RECLAMATION

Managing Water in the West

Hydraulics Laboratory Technical Memorandum PAP-1119
THV-8460-TM-2015-1

Thief Valley Dam Issue Evaluation: Erosion Potential of Spillway and Dam Overtopping Flows

Baker Project, Oregon
Pacific Northwest Region

U.S. Department of the Interior
Bureau of Reclamation
Technical Service Center
Hydraulic Investigations and Laboratory Services Group
Denver, Colorado

June 2015

Hydraulics Laboratory Technical Memorandum PAP-1119
THV-8460-TM-2015-1

Thief Valley Dam Issue Evaluation: Erosion Potential of Spillway and Dam Overtopping Flows

Baker Project, Oregon
Pacific Northwest Region

Tony L. Wahl

Digitally signed by TONY WAHL
DN: c=US, o=U.S. Government, ou=Department of the Interior, ou=Bureau of Reclamation, cn=TONY WAHL, 0.9.2342.19200300.100.1.1=14001000107789
Date: 2015.06.01 17:01:19 -06'00'

Prepared: Tony L. Wahl, P.E.
Hydraulic Engineer, Hydraulic Investigations and Laboratory Services Group, 86-68460

ROBERT EINHELLIG

Digitally signed by ROBERT EINHELLIG
DN: c=US, o=U.S. Government, ou=Department of the Interior, ou=Bureau of Reclamation, cn=ROBERT EINHELLIG, 0.9.2342.19200300.100.1.1=14001000107692
Date: 2015.09.02 14:39:24 -06'00'

Technical Approval: Robert F. Einhellig, P.E.
Manager, Hydraulic Investigations and Laboratory Services Group, 86-68460

JOSEPH KUBITSCHEK

Digitally signed by JOSEPH KUBITSCHEK
DN: c=US, o=U.S. Government, ou=Department of the Interior, ou=Bureau of Reclamation, cn=JOSEPH KUBITSCHEK, 0.9.2342.19200300.100.1.1=14001000107726
Date: 2015.09.02 14:33:47 -06'00'

Peer Review: Joseph P. Kubitschek, Ph.D., P.E.
Hydraulic Engineer, Hydraulic Investigations and Laboratory Services Group, 86-68460

U.S. Department of the Interior
Bureau of Reclamation
Technical Service Center
Hydraulic Investigations and Laboratory Services Group
Denver, Colorado

June 2015

Executive Summary

Analytical studies were performed to estimate the erosion potential of flows passing through the spillway and over the parapet wall of Thief Valley Dam for frequency floods ranging from 100-yr to the PMF. These flows are free jets, relatively thin, high velocity flows that travel through the air from the dam crest or spillway flip bucket down to the tailwater pool. The jets are influenced by gravitational acceleration, air entrainment, and turbulent dissipation as they travel through the air and as they penetrate into the tailwater pool.

Stream power intensities were calculated for jets impinging on areas downstream from the dam, both above and below the surface of the tailwater pool. Jet trajectories were calculated and plotted, and spreading of the jets and dissipation of the jet core were estimated both in the air and in the tailwater pool. The calculated values of stream power intensity and headcut erodibility index values of rock in the impact zones of the jets could be used to determine zones of expected erosion. This study focused on analysis of the jet flows and calculation of stream power intensities; headcut erodibility index values for the downstream rock will be estimated separately.

The highest values of stream power intensity occur just above the surface of the tailwater pool for the 1,000-yr flood. The jets associated with smaller floods are predicted to break up before reaching the tailwater pool. For larger floods, jets remain intact, but the tailwater level increases significantly, and stream power intensity drops off rapidly as the jets penetrate into the tailwater pool. Although maximum stream power intensity drops for floods larger than the 1,000-yr event, the overall erosive capability of those floods may still be significant, since the thicker jets contain more total energy, albeit spread over a larger area. This study did not specifically analyze the erosive capability of flows outside of the jet impingement zones.

A brief review of assumptions regarding discharge coefficients of the spillway and dam crest was made at the outset of this study. That review indicated that discharge coefficients were probably underestimated in previous studies, leading to slightly higher predicted maximum water surfaces to pass given floods. This leads to slightly larger drop heights and greater stream power intensities.

Purpose

This technical memorandum presents the results of analytical studies performed to partially address the following Safety of Dams (SOD) recommendation for Thief Valley Dam:

> **1997-SOD-D** Using stream power and erodibility index relationships or other methods, assess the potential for rock erosion and subsequent instability under high spillway discharges, within a risk assessment framework.

Background

Thief Valley Dam is a water storage feature serving the Lower Division of the Baker Project, located on the Powder River in northeastern Oregon, about 16 miles north of Baker City and 54 river miles downstream from Mason Dam. The dam, completed in 1932, is owned by the Bureau of Reclamation and operated and maintained by the Lower Powder River Irrigation District. The dam is a 390-ft long, reinforced concrete, slab and buttress (Ambursen) structure, with a structural height of 73 ft and a hydraulic height of 48 ft. The original active storage in Thief Valley Reservoir was 17,400 acre-feet. A sedimentation survey completed in 1992 estimated the active capacity at 13,300 acre-feet with a surface area of 685 acres.

The service spillway for the dam is an uncontrolled ogee crest in the center of the dam with a width of 267.83 ft. Spillway capacity is reported to be between 32,200 ft^3/s and 34,000 ft^3/s. Dam segments on the right and left sides of the spillway have lengths of 59.52 ft and 62.65 ft, respectively. Parapet walls at the upstream edge of the dam crest extend up to elevation 3146.0 ft on both sides of the spillway, and the downstream edge of the dam crest is equipped with a handrail. Figure 1 shows a close view of the dam and spillway, and Figure 2 provides a view aligned with the river channel that illustrates some impingement of spillway flows on outcroppings of rock downstream from the dam. Appendix C provides original drawings of the dam and spillway.

Figure 1. — Thief Valley Dam.

Figure 2. — Thief Valley Dam and Reservoir on the Powder River, Oregon.

Probable Maximum Flood (PMF) hydrographs for Spring (May) Rain-on-Snow and Fall (November) General Precipitation events were developed in 1990. A 1992 analysis of hydrologic and hydraulic issues was performed by Harza Engineering Co. (Schickedanz 1992) and determined that the November PMF produced the largest peak outflows from the dam. The reservoir routing study predicted 16 hours of overtopping and a maximum overtopping depth of 11 ft (maximum reservoir water surface elevation 3156.9 ft). Significant assumptions of the Harza study included:

- The dam crest parapet wall remains intact throughout the passage of the PMF. The crest length was assumed to be 120 ft and the discharge coefficient was 2.64. No adjustment was made for an additional increase in crest length as the reservoir rises above the top of the parapet walls and begins to also overflow the sloped abutments above the top of the dam.

- The service spillway rating curve was extended above reservoir elevation 3143.0 ft using a constant discharge coefficient of 4.0, which matches the coefficient corresponding to a discharge of 34,000 ft^3/s at reservoir elevation 3143.0 ft.

The Harza study also estimated the associated tailwater elevations using a DAMBRK computer model simulation of the routed PMF through a 1.6 mi reach of the river downstream from the dam. No tailwater study for lower flow rates is known.

Additional hydrologic studies (Wright 2004) developed reservoir inflow hydrographs for return intervals from 100 to 100,000,000 years. A subsequent routing study (Stowell 2005) produced estimates of peak outflow through the spillway for each of these floods, assuming an initial reservoir water surface elevation of 3133.0 ft. This study also assumed the discharge coefficient of the dam crest to be 2.64. Results from this study are summarized in Table 1, along with the results from the PMF study by Harza. These provide basic input data required to analyze the flow conditions over the spillway and the dam crest with the objective of characterizing the potentially erosive jet flows that are produced downstream from the dam in different flood scenarios.

Table 1. — Flood routing results.

Return period, yr	MWSE	Peak routed Q, cfs
100	3135.56	3828
500	3136.17	5306
1,000	3136.47	6033
10,000	3137.51	9040
100,000	3138.59	12670
1,000,000	3139.75	17187
100,000,000	3142.31	28795
PMF	3159.99	136926*

* Spillway discharge for the PMF is approximately 120,000 ft^3/s and discharge overtopping the dam is about 16,900 ft^3/s.

Discharge Coefficients

A brief review of the previous studies raises some questions about the discharge coefficients used for the spillway and dam crest. The discharge coefficient of 2.64 used for the dam crest in the 1992 and 2005 studies is discussed in the 1992 Harza report. The report states that this discharge coefficient corresponds to a weir breadth of 10 ft, but the total dam crest width is 7.5 ft and the parapet wall thickness is only 1.5 ft. The low C value was also said to account for "turbulence introduced by flow through the hand railing and the short drop from the sharp-crested upstream wall to the parapet deck." This explanation is inconsistent with several characteristics of the flow situation:

1) The hand rail is likely to fail and be removed by the flow and associated debris during a large event,

2) The hand rail is located <u>downstream</u> from the parapet wall and the critical depth location and thus cannot regulate the flow, and

3) The trajectory of flow over the parapet wall will completely miss the entire concrete deck for any head greater than about 5 ft (Hulsing, 1967).

Given these observations, it is likely that flow will spring free from the upstream edge of the parapet wall and the parapet wall will function as a sharp-crested weir with a discharge coefficient in the range of 3.3 or higher.

Figure 3 shows the spillway discharge curves used in the 1992 Harza study and for the 2005 flood routing study by Reclamation. For reservoir elevations below 3143.0 ft, both studies used the discharge curve provided on original design drawings. For higher elevations, the Harza study assumed a constant discharge coefficient of 4.0, while the 2005 study used a discharge curve that implies reduced discharge coefficients for higher reservoir elevations. However, past research on the performance of ogee crest spillways at high heads suggests that the discharge coefficient of this spillway will increase as the operating head exceeds the design value because of suction beneath the nappe that draws additional flow over the crest (Vermeyen 1992). This increase will typically continue for heads as high as 3 to 5 times the design head. The design head for this spillway was estimated at 10.33 ft by matching the shape to idealized ogee crest shape equations given in *Design of Small Dams* (Reclamation, 1987). Thus, the spillway discharge coefficient should continue to increase up to at least reservoir elevation 3164.0 ft (3 times the design head).

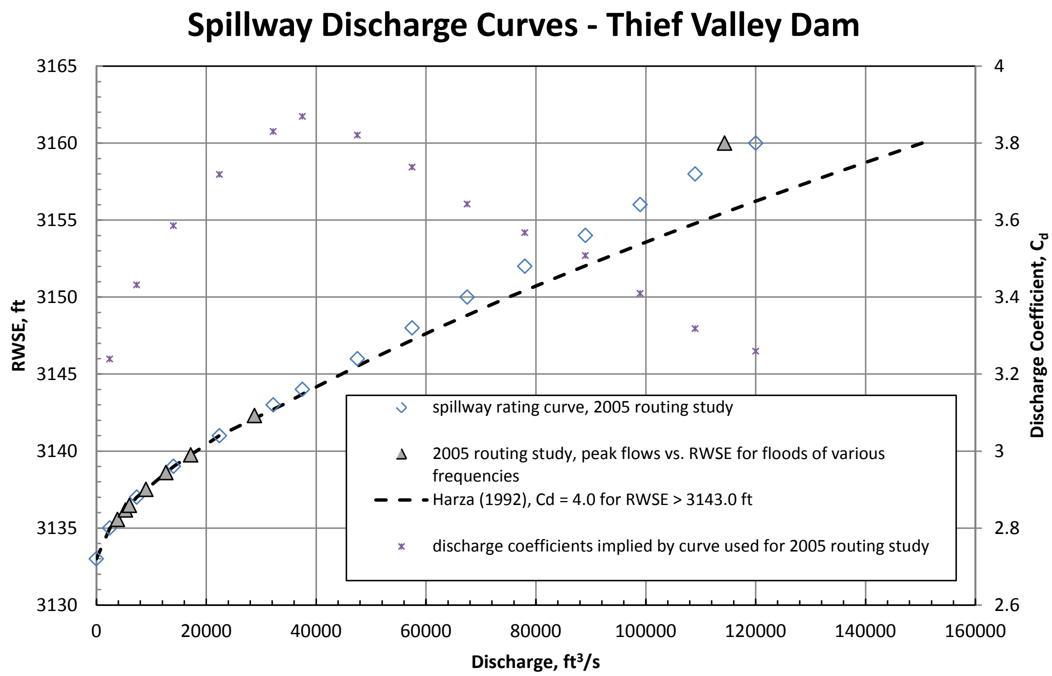

Figure 3. — Spillway discharge curves used in previous hydrologic and hydraulic studies of Thief Valley Dam.

These issues make it likely that the capacity of both the spillway and the dam crest were probably underestimated in the 2005 flood routings, and the 2005 study thus predicts higher reservoir elevations for each given flood event than would actually occur. However, because the volume of the floods considered is much greater than the storage volume of Thief Valley Dam, reservoir attenuation effects were probably small in the routing study, and predicted maximum discharges are probably close to the values that would be obtained if the study were repeated with revised discharge coefficients.

For the purposes of this study, the results of the 2005 flood routing study were considered to be conservative, since they indicate higher reservoir levels for a given flood flow, and these higher reservoir levels and greater drop heights will produce higher-energy jet flows over the spillway and dam. The 2005 flood routing study results were thus accepted and used as the basis for this study of the erosion potential of spillway and dam overtopping flows.

Modeling Spillway and Overtopping Jet Flows

Spillway and dam overtopping flows will produce free jets emanating from the lip of the spillway flip bucket and the crest of the dam parapet wall. These planar or rectangular jets will travel through the air, undergoing changes in thickness and velocity due to gravitational forces, and experiencing air entrainment due to turbulence induced free surface disturbances and interaction with the surrounding air. Figure 4 shows a schematic diagram of the primary physical processes that occur in a free jet as it travels through the air and into a plunge pool. The diagram shows an idealized jet issuing vertically down that is assumed to be initially intact, composed of 100% water with no entrained air. In the case of the Thief Valley Dam spillway, the jet will initially leave the spillway lip at an angle related to the flip bucket geometry. There is some possibility for air entrainment into the spillway flow before the jet leaves the flip bucket, but this will be neglected. As the jet travels through the air, it will entrain air at the edges and the thickness of the "black water" core of the jet will diminish. Eventually the jet may break up fully into clumps and droplets of water with no black water core. Upon entering the tailwater pool, the jet will undergo additional changes as it penetrates into the pool. The core of the jet will diminish rapidly in size and the edges of the jet will experience turbulent mixing as air and water from the tailwater pool are entrained in the shear zone created by the jet as it plunges.

The objective of the analysis described in this section is to estimate the characteristics of the jets associated with spillway and dam overtopping flows that are related to the potential for erosion of soil and rock surfaces downstream from the dam (e.g., abutments, the bottom of the tailwater pool, etc.). The characteristics of the jet that will be the focus of this study are the trajectory (position), the thickness (to map the areal extent of the impingement zone), the velocity, and the associated energy content of the jet. To enable an evaluation of erosion potential, the energy and areal extent of the jet will be combined to determine the amount of energy per unit area being applied at the point of flow impingement. The analysis described in the sections that follow was carried out for the spillway flows associated with each of the frequency flood events shown in Table 1, and for the dam overtopping flow associated with the November PMF event. The spillway flows during the November PMF were not modeled because the predicted tailwater elevation during the PMF submerges the spillway crest by more than 3 ft, and the spillway flip bucket lip is submerged by more than 15 ft. This negates the assumptions made in the analysis of the free jet flows.

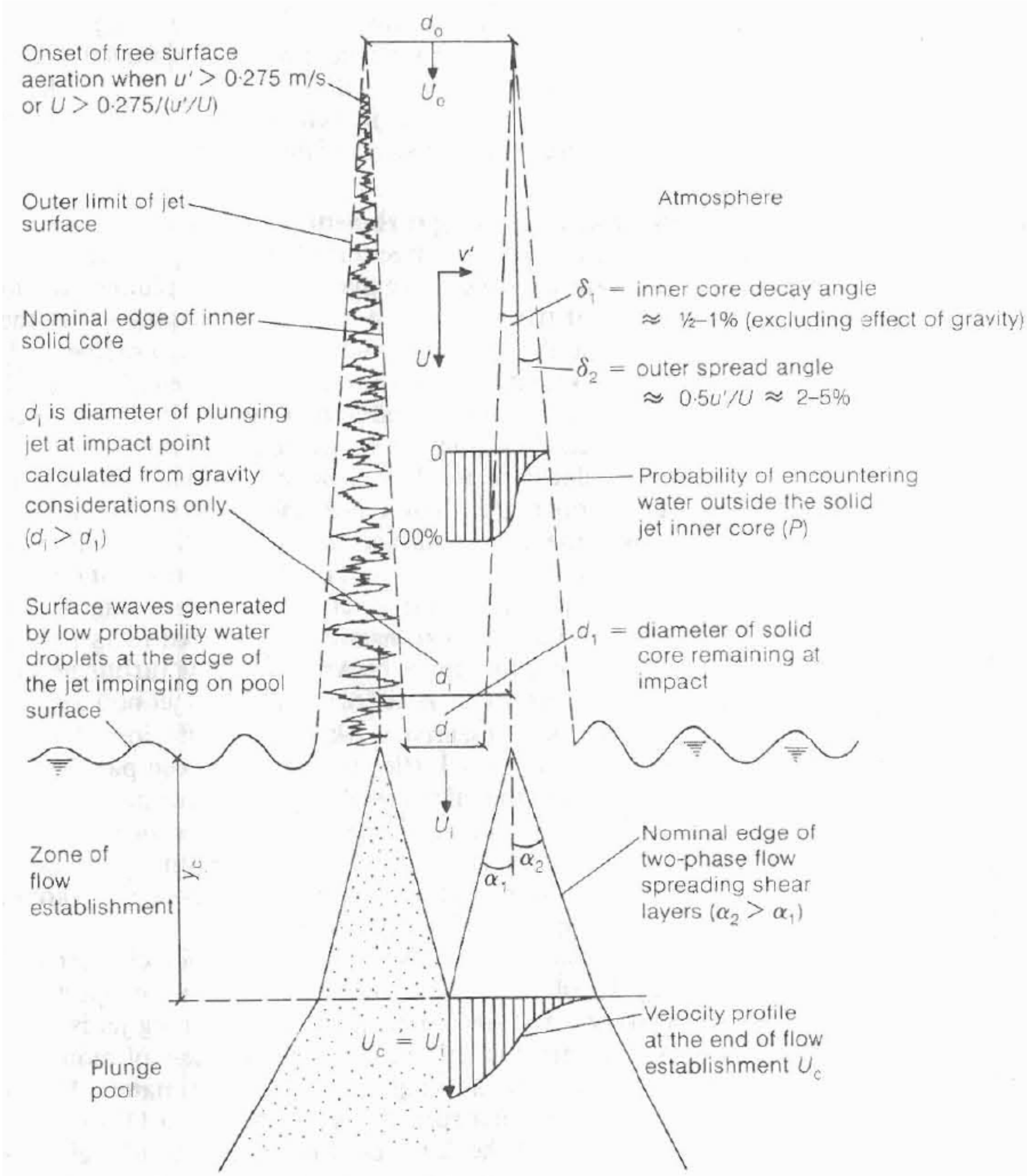

Figure 4. — Schematic representation of a free jet traveling through air and entering a plunge pool (Ervine and Falvey 1987).

Previous studies of similar flow situations have been undertaken for other Reclamation dams. These include:

- Overtopping of Gibson Dam (Frizell 2006);
- Overtopping of Owyhee Dam (Frizell 2006);
- Overtopping of Arrowrock Dam (Frizell 2007); and
- Overtopping of Yellowtail Dam (Frizell 2009).

This study used similar procedures as the previous studies, with consideration of the effects of the spillway chute and flip bucket and new literature published since 2009 relating to the modeling of jet flows.

Jet Trajectory

Jet trajectories were calculated using equations that describe the free-fall motion of a projectile neglecting aerodynamic effects. In a form that is convenient for this application, the elevation of the jet, y, at a given horizontal distance from the take-off point (x = 0) is (Wahl et al. 2008):

$$y = x \tan\theta - \frac{x^2}{4h_v(\cos\theta)^2}$$

where y is the elevation below the takeoff point (y=0 at takeoff), x is the horizontal distance from the takeoff point, θ is the initial angle of the jet from horizontal at the takeoff point, and h_v is the initial velocity head at the takeoff point. This equation was applied to the underside of the nappe and the position of the top side of the nappe was computed relative to the underside based on the jet thickness (see below). For jets overtopping the parapet wall the initial takeoff angle was assumed to be zero (horizontal), and for the jets issuing from the spillway the takeoff angle was assumed to be -25.1°, the angle of the flip bucket lip. The initial flow depth for dam overtopping was computed as (Wahl et al. 2008)

$$d_{\text{brink}}=0.477H_{\text{ovtop}}$$

and the initial velocity and velocity head were determined by continuity. For jets issuing from the spillway, the flow depth and velocity at the takeoff point were determined by applying the energy equation from the reservoir pool to the flip bucket lip, with a conservative assumption of zero energy loss due to friction down the approximately 25-ft long spillway chute. Pfister et al. (2014) showed that the actual jet takeoff angle from a flip bucket is typically less (lower angle) than the physical bucket lip angle, causing the actual jet throw distance to be shorter than one would compute based on the bucket lip angle. However, all of their data were obtained from buckets with larger angles than the Thief Valley spillway and when their equations are extended to the Thief Valley case they predict a takeoff angle that is actually greater (higher) than the flip bucket angle. Since this seems implausible, the bucket lip angle was used here without modification.

The velocity of the free-falling jet was calculated initially by assuming no dissipation or spreading of the jet. Applying the energy equation to the jet, the average velocity at any elevation along the free-fall trajectory can be computed as

$$V_j = \sqrt{V_i^2 + 2gZ}$$

where V_i is the initial average velocity, g is the acceleration due to gravity, and Z is the fall distance. A spreadsheet was used to compute the jet velocities and trajectory coordinates at incremental elevations from the takeoff point to the location at which the jet impacted the tailwater surface. The tailwater elevation for each flow rate was estimated from

$$TW = (Q/207.4)^{(1/1.65)} + 3085$$

This equation was generated by fitting two data points to an assumed equation form:

- tailwater at zero discharge equal to the estimated downstream channel bottom elevation = 3085 ft, and

- estimated PMF tailwater elevation at 138,000 ft^3/s = 3136.4 ft (Schickedanz 1992).

The exponent of 1.65 was based on experience and consideration of the channel shape; it is an estimate that should yield reasonable values for the purpose of this study.

The thickness of the jet neglecting spreading due to breakup was computed by recognizing that for a rectangular jet experiencing no change in its width as it falls, the unit discharge must be the product of the jet thickness and the jet velocity to satisfy continuity. This leads to the equation:

$$t_j = t_i \frac{V_i}{V_j}$$

where t_j is the jet thickness at any point along the trajectory.

Two useful characteristics for any point along the trajectory are the angle of flight and the total distance traveled along the trajectory arc. The flight angle θ from horizontal can be determined from

$$\tan\theta = \frac{V_y}{V_x}$$

with V_x being the horizontal component of velocity and V_y the vertical component. The horizontal velocity is constant since there is no gravitational acceleration and aerodynamic effects that might reduce V_x are neglected. The vertical velocity is computed from

$$V_y = \sqrt{V_j^2 - V_x^2}$$

Finally, the length of the trajectory arc can be calculated from the takeoff point to any horizontal position as:

$$L_j = \int_{x=0}^{x=x} \sqrt{1 + \left(\frac{dy}{dx}\right)^2}\, dx$$

This integration is accomplished by making the following substitutions satisfying the initial conditions:

$A = 2h_v\cos^2(\theta_o)$

$B = dy/dx = \tan(\theta_o)\text{-}x/A$

where h_v is the initial velocity head at the takeoff point and θ_o is the takeoff angle. Then,

$$L_j(x) = \frac{-A}{2}\left[B\sqrt{B^2+1} + ln\left(B + \sqrt{B^2+1}\right)\right]$$

If the initial takeoff is horizontal (θ_o=0), then $L_j(0)=0$ and the integration function must only be evaluated at the final x position. If the takeoff angle is non-zero, then $L_j(0)$ is also non-zero and the net trajectory length is $L_j(x)-L_j(0)$.

The calculations described above were carried out until the centerline of the jet reached the estimated tailwater elevation. Below the tailwater surface, the jet was assumed to penetrate into the tailwater pool at a uniform velocity and angle equal to the conditions at entry through the tailwater surface (i.e., no further gravitational acceleration occurs in the tailwater pool).

Jet Changes in the Air

In addition to the thinning of the jet core under the influence of acceleration due to gravity, as the jet travels through the air it will begin to spread near the edges as air becomes entrained into the surface of the jet. This further reduces the thickness of the jet core. The trajectory calculation spreadsheet was used to calculate the gradual spreading of the jet and the further reduction of the jet core thickness using equations developed by Ervine et al. (1997):

$$t_{spread} = t_j + 2\varepsilon$$

$$\varepsilon = \frac{1.14T_uV_i^2}{g}\left[\sqrt{\frac{2L_j}{t_iFr_i^2} + 1} - 1\right]$$

$$t_{core} = t_j - \frac{2L_j}{200}$$

where Fr_i is the Froude number $V_i/(gD_i)^{0.5}$ at the initial takeoff point and T_u is a turbulence intensity factor that varies from 0.00 to 0.03 for free overfalls and 0.03 to 0.05 for ski jump (flip bucket) outlets (Bollaert 2002). The initial depth D_i is either the brink depth for dam overtopping or the depth calculated at the spillway flip bucket lip using the energy equation as described in the Jet Trajectory section. A value of T_u=0.02 was assumed in this study for flow over the dam parapet wall and a value of T_u=0.04 was assumed for flow leaving the spillway flip bucket. The equation for the thickness of the jet core merely reflects the observation by Ervine et al. (1997) that in addition to the gravitationally-induced thinning, diffusion of the jet causes the core to diminish at each edge at a rate of about 0.5% to 1.0% of the travel distance. The lower value was assumed for a conservative estimate.

Most formulas describing free jet behavior, including those above, were developed for circular jets. Castillo (2006) in a non-peer reviewed publication provides jet spread formulas for rectangular jets, but they are poorly documented with some questionable assumptions made in their development. A new peer-reviewed paper by Castillo et al. (2014) was published after the bulk of the calculations had been performed for this study; that paper provides slightly modified equations compared to Castillo (2006), and quick checks showed that the results are not dramatically different from those obtained with the Ervine et al. (1997) equations.

Jet Break-up Distance

Full break-up of the jet core is implied when the calculated jet core thickness reaches zero. With the conservative assumptions made in the previous section, the jet core is estimated to have an intact core for the 1,000-year flood events and larger.

Several investigators have offered equations for directly estimating the jet break-up distance. Ervine et al. (1997) derived an equation from first principles for round jets:

$$C^2 = (1.14T_uFr_i^2)^2 = \frac{1}{\left(\sqrt{\frac{2L_b}{D_iFr_i^2}+1}\right)\left(\sqrt{\frac{2L_b}{D_iFr_i^2}+1}-1\right)^2}$$

L_b can be determined with this equation by trial. Following the procedure used by Ervine et al. (1997), a similar equation for rectangular jets can be developed:

$$C = 1.14T_u Fr_i^2 = \frac{1}{\left(\sqrt{\frac{2L_b}{t_i Fr_i^2} + 1}\right)\left(\sqrt{\frac{2L_b}{t_i Fr_i^2} + 1} - 1\right)}$$

Ervine et al. (1997) also provided an empirical equation fitted to experimental data for round jets:

$$L_b = \frac{1.05 D_i Fr_i^2}{(1.14 T_u Fr_i^2)^{0.82}}$$

Castillo (2006) developed a similar empirical equation for rectangular jets:

$$L_b = \frac{0.85 t_i Fr_i^2}{\left(K_\varphi T_u Fr_i^2\right)^{0.82}}$$

with K_φ having a value of 1.07. Castillo et al. (2014) proposed the same equation, but with $K_\varphi \approx 1.02$ for two-dimensional (rectangular) jets and $K_\varphi \approx 1.24$ for three-dimensional rectangular jets. One other commonly referenced equation is due to Horeni (1956), $L_b = 6(q)^{0.32}$, where L_b is in meters and q is unit discharge in m^2/s. This equation predicts much longer breakup distances than the others and the basis for its development is not well understood. The reference is cited by many, including Ervine et al. (1997) and Castillo et al. (2014), but the original document (Horeni's Ph.D. thesis) was only obtained by this author after the bulk of this study was complete; furthermore the document is written in the Czech language with only a brief technical summary in English. Given its significantly different results compared to newer works, this equation was not considered further.

Results of applying the break-up length equations are shown in Table 2. For the spillway flows associated with the 10,000-yr event or smaller, the equations predict that the jet will be fully broken up before it reaches the tailwater pool. For the overtopping of the dam during the PMF and for the spillway flows during the 1- and 100-million year events the jets are likely to have an intact core when they reach the surface of the tailwater pool. For the 100-thousand year event the spillway jet is predicted to be close to full breakup when it reaches the tailwater pool.

Jet Dissipation in the Tailwater Pool

Upon entering the tailwater pool a free jet will undergo additional spreading of its outer extents and dissipation of the core. The most common case is a highly turbulent plunging jet like that shown in Figure 5(d). The inner core contracts at about an 8° angle on each edge while the exterior of the jet spreads at an angle of about 14°.

Table 2. — Computed jet break-up distances compared to the length of the flow trajectory to the tailwater surface.

Flood event frequency and flow type	Ervine et al. (1997) theoretical round jet	theoretical rectangular	empirical (round jet)	Castillo (2006) - rectangular	Trajectory arc length at tailwater, L_j
years	*ft*	*ft*	*Ft*	*ft*	*ft*
Dam overtopping					
PMF	401	161	168	143	25.4
Spillway operations					
100	10.5	9.2	13.1	11.1	41.9
500	14.4	12.3	16.9	14.5	40.6
1,000	16.3	13.8	18.8	16.0	40.0
10,000	24.0	19.5	25.9	22.0	37.9
100,000	33.3	26.0	33.7	28.8	35.6
1,000,000	44.8	33.6	42.9	36.6	32.9
100,000,000	73.9	51.7	64.2	54.8	27.0

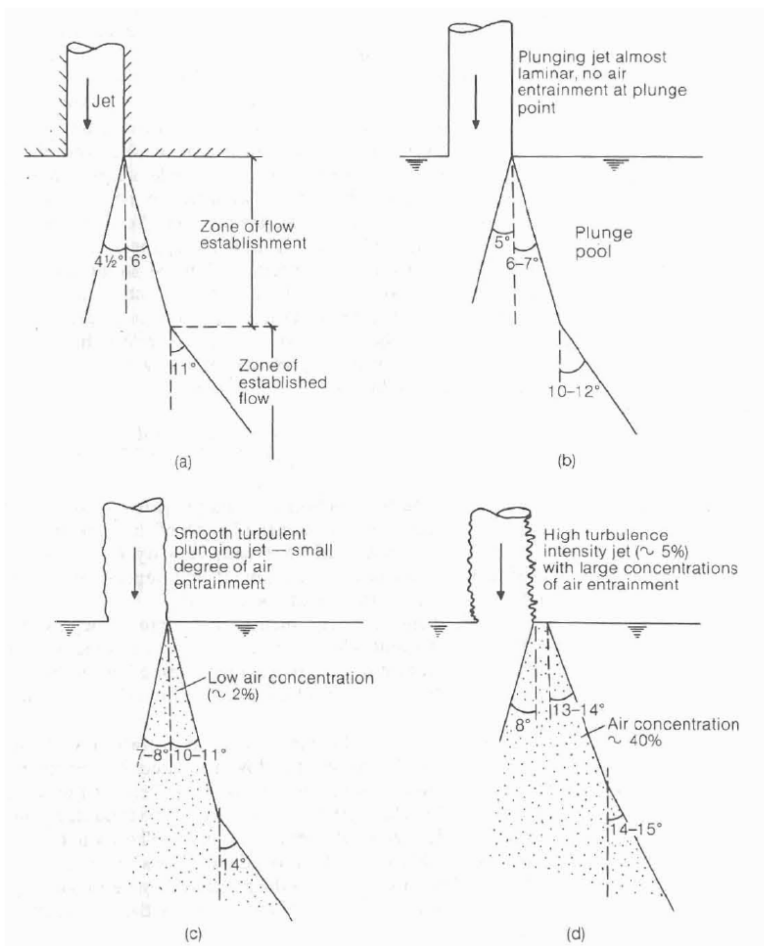

Figure 5. — Characteristics of jet dissipation in a plunge pool (Ervine and Falvey 1987) for: (a) submerged jet in a pool with lid (no aeration of jet boundaries); (b) almost laminar plunging jet (almost never encountered in a prototype flow; (c) smooth turbulent plunging jet (rare in a prototype flow); and (d) highly turbulent plunging jet (typical of almost all prototype flows and most models).

Pressure Fluctuations Produced by Impinging Jets

The erosive capability of an impinging jet can be evaluated based on either the pressures produced against a rock surface and in fissures penetrating that surface, or the rate of energy dissipation that takes place in the near field of that surface. This study focuses on the latter, but for those interested in the pressure-based approach, the newly published work of Castillo et al. (2014) is suggested. That study provides experimental data and equations for estimating the mean and maximum dynamic pressures occurring at plunge pool boundaries for a variety of jet configurations. A significant finding of that study is that the maximum dynamic pressures occur when the drop height from reservoir to tailwater pool is about 1.0 to 1.2 times the jet breakup length (i.e., the jet core breaks up in the air shortly before hitting the tailwater pool) and the pool is shallow (pool depth < $5.5t_{spread}$).

Stream Power Calculations

For each modeled flow condition the stream power of the jet was calculated along its travel path to determine its erosive capability. The total power of the jet was calculated as

$$P = \gamma Q h_v$$

where g is the unit weight of water, Q is the discharge, and h_v is the velocity head at the point of impact. The erosive power of the jet is related to the stream power intensity which is the power divided by the area over which it is applied.

$$p' = \frac{\gamma Q h_v}{A_i}$$

An intact jet core may impinge on a solid boundary either on an abutment above the tailwater surface, or in the tailwater pool. For an intact jet core, the stream power intensity in the core will be equal to that which would be calculated for the jet with no spread or turbulent dissipation of the core thickness, i.e., the impact area is considered to be the jet thickness, t_j, calculated considering only the thinning effect of gravitational acceleration. Depending on local topography, the jet may impinge against the boundary at an oblique angle, but the maximum stream power intensity will be realized when the jet strikes normal to the solid boundary. The stream power intensity for that case is

$$p' = \frac{\gamma q h_v}{t_j}$$

For a jet that is completely broken up in the air or in the tailwater pool, the average stream power intensity over the full extent of the spread jet envelope can be calculated from

$$p' = \frac{\gamma q h_v}{t_{spread}}$$

However, this does not account for the fact that a non-uniform velocity distribution persists for some distance even after the jet core has been dissipated (Figure 6). The peak velocity of the jet for distances beyond the end of the jet core diminishes in proportion to the ratio of the total distance traveled by the jet compared to the length of the jet core (Hanson et al. 1990), and thus the peak stream power intensity of the fully developed jet can be expressed as

$$p' = \frac{\gamma q h_v \left(\frac{L_{core}}{L_{tw}}\right)}{t_j}$$

where L_{core} is the length of the core of the jet and L_{tw} is total distance traveled by the jet into the tailwater pool. In the spreadsheet used to model the jet flows for Thief Valley Dam, the maximum of the two previous expressions was used as the stream power intensity for the fully developed jet in the tailwater pool.

It should be emphasized that these calculations of stream power intensity consider the impact area of the jet against a horizontal surface and do not reflect any reduction due to slope of the abutments.

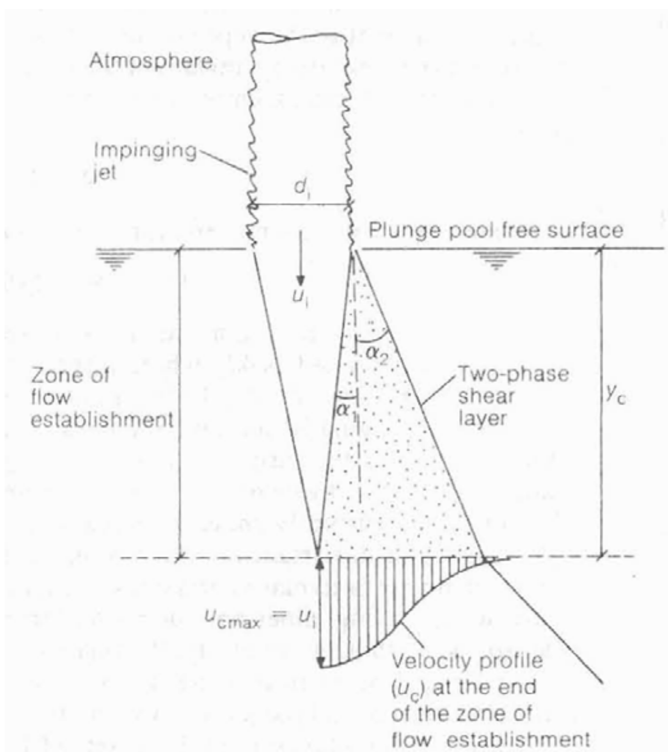

Figure 6. — Velocity profile at the end of the zone of flow establishment (Ervine and Falvey 1987).

Stream Power Estimates

Appendix A provides charts showing the predicted spillway and dam overtopping jet flows for each flood event. For locations above the tailwater surface the stream power intensity of the jet core is plotted and for locations below the water surface the maximum stream power intensity is plotted for the jet core or the fully developed jet. There is uncertainty about where the jet breaks up in the air. The conservative application of the jet thickness and jet spread equations indicates that the jet core retains a finite thickness at impact with the tailwater surface, while the direct jet breakup equations indicate full breakup for the 10,000-yr flood event and smaller. To illustrate the effect of this, each plot also includes a line showing the average stream power intensity if the full power of the jet is evenly distributed over the calculated spread thickness of the jet.

In general, smaller flood events have the potential to produce greater stream power intensity because of the lower tailwater elevations and larger drop heights, but the extent of the area that experiences the high intensity flow impingement will also be small. Larger flood events produce thicker jets with a greater chance for an intact jet at impact, but with lower stream power intensity due to the protection provided by the associated high tailwater levels. Although the focus of SOD Recommendation 1997-SOD-D was on spillway flows, the November PMF which overtops the dam was also modeled. Only the dam overtopping jet trajectory is plotted for that event, since the spillway crest and the entire spillway flip bucket chute will be below the tailwater level.

Table 3 summarizes the jet characteristics and stream power intensities computed for each flood event. The smaller flood events have a wide range of possible stream power intensities, but also the narrowest jets at impact and a good potential that the jets are fully broken up; the peak values of stream power intensity are conservative upper estimates.

Table 3. — Jet thickness and stream power intensities at impact with tailwater.

	Jet core thickness, *ft*		Stream power intensity at tailwater impact, *kW/m²*	
Flood event frequency (years) and flow type	minimum (at tailwater impact)	maximum (at takeoff)	Average (broken up jet)	peak / maximum
Dam overtopping				
PMF	3.65	6.02	525	628
Spillway operations				
100	-	0.47	205	1457**
500	-	0.65	272	1889**
1,000	0.03	0.73	303	2076
10,000	0.27	1.07	419	1980
100,000	0.57	1.46	535	1880
1,000,000	0.95	1.94	649	1768
100,000,000	1.98	3.12	830	1536

** Jet core is broken up at tailwater level according to all modeling methods; value shown is peak stream power intensity at the point of predicted jet breakup based on trajectory and jet core thickness equations

Jet Impingement Areas

Each of the computed trajectories was used to develop an estimate of the impingement zone on the downstream topography. The jet core and spread jet profiles were used to create polylines in AutoCAD that were then intersected with the downstream topographic surface to generate plan view maps of the impact zones. Tailwater levels for each flood event were also illustrated so that zones of direct vs. submerged impingement can be readily seen. Appendix D provides maps depicting the impingement zones for each flood event.

Discussion: Use of Stream Power Estimates for Erosion Analysis

The estimates of stream power intensity developed in this study can be used to evaluate the potential for erosion of the areas impacted by the spillway jet flows. Annandale (1995) established a curve to define the threshold for erosion as a function of stream power intensity and the headcut erosion index of soil and rock materials. The headcut erosion index can be evaluated using a combination of field evaluations and laboratory tests that incorporate the effects of rock mass strength, particle block size, discontinuity and interparticle bond strength, and block structure/orientation to the flow. Wibowo et al. (2005) extended this work, using logistic regression to establish lines of equal probability of erosion on the stream power-headcut index diagram (Figure 7).

Estimates of headcut erodibility index for rock in the jet impact areas have not been developed at this time, but the high values of maximum stream power intensity shown in Table 3 suggest that where jets impact on the stream channel or abutments above the tailwater surface, there is high potential for erosion, even of resistant materials. However, the thickness of the intact jet is relatively small, so the capacity to erode extensive areas seems limited. Additionally, the charts of stream power intensity in Appendix A show that stream power intensity drops rapidly once the jets penetrate below the tailwater level, so the potential for deep erosion is also limited.

Tailwater has a significant effect on the erosion potential of spillway and overtopping flows. The highest stream power intensities occur in zones just above the tailwater pool water surface for the 1,000-yr frequency flood. The jets associated with smaller floods are predicted to break up before reaching the tailwater pool. For larger floods, jets remain intact, but the tailwater level increases significantly, which reduces the maximum drop height of the jets and the maximum stream power intensity. Although the maximum stream power intensities are smaller for these larger floods, the thickness of these jets is greater, so they may cause less intense erosion, but over a more extended area.

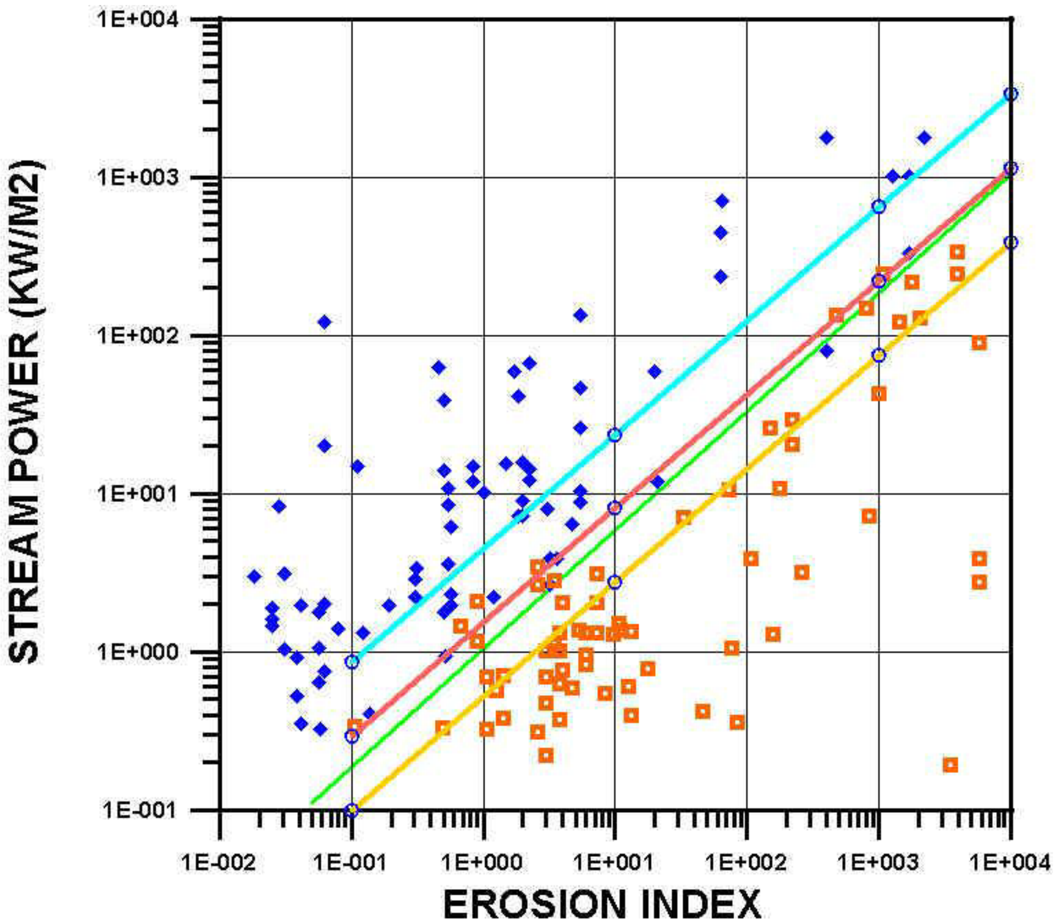

Figure 7. — Probability of erosion as a function of K_h (headcut erosion index) and stream power per unit area (Wibowo et al. 2005). The upper line indicates 99% chance of erosion, the lower line 1% chance, and the middle (orange) line 50% chance. The middle (green) line is the original threshold for erosion proposed by Annandale (1995). Orange data points are case studies with no erosion; blue points are case studies with erosion.

Summary and Conclusions

Estimates of stream power intensity were made for jet flows produced by flow through the spillway or overtopping the parapet wall of Thief Valley Dam for frequency floods ranging from the 100-yr event to the PMF.

Although estimates of headcut erodibility index have not been developed at this time, high values of stream power intensity are present, but with a limited areal extent due to the thinning of the jets as they travel through the air down to the tailwater pool. Potential for erosion of rock and soil above the tailwater level is high, but only in the limited areas impacted by the intact jet. Potential for deep erosion below the level of the tailwater surface seems limited by the fact that stream power intensity drops rapidly when these thin jets penetrate below the tailwater level. The highest flood flows are capable of producing thicker jets whose erosive power could penetrate further into the tailwater pool, but the erosion potential of these jets is limited by the fact that very high tailwater pool levels accompany such high flows and the net head drop is reduced, so stream power intensities at the tailwater surface are actually lower than for smaller flow rates combined with low tailwater levels.

References

Annandale, G., 1995, Erodibility. *Journal of Hydraulic Research*, 33(4):471-494.

Bollaert, Erik, 2002, Transient water pressures in joints and formation of rock scour due to high-velocity jet impact. Communication 13, Laboratoire de Constructions Hydrauliques Ecole Polytechnique Federale de Lausanne, Edited by Professor Dr. A. Schleiss, Lausanne, Switzerland, 2002.

Bureau of Reclamation, 1987. *Design of Small Dams*. Denver, Colorado

Bureau of Reclamation, Data Web. Thief Valley Dam. http://www.usbr.gov/projects/Facility.jsp?fac_Name=Thief+Valley+Dam, accessed 10/3/2014.

Bureau of Reclamation, Data Web. Baker Project. http://www.usbr.gov/projects/Project.jsp?proj_Name=Baker+Project, accessed 10/3/2014.

Capacity Curves, Thief Valley Dam, Plan-Elevation and Sections, Bureau of Reclamation, Drawing 115-D-153, June 1931.

Castillo, L., 2006. Aerated jets and pressure fluctuation in plunge pools. Proceedings of the *Seventh International Conference on Hydroscience and Engineering* (ICHE-2006), Philadelphia, 1–23, M. Piasecki and College of Engineering, Drexel University, USA.

Castillo, Luis G., José M. Carrillo and Antonio Blázquez, 2014. Plunge pool dynamic pressures: a temporal analysis in the nappe flow case, *Journal of Hydraulic Research*, DOI: 10.1080/00221686.2014.968226

Ervine, D.A., and H.T. Falvey, 1987. Behaviour of turbulent water jets in the atmosphere and in plunge pools. *Proc. Instn. Civ. Engrs.*, Part 2, Paper 9136, Vol. 83, March 1987, pp. 295-314.

Ervine, D.A., H.T. Falvey, and W. Withers, 1997. Pressure fluctuations on plunge pool floors. *Journal of Hydraulic Research*, 35:2, 257-279, DOI: 10.1080/00221689709498430

FEMA, 2014. Technical Manual: Overtopping Protection for Dams. FEMA P-1015. Federal Emergency Management Agency, Washington, DC.

Frizell, Kathleen H., 2006. *Hydraulic Investigations of the Erosion Potential of Flows Overtopping Gibson Dam*, Hydraulic Laboratory Report HL-2006-02, Bureau of Reclamation Hydraulic Investigations and Laboratory Services Group, Denver, Colo.

Frizell, Kathleen H., 2006. *Hydraulic Investigations of the Erosion Potential of Flows Overtopping Owyhee Dam*, Report PAP-956, Bureau of Reclamation Hydraulic Investigations and Laboratory Services Group, Denver, Colo. FOR OFFICIAL USE ONLY.

Frizell, Kathleen H., 2007. *Analysis of the Erosion Potential of Flow Overtopping Arrowrock Dam*, Report PAP-963, Technical Memorandum ARR-8560-IE-2007-1, Bureau of Reclamation Hydraulic Investigations and Laboratory Services Group, Denver, Colo. FOR OFFICIAL USE ONLY.

Frizell, Kathleen H., 2009. *Yellowtail Dam Issue Evaluation-Analysis of the Erosion Potential of Flow Overtopping*, Report PAP-1002, Technical Memorandum YEL-8460-IE-2009-1, Bureau of Reclamation Hydraulic Investigations and Laboratory Services Group, Denver, Colo.

Hanson, G. J., K. M. Robinson, and D. M. Temple. 1990. Pressure and stress distributions due to a submerged impinging jet. *Proceedings*, *ASCE National Convention on Hydraulic Engineering*, July 30-August 3, 1990, San Diego, CA, pp. 525−530.

Horeni, P., 1956. Desintegration [sic] of a free jet of water in air. Studie rozpadu volného vodního paprsku ve vzduchu Workbook 93, Hydraulic Research Institute, Prague, Czechoslovakia. 1956. In Czech.

Hulsing, H., 1967. Measurement of peak discharge at dams by indirect method. Techniques of Water Resources Investigations of the United States Geological Survey, Book 3, Chapter A5.

Pfister, Michael, Willi H. Hager, and Robert M. Boes, 2014. Trajectories and air flow features of ski jump-generated jets, *Journal of Hydraulic Research*, DOI: 10.1080/00221686.2013.875072

Schickedanz, Norman L., 1992. Technical Memorandum No. TVY-3110-SEED-93-1, Analysis of hydrologic/hydraulic issues for Thief Valley Dam. December 1992. Submitted by Harza Engineering Company to Bureau of Reclamation, Concrete Dams Branch, Denver, Colorado.

Stowell, Hillery, 2005. Thief Valley flood routing study. Technical Memorandum No. THV-8130-TM-2005-1, Bureau of Reclamation, Waterways and Concrete Dams Group, Denver, Colorado.

Vermeyen, Tracy, 1992. Uncontrolled ogee crest research. Bureau of Reclamation, Hydraulics Laboratory Report PAP-609, Denver, Colorado.

Wahl, Tony L., Kathleen H. Frizell, and Elisabeth A. Cohen, 2008. Computing the trajectory of free jets. *Journal of Hydraulic Engineering*, 134(2):256-260.

Wright, Joseph M., 2004. Thief Valley Dam, Oregon – initial flood characterization. Memorandum to Team Leader, Thief Valley Dam Issue Evaluation, November 24, 2004. Bureau of Reclamation, Flood Hydrology Group, D-8530, Denver, Colorado.

Appendix A – Jet Trajectory and Stream Power Intensity Charts

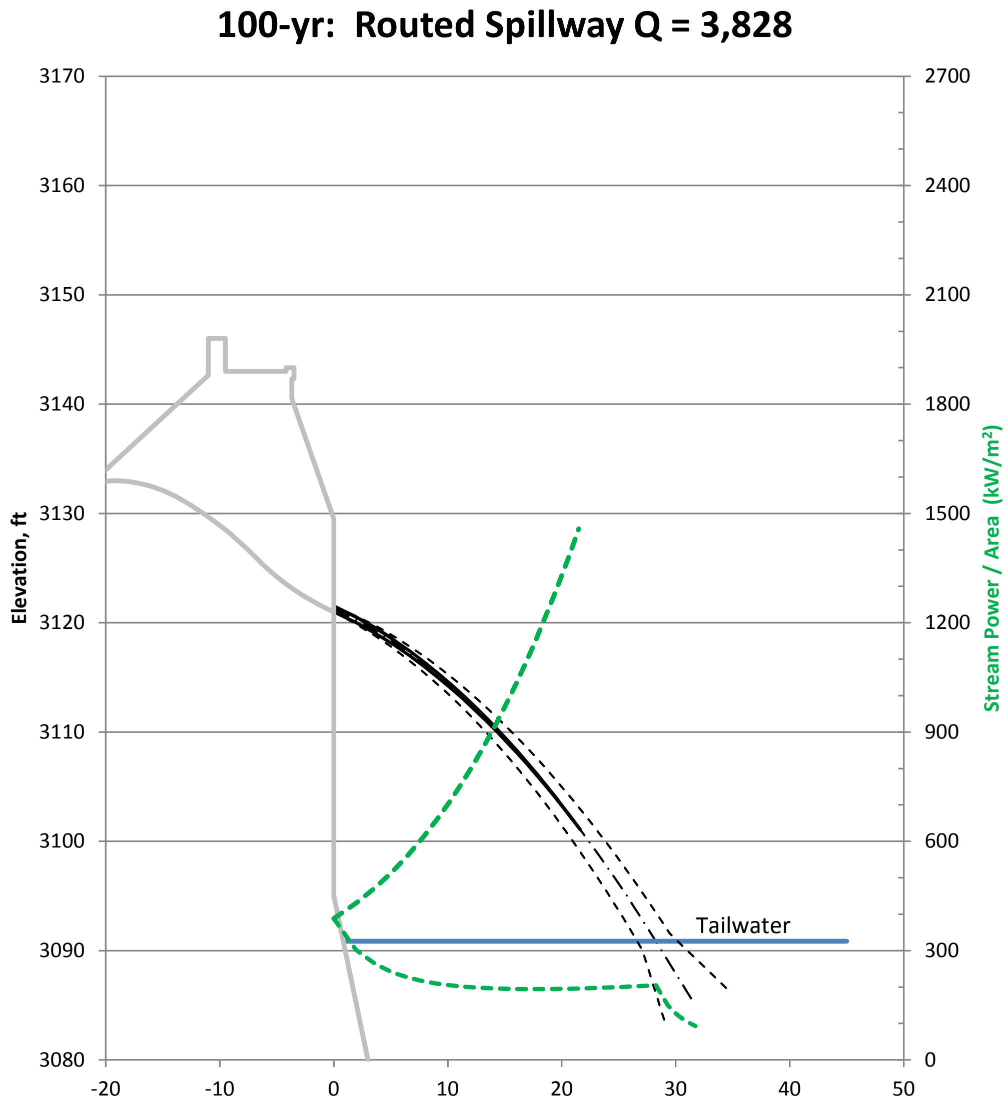

Figure A - 1. — Jet trajectory and stream power intensity for peak spillway flow during the 100-yr frequency flood, Thief Valley Dam, Oregon. Gray lines show the approximate dam and spillway cross section. Light dashed lines indicate the extent of the spread jet, while solid thin lines illustrate a conservative estimate of the thickness of the jet core. Heavy, dashed green lines show the stream power intensity. The upper line is the stream power intensity of the jet core; the lower line is the average stream power across the width of the spread jet. Empirical equations suggest that the jet will be fully broken up after about 10 to 15 ft of flight through the air.

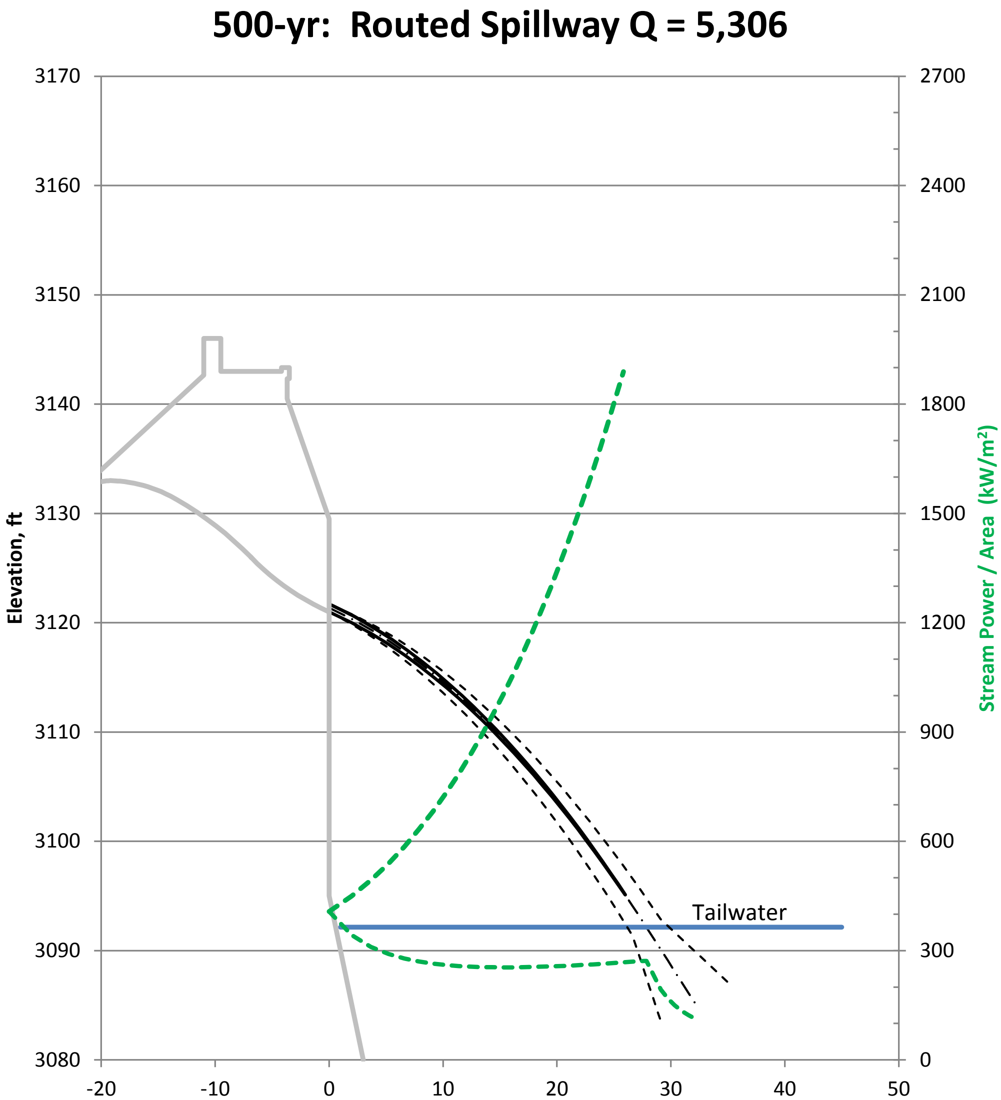

Figure A - 2. — Jet trajectory and stream power intensity for peak spillway flow during the 500-yr frequency flood, Thief Valley Dam, Oregon. Heavy, dashed green lines show the stream power intensity. The upper line is the stream power intensity of the jet core; the lower line is the average stream power across the width of the spread jet. Empirical equations suggest that the jet will be fully broken up after about 15 ft of flight through the air.

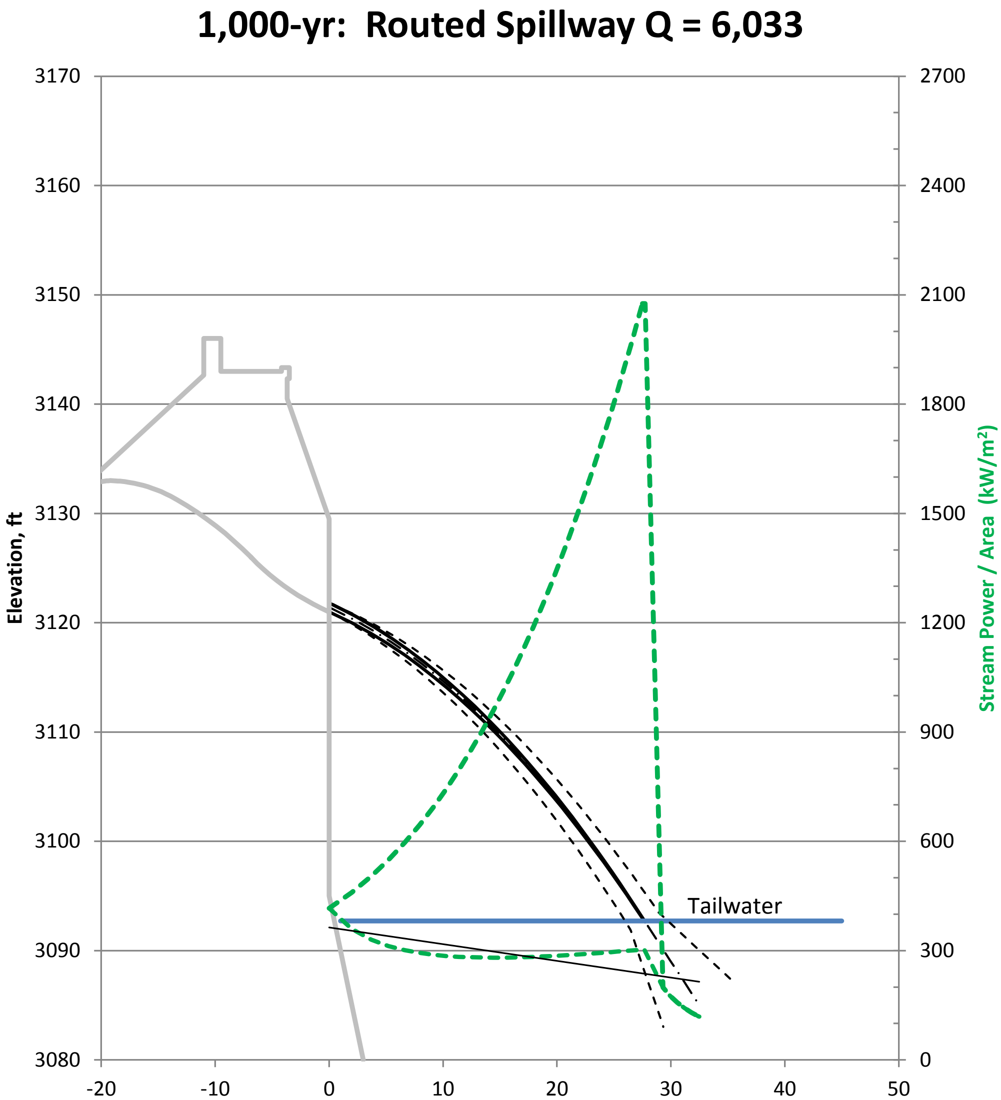

Figure A - 3. — Jet trajectory and stream power intensity for peak spillway flow during the 1,000-yr frequency flood, Thief Valley Dam, Oregon. Heavy, dashed green lines show the stream power intensity. The upper lines are the stream power intensity within the jet core; the lower lines are the average stream power across the width of the spread jet. Empirical equations suggest that the jet will be fully broken up after about 15 to 20 ft of flight through the air.

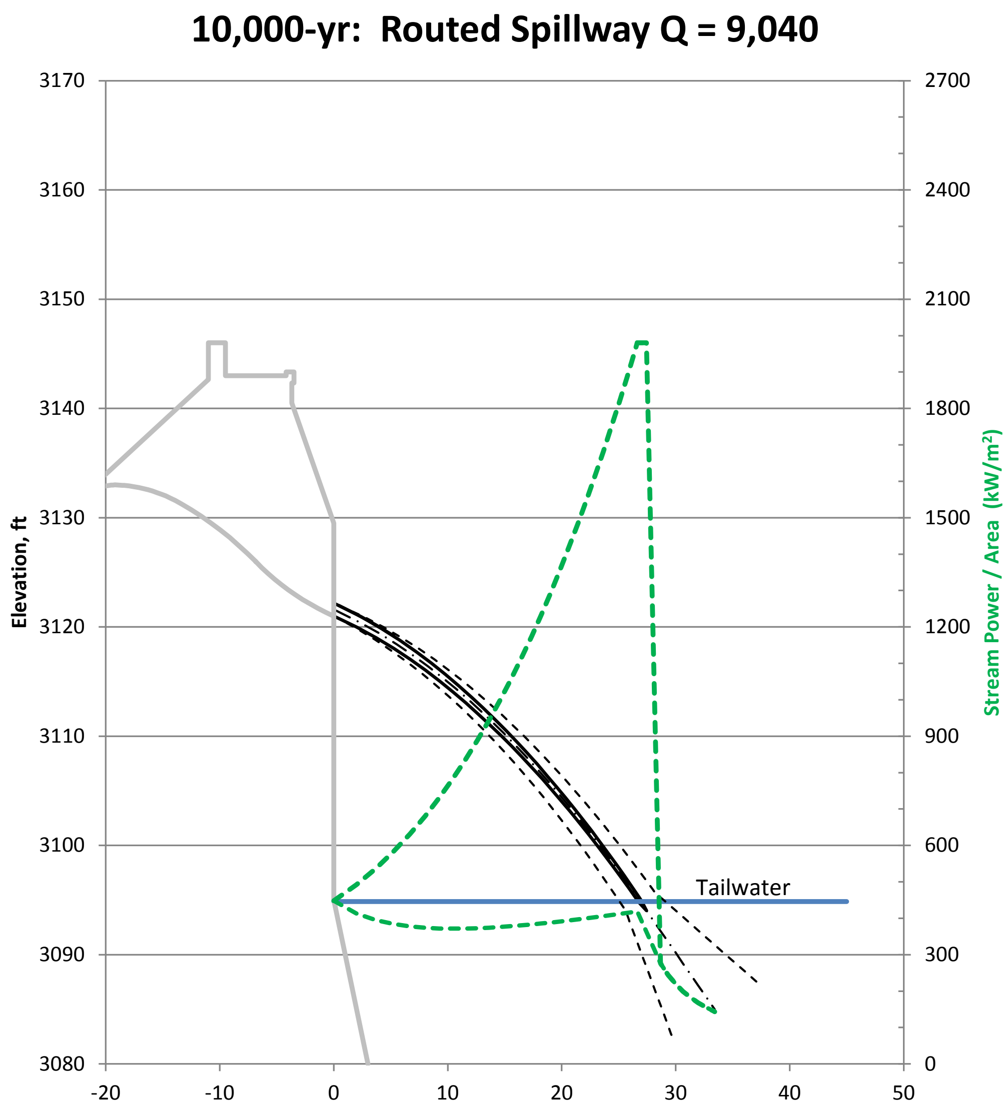

Figure A - 4. — Jet trajectory and stream power intensity for peak spillway flow during the 10,000-yr frequency flood, Thief Valley Dam, Oregon. Heavy, dashed green lines show the stream power intensity. Empirical equations suggest that the jet will be fully broken up after about 20 to 25 ft of flight through the air.

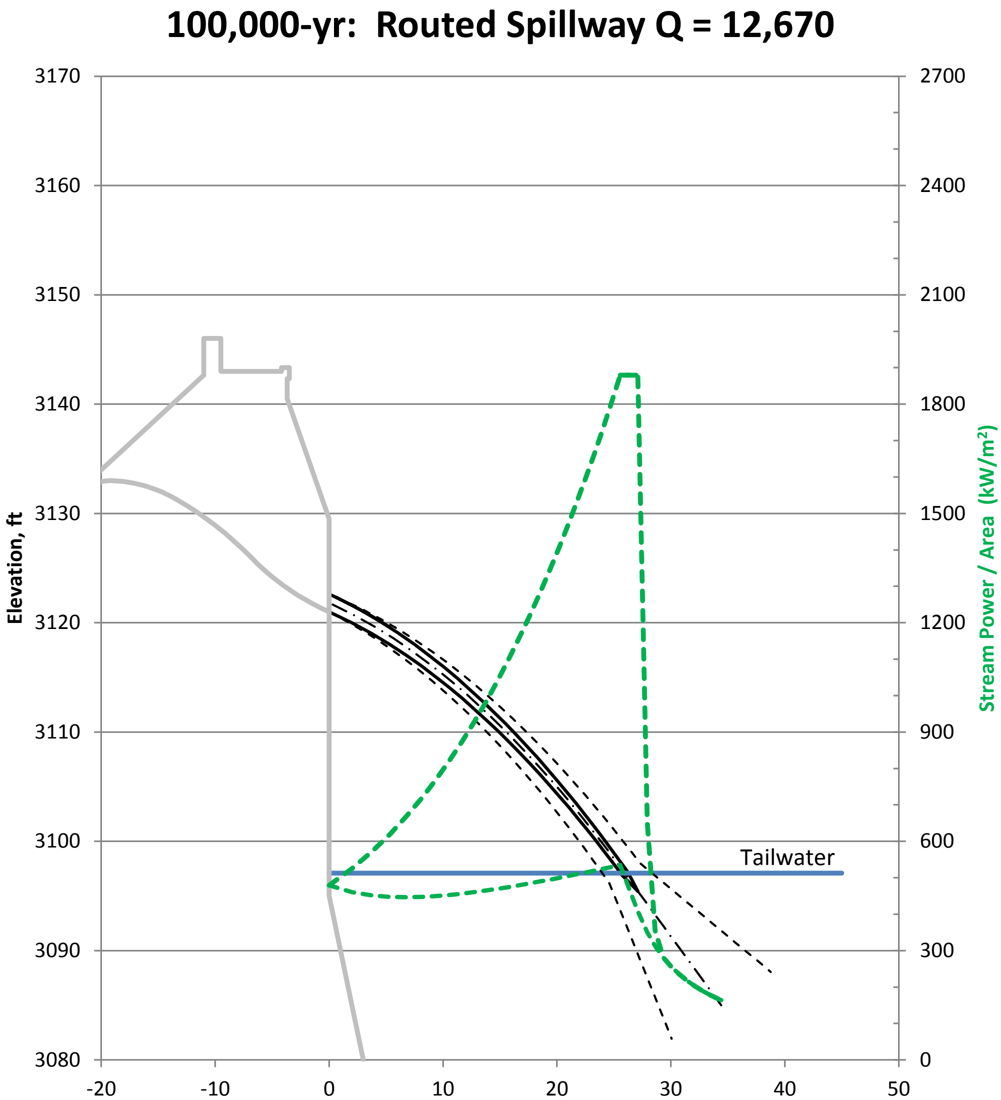

Figure A - 5. — Jet trajectory and stream power intensity for peak spillway flow during the 100,000-yr frequency flood, Thief Valley Dam, Oregon. Heavy, dashed green lines show the stream power intensity. Empirical equations suggest that the jet will be fully broken up after about 25 to 35 ft of flight through the air. The length of the trajectory arc to the tailwater pool is 35.6 ft.

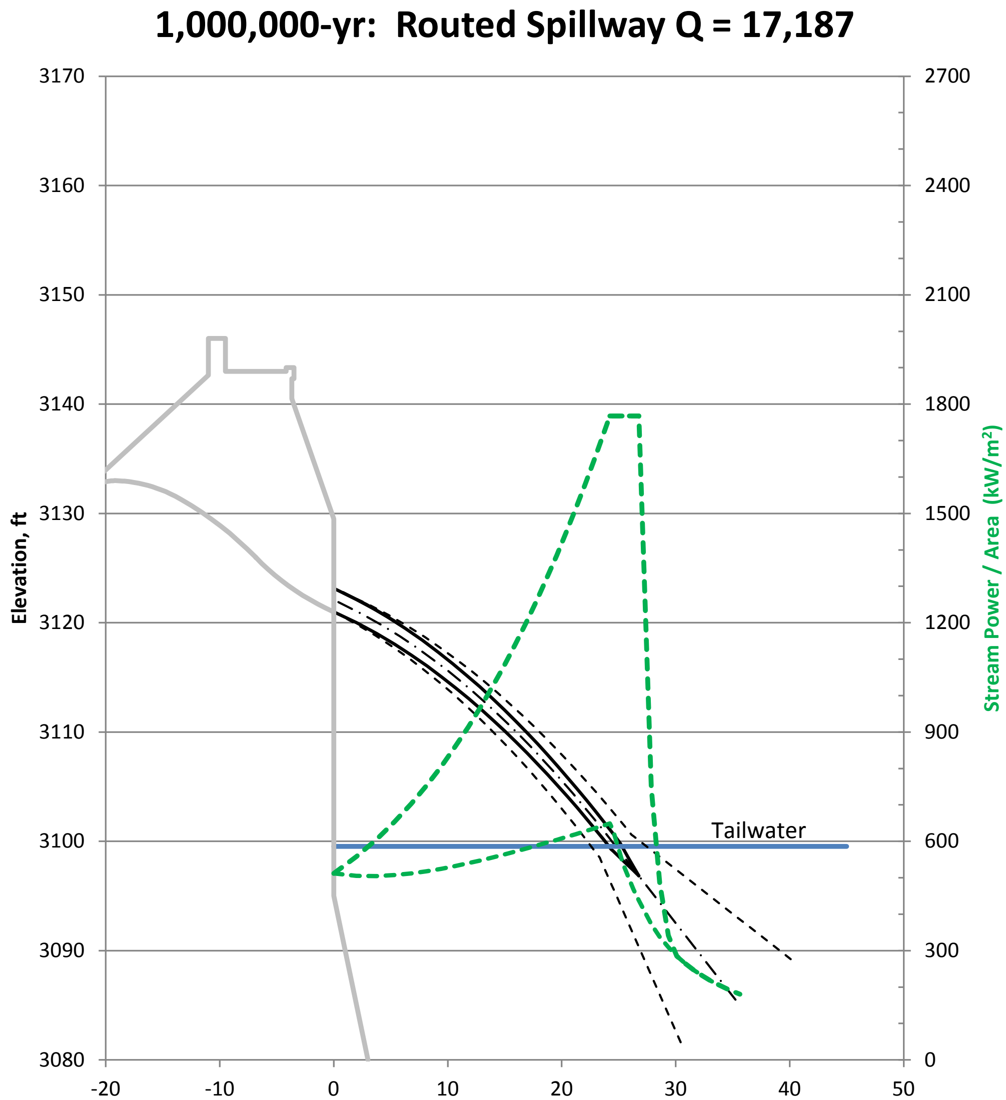

Figure A - 6. — Jet trajectory and stream power intensity for peak spillway flow during the 1,000,000-yr frequency flood, Thief Valley Dam, Oregon. Heavy, dashed green lines show the stream power intensity. The jet is expected to have an intact core when it reaches the tailwater surface.

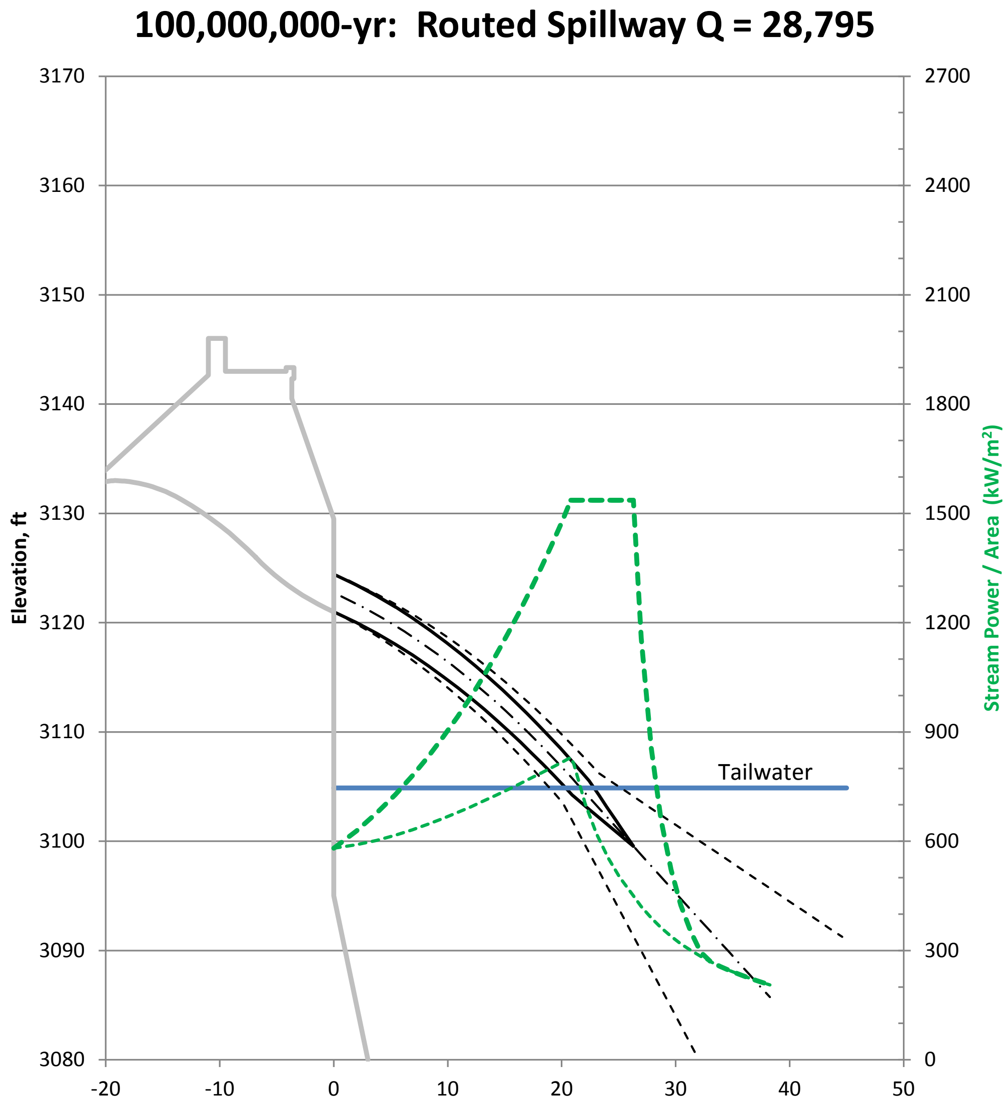

Figure A - 7. — Jet trajectory and stream power intensity for peak spillway flow during the 100,000,000-yr frequency flood, Thief Valley Dam, Oregon. Heavy, dashed green lines show the stream power intensity. The jet is expected to have an intact core when it reaches the tailwater surface.

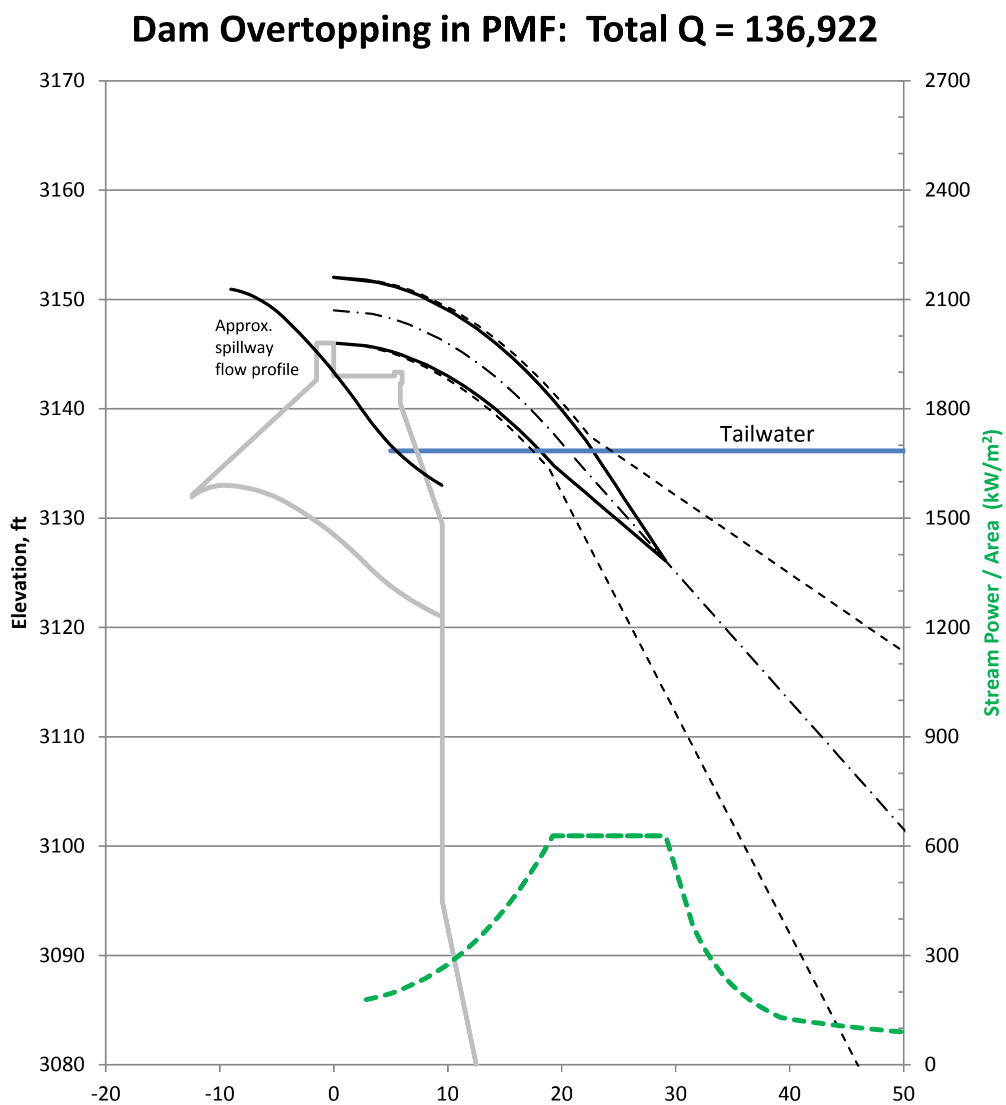

Figure A - 8. — Jet trajectory and stream power intensity for peak dam overtopping flow during the November PMF event, Thief Valley Dam, Oregon. Discharge overtopping the dam is 16,900 ft^3/s, and discharge through the spillway is 120,000 ft^3/s. Heavy, dashed green lines show the stream power intensity. The spillway crest is at elevation 3133.0 ft, so the tailwater is above the crest, but is probably not sufficient to reduce flow through the spillway. A sketch of the spillway flow profile is also shown for illustration, but stream power intensities are not calculated for the spillway flow, since the spillway lip is submerged. Note that at the dam and spillway crests there is significant drawdown of the water surface from the reservoir elevation of 3159.99 ft.

Appendix B – Jet Trajectory and Stream Power Calculation Spreadsheets

Thief Valley Dam - Spillway Plunge Pool Jet

RWSE	3135.56 ft		100
Tailwater	3090.85 ft		
	Q total	3,328	

SPILLWAY

Crest of spillway, elev.	3133 ft			start of bucket angle, φ	47.1°
$H_{spillway}$	2.56 ft			Bucket curve, β	22.03°
Spillway width, L	267.83 ft			flip angle, α	-25.1°
$C_{d,spillway}$	3.49	d_{lip}	0.47 ft	A	-0.464006492
$Q_{spillway}$	3,328 cfs	V_{lip}	30.17 ft/s	$\alpha_{(o)}$	-23.25636234
$q_{spillway}$	14 cfs/ft	$h_{v,lip}$	14.13 ft	α_1	-23.81
Lip of spillway	3121 ft	E_{lip}	14.56 ft	δ	11.43°
Incline angle at lip of spillway	-25.1°	H_{lip}	3135.56 ft	L_b	3.87 ft
A	23.19213			Fr_1	7.723
B_o	-0.46753				
L_p	11.22606		-0.46631		
T_s	0.04				

Use this as the take-off angle.
But this is flatter than flip! (opposite to reported observation)
But this is flatter than flip! (opposite to reported observation)
no theta correction

DAM OVERTOPPING

Top of dam elev.	3146 ft
H_{o-top}	-10.44 ft
Top of dam, length, L_{dam}	122.17 ft
$C_{d,dam}$	2.64
Q_{dam}	0 cfs
Incline angle at top of dam, θ	0°
d_{brink}	-4.98 ft
V_{brink}	#NUM! ft/s
$h_{v,brink}$	#NUM! ft
A	
Fr_1	#NUM!

This should be modified if the incline angle is not zero
This should be modified if the incline angle is not zero

Simple breakup length equation (Ervine et al. 1997), based on experimental data
13.1 ft

simple breakup length, Castillo (2006) - rectangular jet
11.1 ft

Castillo (2006)
φ 0.0321

Complex calculation of breakup length (round jet)		rectangular jet	
C^2	7.3988092	C	2.720075
right side	7.3988109	right side	2.720079
difference	5.513E-06		
L_b	10.5 ft	L_b	9.234974 ft

Extremely simple estimate of breakup length (Ervin
L_b = 50 to 100 times initial diameter (thick

L_b low	24 ft
L_b high	47 ft

Horeni estimate for rectangular jets (must use metr
L_b=6q^0.32
L_b= 6.6 m
L_b= 21.6 ft

Jet Discharging from Spillway Flip Bucket

NO SPREAD

Drop z (ft)	Distance from brink x (ft)	Lower nappe elev. (ft)	Upper nappe elev. (ft)	V_j (ft/s)	V_x (ft/s)	V_y (ft/s)	t_j/t_{gw}, gravitational thickness (ft)	θ		upper nappe, coordinate, perpendicular to lower nappe x	Elev.
0	0	3121	3121.52	30.17	27.33	12.77	0.47	25.1		0.20	3121.43
-1	1.962071	3120	3120.52	31.22	27.33	15.08	0.46	28.9		2.18	3120.40
-2	3.661061	3119	3119.52	32.23	27.33	17.09	0.44	32.0		3.90	3119.38
-3	5.180886	3118	3118.52	33.21	27.33	18.88	0.43	34.6		5.43	3118.35
-4	6.568531	3117	3117.52	34.17	27.33	20.51	0.42	36.9		6.82	3117.33
-5	7.853455	3116	3116.52	35.10	27.33	22.03	0.41	38.9		8.11	3116.32
-6	9.05557	3115	3115.52	36.01	27.33	23.44	0.40	40.6		9.31	3115.30
-7	10.18908	3114	3114.52	36.89	27.33	24.78	0.39	42.2		10.45	3114.29
-8	11.26454	3113	3113.52	37.75	27.33	26.05	0.38	43.6		11.53	3113.27
-9	12.29006	3112	3112.52	38.60	27.33	27.25	0.37	44.9		12.55	3112.26
-10	13.27199	3111	3111.52	39.42	27.33	28.41	0.36	46.1		13.53	3111.25
-11	14.21548	3110	3110.52	40.23	27.33	29.52	0.36	47.2		14.48	3110.24
-12	15.1247	3109	3109.52	41.02	27.33	30.59	0.35	48.2		15.38	3109.23
-13	16.00315	3108	3108.52	41.80	27.33	31.63	0.34	49.2		16.26	3108.22
-14	16.85374	3107	3107.52	42.56	27.33	32.63	0.34	50.1		17.11	3107.22
-15	17.67898	3106	3106.52	43.31	27.33	33.60	0.33	50.9		17.93	3106.21
-16	18.48101	3105	3105.52	44.05	27.33	34.55	0.32	51.7	0.4	18.74	3105.20
-17	19.26167	3104	3104.52	44.78	27.33	35.47	0.32	52.4	0.4	19.51	3104.19
-18	20.02259	3103	3103.52	45.49	27.33	36.36	0.31	53.1	0.4	20.27	3103.19
-19	20.7652	3102	3102.52	46.19	27.33	37.24	0.31	53.7	0.4	21.01	3102.18
-20	21.49075	3101	3101.52	46.88	27.33	38.09	0.30	54.3	0.4	21.74	3101.18
-21	22.20038	3100	3100.52	47.56	27.33	38.93	0.30	54.9	0.4	22.45	3100.17
-22	22.89508	3099	3099.52	48.24	27.33	39.75	0.30	55.5	0.4	23.14	3099.17
-23	23.57576	3098	3098.52	48.90	27.33	40.55	0.29	56.0	0.4	23.82	3098.16
-24	24.24324	3097	3097.52	49.55	27.33	41.34	0.29	56.5	0.3	24.48	3097.16
-25	24.89826	3096	3096.52	50.20	27.33	42.11	0.28	57.0	0.3	25.14	3096.15
-26	25.54148	3095	3095.52	50.84	27.33	42.87	0.28	57.5	0.3	25.78	3095.15
-27	26.17353	3094	3094.52	51.47	27.33	43.61	0.28	57.9	0.3	26.41	3094.15
-28	26.79496	3093	3093.52	52.09	27.33	44.34	0.27	58.4	0.3	27.03	3093.14
-29	27.4063	3092	3092.52	52.70	27.33	45.06	0.27	58.8	0.3	27.64	3092.14
-30	28.00802	3091	3091.52	53.31	27.33	45.77	0.27	59.2	0.3	28.24	3091.14
-30.22	28.14	3090.78	3091.30	53.44	27.33	45.93	0.27	59.2		28.37	3090.92
-30.22	28.14	3090.78	3091.30	53.44			0.27	59.2		28.36897709	3090.92
-30.22	28.25	#N/A						59.2		#N/A	3090.85
-32	29.31	#N/A						59.2		#N/A	3089.07
-33	29.91	#N/A						59.2		#N/A	3088.07
-34	30.50	#N/A						59.2		#N/A	3087.07
-35	31.10	#N/A						59.2		#N/A	3086.07
-36	31.69	#N/A						59.2		#N/A	3085.07
-36.07	31.74	#N/A						59.2		#N/A	3085.00

Jet spread in the air, Ervine et al. (1997)

z (ft)	x	CL nappe Elev.	B	Arc length of jet, L_j (ft)	ε (ft)	t_{outer} spread thickness (Ervine et al. 1997) (ft)	Outer jet spread thickness (Ervine & Falvey 1987) (ft)	Castillo (2006) (ft)	t_{core}, Inner jet thickness (0.5-1% angle of decay on each side) 0.50%	Jet core streampower at water surface impact, $q\gamma H/t_{core}$ (ft-lb/s)/ft²	kW/m²
0	0.10	3121.21	-0.47	0.00	0.00	0.47	0.47	0.47	0.47	26600	388
-1	2.07	3120.20	-0.55	2.20	0.10	0.65	0.54	0.52	0.44	29473	430
-2	3.78	3119.19	-0.63	4.17	0.18	0.80	0.60	0.57	0.40	32442	473
-3	5.30	3118.18	-0.69	5.99	0.25	0.93	0.66	0.61	0.37	35505	518
-4	6.69	3117.17	-0.75	7.70	0.31	1.04	0.71	0.66	0.34	38659	564
-5	7.98	3116.16	-0.81	9.33	0.37	1.15	0.76	0.70	0.31	41901	612
-6	9.18	3115.15	-0.86	10.90	0.43	1.25	0.81	0.75	0.29	45229	660
-7	10.32	3114.14	-0.91	12.41	0.48	1.34	0.85	0.79	0.26	48641	710
-8	11.40	3113.14	-0.95	13.88	0.53	1.43	0.90	0.83	0.24	52134	761
-9	12.42	3112.13	-1.00	15.31	0.57	1.51	0.94	0.88	0.22	55708	813
-10	13.40	3111.13	-1.04	16.71	0.62	1.59	0.98	0.92	0.20	59359	866
-11	14.35	3110.12	-1.08	18.09	0.66	1.67	1.02	0.96	0.17	63087	921
-12	15.25	3109.12	-1.12	19.44	0.70	1.74	1.06	1.00	0.15	66889	976
-13	16.13	3108.11	-1.16	20.77	0.74	1.82	1.11	1.04	0.13	70766	1033
-14	16.98	3107.11	-1.19	22.08	0.77	1.88	1.15	1.08	0.11	74714	1090
-15	17.81	3106.10	-1.23	23.38	0.81	1.95	1.18	1.12	0.10	78733	1149
-16	18.61	3105.10	-1.26	24.66	0.85	2.02	1.22	1.16	0.08	82822	1209
-17	19.39	3104.10	-1.30	25.93	0.88	2.08	1.26	1.20	0.06	86979	1269
-18	20.15	3103.09	-1.33	27.19	0.91	2.14	1.30	1.24	0.04	91203	1331
-19	20.89	3102.09	-1.36	28.43	0.95	2.21	1.34	1.27	0.03	95494	1394
-20	21.61	3101.09	-1.39	29.67	0.98	2.27	1.38	1.31	0.01	99850	1457
-21	22.32	3100.09	-1.42	30.90	1.01	2.32	1.41	1.35	-0.01	#N/A	#N/A
-22	23.02	3099.08	-1.45	32.11	1.04	2.38	1.45	1.38	-0.02	#N/A	#N/A
-23	23.70	3098.08	-1.48	33.32	1.07	2.44	1.49	1.42	-0.04	#N/A	#N/A
-24	24.36	3097.08	-1.51	34.53	1.10	2.49	1.52	1.45	-0.06	#N/A	#N/A
-25	25.02	3096.08	-1.54	35.72	1.13	2.55	1.56	1.49	-0.07	#N/A	#N/A
-26	25.66	3095.08	-1.57	36.91	1.16	2.60	1.60	1.52	-0.09	#N/A	#N/A
-27	26.29	3094.07	-1.60	38.09	1.19	2.66	1.63	1.56	-0.10	#N/A	#N/A
-28	26.91	3093.07	-1.62	39.27	1.22	2.71	1.67	1.59	-0.12	#N/A	#N/A
-29	27.52	3092.07	-1.65	40.44	1.24	2.76	1.70	1.63	-0.13	#N/A	#N/A
-30	28.12	3091.07	-1.68	41.61	1.27	2.81	1.74	1.66	-0.15	#N/A	#N/A
-30.22	28.25	3090.85	-1.68	41.87	1.28	2.82	1.75	1.67	-0.15	#N/A	#N/A
-30.22	28.25407	3090.843	-1.68	41.87	1.28	2.82	1.75	1.67	-0.15	#N/A	#N/A
-30.22	28.25	3090.85		41.87						#N/A	#N/A
-32	29.31	3089.07		43.94						#N/A	#N/A
-33	29.91	3088.07		45.10						#N/A	#N/A
-34	30.50	3087.07		46.26						#N/A	#N/A
-35	31.10	3086.07		47.43						#N/A	#N/A
-36	31.69	3085.07		48.59						#N/A	#N/A
-36.07	31.74	3085.00		48.67						#N/A	#N/A

Jet dissipation in the water / Spread jet boundaries / Jet core boundaries for plotting...

z (ft)	Jet core thickness, assume t_{core} at impact, tapering by 8° thereafter (ft)	Jet spread, assume t_{outer} at impact, spreading by 14° (ft)	Spread jet streampower per area in pool (ft-lb/s)/ft²	kW/m²	Lower edge x	Elev	Upper edge x	Elev	Peak streampower in spread jet	Average stream power intensity if broken up (kW/m²)	Lower core x	Elev	Upper core x	Elev
0					0.00	3121	0.20	3121.43		388	0.00	3121.00	0.20	3121.43
-1					1.92	3119.915	2.23	3120.49		302	1.97	3120.01	2.18	3120.39
-2					3.57	3118.849	3.99	3119.53		263	3.67	3119.02	3.89	3119.36
-3					5.04	3117.795	5.57	3118.56		240	5.20	3118.02	5.41	3118.33
-4					6.38	3116.749	7.01	3117.59		226	6.59	3117.03	6.80	3117.30
-5					7.62	3115.71	8.34	3116.61		216	7.88	3116.04	8.08	3116.28
-6					8.78	3114.676	9.59	3115.62		210	9.09	3115.04	9.28	3115.26
-7					9.87	3113.646	10.77	3114.64		205	10.23	3114.05	10.41	3114.24
-8					10.90	3112.619	11.89	3113.65		201	11.31	3113.05	11.48	3113.22
-9					11.89	3111.595	12.96	3112.67		199	12.34	3112.05	12.50	3112.21
-10					12.83	3110.573	13.98	3111.68		197	13.33	3111.06	13.47	3111.19
-11					13.73	3109.554	14.96	3110.69		196	14.28	3110.06	14.41	3110.18
-12					14.60	3108.535	15.90	3109.70		195	15.20	3109.06	15.31	3109.17
-13					15.45	3107.518	16.82	3108.71		195	16.08	3108.07	16.18	3108.16
-14					16.26	3106.503	17.70	3107.71		194	16.94	3107.07	17.03	3107.14
-15					17.05	3105.488	18.56	3106.72		194	17.77	3106.07	17.84	3106.13
-16					17.82	3104.475	19.40	3105.73		194	18.58	3105.08	18.64	3105.12
-17					18.56	3103.462	20.21	3104.73		195	19.36	3104.08	19.41	3104.12
-18					19.29	3102.45	21.01	3103.74		195	20.13	3103.08	20.17	3103.11
-19					20.00	3101.439	21.78	3102.74		196	20.88	3102.08	20.90	3102.10
-20					20.69	3100.429	22.53	3101.75		196	21.61	3101.09	21.62	3101.09
-21					21.37	3099.419	23.27	3100.75		197	#N/A	#N/A	#N/A	#N/A
-22					22.04	3098.409	24.00	3099.76		197	#N/A	#N/A	#N/A	#N/A
-23					22.69	3097.4	24.71	3098.76		198	#N/A	#N/A	#N/A	#N/A
-24					23.32	3096.392	25.40	3097.77		199	#N/A	#N/A	#N/A	#N/A
-25					23.95	3095.384	26.09	3096.77		200	#N/A	#N/A	#N/A	#N/A
-26					24.56	3094.376	26.76	3095.78		201	#N/A	#N/A	#N/A	#N/A
-27					25.17	3093.369	27.42	3094.78		202	#N/A	#N/A	#N/A	#N/A
-28					25.76	3092.362	28.06	3093.78		203	#N/A	#N/A	#N/A	#N/A
-29					26.34	3091.355	28.70	3092.79		203	#N/A	#N/A	#N/A	#N/A
-30					26.92	3090.349	29.33	3091.79		204	#N/A	#N/A	#N/A	#N/A
-30.22	-0.15	2.82			27.04	3090.127	29.47	3091.57		205	#N/A	#N/A	#N/A	#N/A
-30.22	0.00	2.82	14022	205	27.04	3090.127	29.47	3091.57	#N/A	205	#N/A	#N/A	#N/A	#N/A
-30.22	0.0000	2.82	14022	205	27.04	3090.127	29.47	3091.57	#N/A	205	#N/A	#N/A	#N/A	#N/A
-32	0.00	3.85	10264	150	27.66	3088.083	30.97	3090.05	#N/A	150	#N/A	#N/A	#N/A	#N/A
-33	0.00	4.43	8921	130	28.00	3086.935	31.81	3089.20	#N/A	130	#N/A	#N/A	#N/A	#N/A
-34	0.00	5.01	7888	115	28.35	3085.786	32.66	3088.35	#N/A	115	#N/A	#N/A	#N/A	#N/A
-35	0.00	5.59	7070	103	28.69	3084.618	33.50	3087.50	#N/A	103	#N/A	#N/A	#N/A	#N/A
-36	0.00	6.17	6406	93	29.04	3083.49	34.35	3086.65	#N/A	93	#N/A	#N/A	#N/A	#N/A
-36.07	0.00	6.22	6364	93	29.06	3083.409	34.41	3086.59	#N/A	93	#N/A	#N/A	#N/A	#N/A

Thief Valley Dam - Spillway Plunge Pool Jet

RWSE	3136.17 ft	500
Tailwater	3092.13 ft	
Q total	5,306	

SPILLWAY

Crest of spillway, elev.	3133 ft			start of bucket angle, ψ	47.1 °	
$H_{spillway}$	3.17 ft			Bucket curve, β	22.03 °	
Spillway width, L	267.83 ft			flip angle, α	-25.1 °	Use this as the take-off angle
$C_{d,spillway}$	3.51	d_{lip}	0.65 ft	A	-0.462768514	
$Q_{spillway}$	5,306 cfs	V_{lip}	30.65 ft/s	α_U	-23.20605045	But this is flatter than flip! (opposite to reported observation)
$q_{spillway}$	20 cfs/ft	$h_{v,lip}$	14.58 ft	α_L	-23.76	But this is flatter than flip! (opposite to reported observation)
Lip of spillway	3121 ft	E_{lip}	15.17 ft	δ	11.43 °	
Incline angle at lip of spillway	-25.1 °	H_{lip}	3136.17 ft	L_b	6.07 ft	
A	23.93661			Fr_j	6.717	no theta correction
B_o	-0.46753					
L_p	11.58643					
T_s	0.04					

DAM OVERTOPPING

Top of dam elev.	3146 ft	
$H_{o,top}$	-9.83 ft	
Top of dam length, L_{dam}	122.17 ft	
$C_{d,dam}$	2.64	
Q_{dam}	0 cfs	
Incline angle at top of dam, θ	0 °	
d_{brink}	-4.69 ft	This should be modified if the incline angle is not zero
V_{brink}	#NUM! ft/s	This should be modified if the incline angle is not zero
$h_{v,brink}$	#NUM! ft	
A		
Fr_j	#NUM!	

Simple breakup length equation (Ervine et al. 1997), based on experimental data
16.9 ft

simple breakup length, Castillo (2006) - rectangular jet — Castillo (2006)
14.5 ft — φ 0.0321

Complex calculation of breakup length (round jet) — rectangular jet

C^2	4.2338719	C	2.057637
right side	4.2338719	right side	2.057627
difference	1.025E-05		
L_b	14.4 ft	L_b	12.30778 ft

Extremely simple estimate of breakup length (Ervin

L_b = 50 to 100 times initial diameter (thick

L_b low	32 ft
L_b high	65 ft

Horeni estimate for rectangular jets (must use metr

$L_b = 6q^{0.32}$

L_b = 7.3 m

L_b = 23.9 ft

Jet Discharging from Spillway Flip Bucket

NO SPREAD — Jet spread in the air, Ervine et al. (1997)

Drop z (ft)	Distance from brink x (ft)	Lower nappe elev. (ft)	Upper nappe elev. (ft)	V_j (ft/s)	V_x (ft/s)	V_y (ft/s)	t_{gw}, gravitational thickness (ft)	θ		upper nappe, coordinate, perpendicular to lower nappe x	Elev.	CL nappe x	Elev.	B	Arc length of jet, L_j (ft)	ε (ft)	t_{outer} spread thickness (Ervine et al. 1997) (ft)	Outer jet spread thickness (Ervine & Falvey 1997) (ft)	Castillo (2006) (ft)
0	0	3121	3121.71	30.65	27.76	12.98	0.65	25.1		0.27	3121.59	0.14	3121.29	-0.47	0.00	0.00	0.65	0.65	0.65
-1	1.966768	3120	3120.71	31.68	27.76	15.26	0.63	28.8		2.27	3120.55	2.12	3120.27	-0.55	2.21	0.10	0.82	0.71	0.69
-2	3.675541	3119	3119.71	32.68	27.76	17.24	0.61	31.8		4.00	3119.51	3.84	3119.26	-0.62	4.19	0.18	0.96	0.77	0.73
-3	5.207183	3118	3118.71	33.65	27.76	19.02	0.59	34.4		5.54	3118.49	5.37	3118.24	-0.69	6.02	0.25	1.09	0.83	0.77
-4	6.607487	3117	3117.71	34.60	27.76	20.64	0.57	36.6		6.95	3117.46	6.78	3117.23	-0.74	7.74	0.32	1.20	0.88	0.81
-5	7.905371	3116	3116.71	35.51	27.76	22.14	0.56	38.6		8.25	3116.44	8.08	3116.22	-0.80	9.38	0.37	1.31	0.93	0.86
-6	9.120481	3115	3115.71	36.41	27.76	23.55	0.54	40.3		9.47	3115.41	9.30	3115.21	-0.85	10.95	0.43	1.40	0.98	0.90
-7	10.26688	3114	3114.71	37.28	27.76	24.88	0.53	41.9		10.62	3114.40	10.44	3114.20	-0.90	12.47	0.48	1.49	1.03	0.94
-8	11.35507	3113	3113.71	38.14	27.76	26.15	0.52	43.3		11.71	3113.38	11.53	3113.19	-0.94	13.95	0.53	1.58	1.07	0.98
-9	12.39309	3112	3112.71	38.97	27.76	27.35	0.51	44.6		12.75	3112.36	12.57	3112.18	-0.99	15.39	0.58	1.66	1.11	1.02
-10	13.3873	3111	3111.71	39.79	27.76	28.50	0.50	45.8		13.74	3111.35	13.57	3111.17	-1.03	16.80	0.62	1.74	1.16	1.06
-11	14.34283	3110	3110.71	40.59	27.76	29.61	0.49	46.8		14.70	3110.33	14.52	3110.17	-1.07	18.18	0.66	1.82	1.20	1.10
-12	15.26387	3109	3109.71	41.38	27.76	30.68	0.48	47.9		15.62	3109.32	15.44	3109.16	-1.11	19.54	0.70	1.89	1.24	1.13
-13	16.1539	3108	3108.71	42.15	27.76	31.71	0.47	48.8		16.51	3108.31	16.33	3108.15	-1.14	20.88	0.74	1.96	1.28	1.17
-14	17.01586	3107	3107.71	42.90	27.76	32.71	0.46	49.7		17.37	3107.30	17.19	3107.15	-1.18	22.20	0.78	2.03	1.32	1.21
-15	17.85224	3106	3106.71	43.65	27.76	33.68	0.45	50.5		18.20	3106.29	18.03	3106.14	-1.21	23.51	0.82	2.09	1.36	1.25
-16	18.6652	3105	3105.71	44.38	27.76	34.62	0.45	51.3	0.6	19.01	3105.28	18.84	3105.14	-1.25	24.80	0.86	2.16	1.40	1.29
-17	19.4566	3104	3104.71	45.10	27.76	35.54	0.44	52.0	0.6	19.80	3104.27	19.63	3104.14	-1.28	26.07	0.89	2.22	1.44	1.32
-18	20.22808	3103	3103.71	45.81	27.76	36.44	0.43	52.7	0.5	20.57	3103.26	20.40	3103.13	-1.31	27.34	0.92	2.28	1.48	1.36
-19	20.98106	3102	3102.71	46.51	27.76	37.31	0.43	53.3	0.5	21.32	3102.25	21.15	3102.13	-1.34	28.59	0.96	2.34	1.52	1.40
-20	21.71681	3101	3101.71	47.19	27.76	38.16	0.42	54.0	0.5	22.06	3101.25	21.89	3101.12	-1.37	29.83	0.99	2.40	1.55	1.43
-21	22.43646	3100	3100.71	47.87	27.76	39.00	0.41	54.6	0.5	22.77	3100.24	22.61	3100.12	-1.40	31.06	1.02	2.46	1.59	1.47
-22	23.14104	3099	3099.71	48.54	27.76	39.81	0.41	55.1	0.5	23.48	3099.23	23.31	3099.12	-1.43	32.28	1.05	2.52	1.63	1.50
-23	23.83144	3098	3098.71	49.20	27.76	40.62	0.40	55.6	0.5	24.16	3098.23	24.00	3098.11	-1.46	33.50	1.09	2.57	1.66	1.54
-24	24.50349	3097	3097.71	49.85	27.76	41.40	0.40	56.2	0.5	24.84	3097.22	24.67	3097.11	-1.49	34.71	1.12	2.63	1.70	1.57
-25	25.17294	3096	3096.71	50.49	27.76	42.17	0.39	56.6	0.5	25.50	3096.22	25.34	3096.11	-1.52	35.91	1.14	2.68	1.74	1.60
-26	25.82546	3095	3095.71	51.12	27.76	42.93	0.39	57.1	0.5	26.15	3095.21	25.99	3095.11	-1.55	37.10	1.17	2.74	1.77	1.64
-27	26.46667	3094	3094.71	51.75	27.76	43.67	0.38	57.6	0.5	26.79	3094.21	26.63	3094.10	-1.57	38.29	1.20	2.79	1.81	1.67
-28	27.09715	3093	3093.71	52.37	27.76	44.40	0.38	58.0	0.4	27.42	3093.20	27.26	3093.10	-1.60	39.47	1.23	2.84	1.85	1.71
-28.97	27.70	3092.03	3092.74	52.96	27.76	45.10	0.37	58.4		28.02	3092.23	27.86	3092.13	-1.62	40.61	1.26	2.89	1.88	1.74
-28.97	27.70	3092.03	3092.74	52.96			0.37	58.4		28.01748858	3092.23	27.85822	3092.128	-1.62	40.61	1.26	2.89	1.88	1.74
-28.97	27.86	#N/A						58.4		#N/A	3092.13	27.86	3092.13		40.61				
-28.97	27.86	#N/A						58.4		#N/A	3092.13	27.86	3092.13		40.61				
-31	29.11	#N/A						58.4		#N/A	3090.10	29.11	3090.10		43.00				
-32	29.72	#N/A						58.4		#N/A	3089.10	29.72	3089.10		44.17				
-33	30.34	#N/A						58.4		#N/A	3088.10	30.34	3088.10		45.35				
-34	30.95	#N/A						58.4		#N/A	3087.10	30.95	3087.10		46.52				
-35	31.57	#N/A						58.4		#N/A	3086.10	31.57	3086.10		47.70				
-36	32.19	#N/A						58.4		#N/A	3085.10	32.19	3085.10		48.87				
-36.1	32.25	#N/A						58.4		#N/A	3085.00	32.25	3085.00		48.99				

Jet dissipation in the water — Spread jet boundaries — Jet core boundaries for plotting...

Drop z (ft)	t_{core}, Inner jet thickness (0.5-1% angle of decay on each side) 0.50%	Jet core streampower at water surface impact, $\gamma qH/t_{gw}$ (ft-lb/s)/ft²	kW/m²	Jet core thickness, assume t_{core} at impact, tapering by 8° thereafter (ft)	Jet spread, assume t_{outer} at impact, spreading by 14° (ft)	Spread jet streampower per area in pool (ft-lb/s)/ft²	kW/m²	Lower edge x	Elev	Upper edge x	Elev	Peak streampower in spread jet	Average stream power intensity if broken up (kW/m²)	Lower core x	Elev	Upper core x	Elev
0	0.65	27891	407					0.00	3121	0.27	3121.59		407	0.00	3121.00	0.27	3121.59
-1	0.60	30808	450					1.92	3119.915	2.31	3120.63		343	1.97	3120.01	2.26	3120.54
-2	0.56	33820	494					3.58	3118.848	4.09	3119.67		310	3.69	3119.02	3.98	3119.50
-3	0.53	36925	539					5.07	3117.793	5.68	3118.69		291	5.22	3118.02	5.52	3118.46
-4	0.50	40119	585					6.42	3116.747	7.14	3117.71		279	6.63	3117.03	6.93	3117.43
-5	0.46	43400	633					7.67	3115.707	8.49	3116.73		270	7.93	3116.04	8.22	3116.40
-6	0.43	46767	683					8.84	3114.672	9.75	3115.74		265	9.16	3115.04	9.44	3115.37
-7	0.41	50216	733					9.95	3113.641	10.94	3114.75		261	10.31	3114.05	10.58	3114.35
-8	0.38	53745	784					10.99	3112.614	12.07	3113.76		258	11.40	3113.05	11.66	3113.33
-9	0.35	57354	837					11.99	3111.589	13.15	3112.77		256	12.45	3112.05	12.70	3112.31
-10	0.33	61040	891					12.94	3110.567	14.19	3111.78		255	13.45	3111.06	13.68	3111.29
-11	0.31	64802	946					13.86	3109.546	15.18	3110.79		254	14.41	3110.06	14.63	3110.27
-12	0.28	68639	1002					14.74	3108.527	16.14	3109.79		254	15.34	3109.07	15.55	3109.26
-13	0.26	72548	1059					15.59	3107.51	17.07	3108.80		254	16.23	3108.07	16.43	3108.24
-14	0.24	76528	1117					16.42	3106.494	17.96	3107.81		254	17.10	3107.07	17.28	3107.23
-15	0.22	80579	1176					17.22	3105.479	18.83	3106.81		255	17.94	3106.07	18.11	3106.21
-16	0.20	84699	1236					18.00	3104.465	19.68	3105.81		256	18.76	3105.08	18.92	3105.20
-17	0.18	88887	1297					18.75	3103.452	20.50	3104.82		257	19.56	3104.08	19.70	3104.19
-18	0.16	93141	1359					19.49	3102.439	21.31	3103.82		258	20.34	3103.08	20.46	3103.18
-19	0.14	97462	1422					20.21	3101.428	22.09	3102.83		259	21.10	3102.09	21.21	3102.17
-20	0.12	101847	1486					20.92	3100.417	22.86	3101.83		260	21.84	3101.09	21.94	3101.16
-21	0.10	106296	1551					21.60	3099.407	23.61	3100.83		261	22.56	3100.09	22.65	3100.15
-22	0.09	110808	1617					22.28	3098.397	24.34	3099.84		262	23.27	3099.09	23.34	3099.14
-23	0.07	115382	1684					22.94	3097.388	25.06	3098.84		264	23.97	3098.09	24.03	3098.13
-24	0.05	120018	1752					23.58	3096.379	25.76	3097.84		265	24.65	3097.10	24.69	3097.12
-25	0.03	124714	1820					24.22	3095.37	26.46	3096.85		266	25.32	3096.10	25.35	3096.12
-26	0.02	129469	1889					24.84	3094.362	27.14	3095.85		268	25.98	3095.10	26.00	3095.11
-27	0.00	#N/A	#N/A					25.45	3093.355	27.80	3094.85		269	#N/A	#N/A	#N/A	#N/A
-28	-0.02	#N/A	#N/A					26.05	3092.348	28.46	3093.85		271	#N/A	#N/A	#N/A	#N/A
-28.97	-0.03	#N/A	#N/A	-0.03	2.89			26.63	3091.371	29.09	3092.89		272	#N/A	#N/A	#N/A	#N/A
-28.97	-0.03	#N/A	#N/A	0.00	2.89	18636	272	26.63	3091.371	29.09	3092.89	#N/A	272	#N/A	#N/A	#N/A	#N/A
-28.97		#N/A	#N/A	0.00	2.89	18636	272	26.63	3091.371	29.09	3092.89	#N/A	272	#N/A	#N/A	#N/A	#N/A
-28.97		#N/A	#N/A	0.0000	2.89	18636	272	26.63	3091.371	29.09	3092.89	#N/A	272	#N/A	#N/A	#N/A	#N/A
-31		#N/A	#N/A	0.00	4.08	13203	193	27.37	3089.029	30.84	3091.17	#N/A	193	#N/A	#N/A	#N/A	#N/A
-32		#N/A	#N/A	0.00	4.66	11545	168	27.74	3087.876	31.71	3090.32	#N/A	168	#N/A	#N/A	#N/A	#N/A
-33		#N/A	#N/A	0.00	5.25	10257	150	28.10	3086.722	32.57	3089.47	#N/A	150	#N/A	#N/A	#N/A	#N/A
-34		#N/A	#N/A	0.00	5.83	9223	135	28.47	3085.569	33.44	3088.63	#N/A	135	#N/A	#N/A	#N/A	#N/A
-35		#N/A	#N/A	0.00	6.42	8386	122	28.84	3084.415	34.30	3087.78	#N/A	122	#N/A	#N/A	#N/A	#N/A
-36		#N/A	#N/A	0.00	7.01	7685	112	29.20	3083.262	35.17	3086.93	#N/A	112	#N/A	#N/A	#N/A	#N/A
-36.1		#N/A	#N/A	0.00	7.06	7622	111	29.24	3083.146	35.26	3086.85	#N/A	111	#N/A	#N/A	#N/A	#N/A

Thief Valley Dam - Spillway Plunge Pool Jet

RWSE	3136.47 ft		1.000
Tailwater	3092.71 ft		
Q total	6,033		

SPILLWAY

Crest of spillway, elev.	3133 ft			start of bucket angle, φ	47.1 °		
$H_{spillway}$	3.47 ft			Bucket curve, β	22.03 °		
Spillway width, L	267.83 ft			flip angle, α	-25.1 °	Use this as the take-off angle.	
$C_{d,spillway}$	3.48	d_{lip}	0.73 ft	Λ	-0.462171182		
$Q_{spillway}$	6,033 cfs	V_{lip}	30.88 ft/s	α_{φ}	-23.18176109	But this is flatter than flip! (opposite to reported observation)	
$q_{spillway}$	23 cfs/ft	$h_{v,lip}$	14.81 ft	α_{j}	-23.74	But this is flatter than flip! (opposite to reported observation)	
Lip of spillway	3121 ft	E_{lip}	15.47 ft	δ	11.43 °		
Incline angle at lip of spillway	-25.1 °	H_{lip}	3136.47 ft	L_b	7.21 ft		
A	24.30563			Fr_j	6.372	no theta correction	
B_o	-0.46753						
L_p	11.76505						
T_x	0.04						

DAM OVERTOPPING

Top of dam elev.	3146 ft	
H_{o-top}	-9.53 ft	
Top of dam, length, L_{dam}	122.17 ft	
$C_{d,dam}$	2.64	
Q_{dam}	0 cfs	
Incline angle at top of dam, θ	0 °	
d_{brink}	-4.55 ft	This should be modified if the incline angle is not zero
V_{brink}	#NUM! ft/s	This should be modified if the incline angle is not zero
$h_{v,brink}$	#NUM! ft	
A		
Fr_j	#NUM!	

Simple breakup length equation (Ervine et al. 1997), based on experimental data

18.8 ft

simple breakup length, Castillo (2006) - rectangular jet

16.0 ft

Castillo (2006) φ 0.0321

Complex calculation of breakup length (round jet) / rectangular jet

round jet		rectangular jet	
C^2	3.4287686	C	1.851693
right side	3.4287703	right side	1.851703
difference	1.096E-05		
L_b	16.3 ft	L_b	13.75613 ft

Extremely simple estimate of breakup length (Ervin

L_b = 50 to 100 times initial diameter (thick

L_b low	36 ft
L_b high	73 ft

Horeni estimate for rectangular jets (must use metr

$L_b = 6q^{0.32}$

L_b =	7.6 m
L_b =	24.9 ft

Jet Discharging from Spillway Flip Bucket

NO SPREAD

Drop z (ft)	Distance from brink x (ft)	Lower nappe elev. (ft)	Upper nappe elev. (ft)	V_j (ft/s)	V_x (ft/s)	V_z (ft/s)	t_{gw} - gravitational thickness (ft)	θ		upper nappe, coordinate, perpendicular to lower nappe x	Elev.	CL nappe x	CL nappe Elev.
0	0	3121	3121.81	30.88	27.98	13.08	0.73	25.1		0.31	3121.66	0.15	3121.33
-1	1.969005	3120	3120.81	31.91	27.98	15.34	0.71	28.7		2.31	3120.62	2.14	3120.31
-2	3.682465	3119	3119.81	32.90	27.98	17.31	0.68	31.8		4.04	3119.58	3.86	3119.29
-3	5.219793	3118	3118.81	33.87	27.98	19.08	0.67	34.3		5.59	3118.55	5.41	3118.27
-4	6.626206	3117	3117.81	34.80	27.98	20.70	0.65	36.5		7.01	3117.52	6.82	3117.26
-5	7.930358	3116	3116.81	35.72	27.98	22.20	0.63	38.4		8.32	3116.49	8.13	3116.25
-6	9.151763	3115	3115.81	36.61	27.98	23.61	0.62	40.2		9.55	3115.47	9.35	3115.24
-7	10.30442	3114	3114.81	37.48	27.98	24.94	0.60	41.7		10.70	3114.45	10.50	3114.22
-8	11.39878	3113	3113.81	38.33	27.98	26.19	0.59	43.1		11.80	3113.43	11.60	3113.21
-9	12.44287	3112	3112.81	39.16	27.98	27.40	0.58	44.4		12.85	3112.41	12.64	3112.21
-10	13.44306	3111	3111.81	39.97	27.98	28.55	0.56	45.6		13.85	3111.39	13.64	3111.20
-11	14.40445	3110	3110.81	40.77	27.98	29.65	0.55	46.7		14.81	3110.38	14.61	3110.19
-12	15.33124	3109	3109.81	41.55	27.98	30.72	0.54	47.7		15.73	3109.37	15.53	3109.18
-13	16.22691	3108	3108.81	42.32	27.98	31.75	0.53	48.6		16.63	3108.35	16.43	3108.18
-14	17.0944	3107	3107.81	43.07	27.98	32.75	0.52	49.5		17.49	3107.34	17.29	3107.17
-15	17.93621	3106	3106.81	43.81	27.98	33.72	0.51	50.3		18.33	3106.33	18.13	3106.16
-16	18.75451	3105	3105.81	44.54	27.98	34.66	0.51	51.1	0.6	19.15	3105.32	18.95	3105.16
-17	19.55115	3104	3104.81	45.26	27.98	35.58	0.50	51.8	0.6	19.94	3104.31	19.75	3104.15
-18	20.32777	3103	3103.81	45.97	27.98	36.47	0.49	52.5	0.6	20.72	3103.30	20.52	3103.15
-19	21.0858	3102	3102.81	46.66	27.98	37.34	0.48	53.2	0.6	21.47	3102.29	21.28	3102.14
-20	21.82653	3101	3101.81	47.35	27.98	38.20	0.48	53.8	0.6	22.21	3101.28	22.02	3101.14
-21	22.55108	3100	3100.81	48.02	27.98	39.03	0.47	54.4	0.6	22.93	3100.27	22.74	3100.14
-22	23.26047	3099	3099.81	48.69	27.98	39.85	0.46	54.9	0.6	23.64	3099.27	23.45	3099.13
-23	23.95562	3098	3098.81	49.34	27.98	40.65	0.46	55.5	0.6	24.33	3098.26	24.14	3098.13
-24	24.63734	3097	3097.81	49.99	27.98	41.43	0.45	56.0	0.5	25.01	3097.25	24.82	3097.13
-25	25.30639	3096	3096.81	50.63	27.98	42.20	0.44	56.5	0.5	25.68	3096.25	25.49	3096.12
-26	25.96345	3095	3095.81	51.27	27.98	42.96	0.44	56.9	0.5	26.33	3095.24	26.15	3095.12
-27	26.60914	3094	3094.81	51.89	27.98	43.70	0.43	57.4	0.5	26.97	3094.23	26.79	3094.12
-28	27.24404	3093	3093.81	52.51	27.98	44.43	0.43	57.8	0.5	27.61	3093.23	27.43	3093.11
-28.4	27.50	3092.6	3093.41	52.75	27.98	44.72	0.43	58.0		27.86	3092.83	27.68	3092.71
-28.4	27.50	3092.6	3093.41	52.75			0.43	58.0		27.85709456	3092.83	27.67609	3092.713
-28.41	27.67	3092.697						58.0		27.69	3092.71	27.68	3092.70
-28.48	27.73	3092.633						58.0		27.73	3092.63	27.73	3092.63
-31	29.30	#N/A						58.0		#N/A	3090.11	29.30	3090.11
-32	29.93	#N/A						58.0		#N/A	3089.11	29.93	3089.11
-33	30.55	#N/A						58.0		#N/A	3088.11	30.55	3088.11
-34	31.18	#N/A						58.0		#N/A	3087.11	31.18	3087.11
-35	31.81	#N/A						58.0		#N/A	3086.11	31.81	3086.11
-36	32.43	#N/A						58.0		#N/A	3085.11	32.43	3085.11
-36.11	32.50	#N/A						58.0		#N/A	3085.00	32.50	3085.00

Jet spread in the air, Ervine et al. (1997)

Drop z (ft)	B	Arc length of jet, L_j (ft)	ε (ft)	t_{outer} spread thickness (Ervine et al. 1997) (ft)	Outer jet, spread thickness (Ervine & Falvey 1987) (ft)	Castillo (2006) (ft)	t_{core}, Inner jet thickness (0.5-1% angle of decay on each side) 0.50%	Jet core streampower at water surface impact, $q\gamma H/t_{gw}$ (ft-lb/s)/ft²	kW/m²
0	-0.47	0.00	0.00	0.73	0.73	0.73	0.73	28533	416
-1	-0.55	2.21	0.10	0.90	0.80	0.77	0.68	31477	459
-2	-0.62	4.19	0.18	1.04	0.86	0.81	0.64	34510	504
-3	-0.68	6.03	0.25	1.17	0.91	0.85	0.60	37635	549
-4	-0.74	7.75	0.32	1.28	0.97	0.89	0.57	40849	596
-5	-0.79	9.40	0.38	1.38	1.02	0.93	0.54	44150	644
-6	-0.84	10.98	0.43	1.48	1.06	0.97	0.51	47535	694
-7	-0.89	12.50	0.48	1.57	1.11	1.01	0.48	51002	744
-8	-0.94	13.98	0.53	1.65	1.15	1.05	0.45	54550	796
-9	-0.98	15.43	0.58	1.73	1.20	1.08	0.42	58176	849
-10	-1.02	16.85	0.62	1.81	1.24	1.12	0.40	61880	903
-11	-1.06	18.23	0.67	1.89	1.28	1.16	0.37	65658	958
-12	-1.10	19.60	0.71	1.96	1.33	1.20	0.35	69511	1014
-13	-1.14	20.94	0.75	2.03	1.37	1.24	0.32	73436	1072
-14	-1.17	22.26	0.79	2.10	1.41	1.27	0.30	77433	1130
-15	-1.21	23.57	0.82	2.16	1.45	1.31	0.28	81499	1189
-16	-1.24	24.86	0.86	2.23	1.49	1.35	0.26	85635	1250
-17	-1.27	26.14	0.90	2.29	1.52	1.38	0.24	89838	1311
-18	-1.30	27.41	0.93	2.35	1.56	1.42	0.22	94107	1373
-19	-1.34	28.66	0.96	2.41	1.60	1.45	0.20	98442	1437
-20	-1.37	29.91	1.00	2.47	1.64	1.49	0.18	102842	1501
-21	-1.40	31.14	1.03	2.53	1.68	1.52	0.16	107305	1566
-22	-1.42	32.37	1.06	2.58	1.71	1.56	0.14	111831	1632
-23	-1.45	33.59	1.09	2.64	1.75	1.59	0.12	116419	1699
-24	-1.48	34.80	1.12	2.69	1.79	1.63	0.10	121068	1767
-25	-1.51	36.00	1.15	2.75	1.82	1.66	0.08	125778	1836
-26	-1.54	37.20	1.18	2.80	1.86	1.69	0.07	130547	1905
-27	-1.56	38.39	1.21	2.85	1.90	1.73	0.05	135374	1976
-28	-1.59	39.57	1.24	2.90	1.93	1.76	0.03	140260	2047
-28.4	-1.60	40.04	1.25	2.92	1.95	1.77	0.03	142231	2076
-28.4	-1.60	40.03	1.25	2.92	1.95	1.77	0.03	142231	2076
-28.41		40.06						142231	2076
-28.48		40.14						142231	2076
-31		43.11						#N/A	#N/A
-32		44.29						#N/A	#N/A
-33		45.47						#N/A	#N/A
-34		46.65						#N/A	#N/A
-35		47.83						#N/A	#N/A
-36		49.01						#N/A	#N/A
-36.11		49.14						#N/A	#N/A

Jet dissipation in the water / Spread jet boundaries / Jet core boundaries for plotting...

Drop z (ft)	Jet core thickness, assume t_{core} at impact, tapering by 8° thereafter (ft)	Jet spread, assume t_{outer} at impact, spreading by 14° (ft)	Spread jet streampower per area in pool (ft-lb/s)/ft²	kW/m²	Lower edge x	Lower edge Elev	Upper edge x	Upper edge Elev	Peak streampower in spread jet	Average stream power intensity if broken up kW/m²	Lower core x	Lower core Elev	Upper core x	Upper core Elev
0					0.00	3121	0.31	3121.66		416	0.00	3121.00	0.31	3121.66
-1					1.92	3119.915	2.36	3120.70		360	1.97	3120.01	2.30	3120.61
-2					3.59	3118.848	4.14	3119.73		331	3.69	3119.02	4.03	3119.56
-3					5.08	3117.792	5.74	3118.76		313	5.24	3118.02	5.58	3118.52
-4					6.44	3116.746	7.20	3117.77		301	6.65	3117.03	6.99	3117.49
-5					7.70	3115.705	8.56	3116.79		294	7.96	3116.04	8.29	3116.46
-6					8.87	3114.67	9.83	3115.80		289	9.19	3115.04	9.51	3115.43
-7					9.98	3113.639	11.03	3114.81		285	10.35	3114.05	10.66	3114.40
-8					11.03	3112.611	12.16	3113.82		283	11.45	3113.05	11.75	3113.38
-9					12.04	3111.586	13.25	3112.82		282	12.50	3112.06	12.79	3112.36
-10					13.00	3110.563	14.29	3111.83		281	13.50	3111.06	13.79	3111.34
-11					13.92	3109.542	15.29	3110.84		281	14.47	3110.06	14.74	3110.32
-12					14.81	3108.523	16.26	3109.84		281	15.40	3109.07	15.66	3109.30
-13					15.67	3107.506	17.19	3108.85		281	16.31	3108.07	16.55	3108.28
-14					16.50	3106.489	18.09	3107.85		282	17.18	3107.07	17.41	3107.27
-15					17.30	3105.474	18.97	3106.85		283	18.03	3106.08	18.24	3106.25
-16					18.09	3104.46	19.82	3105.86		284	18.85	3105.08	19.05	3105.24
-17					18.85	3103.447	20.65	3104.86		285	19.65	3104.08	19.84	3104.23
-18					19.59	3102.434	21.45	3103.86		286	20.44	3103.08	20.61	3103.21
-19					20.31	3101.422	22.24	3102.87		288	21.20	3102.09	21.36	3102.20
-20					21.02	3100.411	23.01	3101.87		289	21.95	3101.09	22.09	3101.19
-21					21.72	3099.401	23.77	3100.87		291	22.68	3100.09	22.81	3100.18
-22					22.39	3098.391	24.51	3099.87		292	23.39	3099.09	23.51	3099.17
-23					23.06	3097.381	25.23	3098.88		294	24.09	3098.10	24.19	3098.16
-24					23.71	3096.373	25.94	3097.88		296	24.78	3097.10	24.87	3097.15
-25					24.35	3095.364	26.64	3096.88		297	25.46	3096.10	25.53	3096.15
-26					24.97	3094.356	27.32	3095.88		299	26.12	3095.10	26.18	3095.14
-27					25.59	3093.348	27.99	3094.89		301	26.77	3094.10	26.81	3094.13
-28					26.20	3092.341	28.65	3093.89		302	27.41	3093.11	27.44	3093.12
-28.4	0.03	2.92			26.44	3091.938	28.92	3093.49		303	27.66	3092.71	27.69	3092.72
-28.4	0.03	2.92	20767	303	26.44	3091.938	28.92	3093.49	2076	303	27.66	3092.71	27.69	3092.72
-28.41	0.02	2.93	20726	302	26.44	3091.926	28.92	3093.48	2076	302	27.67	3092.70	27.69	3092.71
-28.48	0.0000	2.97	20438	298	26.47	3091.845	28.99	3093.42	2076	298	27.73	3092.63	27.73	3092.63
-31	0.00	4.45	13636	199	27.41	3088.932	31.19	3091.29	199	199	#N/A	#N/A	#N/A	#N/A
-32	0.00	5.04	12046	176	27.79	3087.776	32.07	3090.45	176	176	#N/A	#N/A	#N/A	#N/A
-33	0.00	5.63	10787	157	28.17	3086.62	32.94	3089.61	157	157	#N/A	#N/A	#N/A	#N/A
-34	0.00	6.22	9767	143	28.54	3085.464	33.82	3088.76	143	143	#N/A	#N/A	#N/A	#N/A
-35	0.00	6.81	8923	130	28.92	3084.308	34.69	3087.92	130	130	#N/A	#N/A	#N/A	#N/A
-36	0.00	7.39	8213	120	29.30	3083.152	35.57	3087.07	120	120	#N/A	#N/A	#N/A	#N/A
-36.11	0.00	7.46	8142	119	29.34	3083.025	35.66	3086.98	119	119	#N/A	#N/A	#N/A	#N/A

Thief Valley Dam - Spillway Plunge Pool Jet

RWSE	3137.51 ft	10,000
Tailwater	3094.85 ft	
Q total	9,040	

SPILLWAY

Crest of spillway, elev.	3133 ft			start of bucket angle, ψ	47.1 °
$H_{spillway}$	4.51 ft			Bucket curve, β	22.03 °
Spillway width, L	267.83 ft			Flip angle, α	-25.1 ° Use this as the take-off angle.
$C_{spillway}$	3.52	d_{lip}	1.07 ft	A	-0.459725892
$Q_{spillway}$	9,040 cfs	V_{lip}	31.64 ft/s	α_u	-23.08223607 But this is flatter than flip! (opposite to reported observation)
$q_{spillway}$	34 cfs/ft	$h_{v,lip}$	15.54 ft	α_l	-23.64 But this is flatter than flip! (opposite to reported observation)
Lip of spillway	3121 ft	E_{lip}	16.51 ft	δ	11.43 °
Incline angle at lip of spillway	-25.1 °	H_{lip}	3137.51 ft	L_b	12.46 ft
A	25.51087			Fr_j	5.398 no theta correction
B_p	-0.46753				
L_p	12.34844				
T_s	0.04				

DAM OVERTOPPING

Top of dam elev.	3146 ft	
$H_{o\text{-}top}$	-8.49 ft	
Top of dam, length, L_{dam}	122.17 ft	
C_{dam}	2.64	
Q_{dam}	0 cfs	
Incline angle at top of dam, θ	0 °	
d_{brink}	-4.05 ft	This should be modified if the incline angle is not zero
V_{brink}	#NUM! ft/s	This should be modified if the incline angle is not zero
$h_{v,brink}$	#NUM! ft	
A		
Fr_j	#NUM!	

Simple breakup length equation (Ervine et al. 1997), based on experimental data
25.9 ft

simple breakup length, Castillo (2006) - rectangular jet
22.0 ft

Castillo (2006)
φ 0.0321

Complex calculation of breakup length (round jet) | rectangular jet

round jet		rectangular jet	
C^2	1.7657238	C	1.328805
right side	1.7657239	right side	1.328808
difference	2.383E-06		
L_b	24.0 ft	L_b	19.48904 ft

Extremely simple estimate of breakup length (Ervin
L_b = 50 to 100 times initial diameter (thick

L_b low	53 ft
L_b high	107 ft

Horeni estimate for rectangular jets (must use metr
$L_b = 6q^{0.32}$

L_b =	8.6 m
L_b =	28.4 ft

Jet Discharging from Spillway Flip Bucket

NO SPREAD

Drop z (ft)	Distance from brink x (ft)	Lower nappe elev. (ft)	Upper nappe elev. (ft)	V_j (ft/s)	V_x (ft/s)	V_y (ft/s)	t_{grav}, gravitational thickness (ft)	θ		upper nappe, coordinate, perpendicular to lower nappe x	Elev.	CL nappe x	Elev.
0	0	3121	3122.18	31.64	28.66	13.40	1.07	25.1		0.45	3121.97	0.23	3121.48
-1	1.975922	3120	3121.18	32.64	28.66	15.62	1.03	28.6		2.47	3120.91	2.22	3120.45
-2	3.703993	3119	3120.18	33.61	28.66	17.56	1.00	31.5		4.23	3119.86	3.97	3119.43
-3	5.25915	3118	3119.18	34.56	28.66	19.30	0.98	34.0		5.80	3118.81	5.53	3118.41
-4	6.684796	3117	3118.18	35.48	28.66	20.91	0.95	36.1		7.25	3117.77	6.97	3117.38
-5	8.008737	3116	3117.18	36.37	28.66	22.39	0.93	38.0		8.58	3116.73	8.29	3116.37
-6	9.25006	3115	3116.18	37.25	28.66	23.79	0.91	39.7		9.83	3115.70	9.54	3115.35
-7	10.42254	3114	3115.18	38.10	28.66	25.10	0.89	41.2		11.01	3114.67	10.71	3114.33
-8	11.53649	3113	3114.18	38.94	28.66	26.36	0.87	42.6		12.12	3113.64	11.83	3113.32
-9	12.5999	3112	3113.18	39.76	28.66	27.55	0.85	43.9		13.19	3112.61	12.89	3112.31
-10	13.61907	3111	3112.18	40.56	28.66	28.70	0.83	45.0		14.21	3111.59	13.91	3111.29
-11	14.59912	3110	3111.18	41.34	28.66	29.80	0.82	46.1		15.19	3110.57	14.89	3110.28
-12	15.54422	3109	3110.18	42.12	28.66	30.86	0.80	47.1		16.13	3109.55	15.84	3109.27
-13	16.45786	3108	3109.18	42.87	28.66	31.89	0.79	48.0		17.04	3108.53	16.75	3108.26
-14	17.343	3107	3108.18	43.62	28.66	32.88	0.77	48.9		17.93	3107.51	17.63	3107.25
-15	18.20214	3106	3107.18	44.35	28.66	33.84	0.76	49.7		18.78	3106.49	18.49	3106.25
-16	19.03745	3105	3106.18	45.07	28.66	34.78	0.75	50.5	1.0	19.62	3105.48	19.33	3105.24
-17	19.85081	3104	3105.18	45.78	28.66	35.70	0.74	51.2	0.9	20.43	3104.46	20.14	3104.23
-18	20.64387	3103	3104.18	46.48	28.66	36.59	0.73	51.9	0.9	21.22	3103.45	20.93	3103.22
-19	21.41807	3102	3103.18	47.17	28.66	37.46	0.72	52.6	0.9	21.99	3102.43	21.70	3102.22
-20	22.17469	3101	3102.18	47.84	28.66	38.31	0.71	53.2	0.9	22.74	3101.42	22.46	3101.21
-21	22.91489	3100	3101.18	48.51	28.66	39.14	0.70	53.8	0.9	23.48	3100.41	23.20	3100.21
-22	23.63968	3099	3100.18	49.17	28.66	39.95	0.69	54.3	0.8	24.20	3099.40	23.92	3099.20
-23	24.34999	3098	3099.18	49.82	28.66	40.75	0.68	54.9	0.8	24.90	3098.39	24.63	3098.19
-24	25.04667	3097	3098.18	50.46	28.66	41.53	0.67	55.4	0.8	25.60	3097.38	25.32	3097.19
-25	25.73045	3096	3097.18	51.10	28.66	42.30	0.66	55.9	0.8	26.28	3096.37	26.00	3096.19
-26	26.40203	3095	3096.18	51.72	28.66	43.06	0.65	56.3	0.8	26.95	3095.36	26.67	3095.18
-26.33	26.62	3094.67	3095.85	51.93	28.66	43.30	0.65	56.5		27.16	3095.03	26.89	3094.85
-26.33	26.62	3094.67	3095.85	51.93			0.65	56.5		27.16307833	3095.03	26.89208	3094.849
-27	27.32	3094.167						56.5		27.35	3094.19	27.34	3094.18
-27.13	27.42	3094.049						56.5		27.42	3094.05	27.42	3094.05
-29	28.66	#N/A						56.5		#N/A	3092.18	28.66	3092.18
-30	29.32	#N/A						56.5		#N/A	3091.18	29.32	3091.18
-31	29.98	#N/A						56.5		#N/A	3090.18	29.98	3090.18
-32	30.65	#N/A						56.5		#N/A	3089.18	30.65	3089.18
-33	31.31	#N/A						56.5		#N/A	3088.18	31.31	3088.18
-34	31.97	#N/A						56.5		#N/A	3087.18	31.97	3087.18
-35	32.63	#N/A						56.5		#N/A	3086.18	32.63	3086.18
-36	33.29	#N/A						56.5		#N/A	3085.18	33.29	3085.18
-36.18	33.41	#N/A						56.5		#N/A	3085.00	33.41	3085.00

Jet spread in the air, Ervine et al. (1997)

z (ft)	B	Arc length of jet, L_j (ft)	ε (ft)	t_{outer} spread thickness (Ervine et al. 1997) (ft)	Outer jet, spread thickness (Ervine & Falvey 1987) (ft)	Castillo (2006) (ft)	t_{core}, Inner jet thickness (0.5-1% angle of decay on each side) 0.50%	Jet core streampower at water surface impact, $q\gamma H/t_{grav}$ (ft-lb/s)/ft²	kW/m²
0	-0.47	0.00	0.00	1.07	1.07	1.07	1.07	30687	448
-1	-0.54	2.22	0.10	1.23	1.13	1.10	1.01	33696	492
-2	-0.61	4.21	0.18	1.37	1.19	1.13	0.96	36796	537
-3	-0.67	6.06	0.25	1.48	1.25	1.16	0.92	39987	584
-4	-0.73	7.80	0.32	1.59	1.30	1.19	0.87	43265	631
-5	-0.78	9.46	0.38	1.69	1.35	1.23	0.83	46628	680
-6	-0.83	11.06	0.44	1.78	1.40	1.26	0.80	50073	731
-7	-0.88	12.60	0.49	1.87	1.45	1.29	0.76	53600	782
-8	-0.92	14.09	0.54	1.95	1.50	1.33	0.73	57205	835
-9	-0.96	15.55	0.59	2.02	1.54	1.36	0.69	60888	889
-10	-1.00	16.98	0.63	2.10	1.58	1.39	0.66	64647	943
-11	-1.04	18.38	0.68	2.17	1.63	1.43	0.63	68481	999
-12	-1.08	19.76	0.72	2.24	1.67	1.46	0.60	72387	1056
-13	-1.11	21.11	0.76	2.31	1.71	1.50	0.58	76364	1114
-14	-1.15	22.45	0.80	2.37	1.75	1.53	0.55	80412	1174
-15	-1.18	23.77	0.84	2.43	1.79	1.56	0.52	84529	1234
-16	-1.21	25.07	0.87	2.50	1.83	1.60	0.50	88714	1295
-17	-1.25	26.36	0.91	2.56	1.87	1.63	0.47	92966	1357
-18	-1.28	27.64	0.95	2.62	1.91	1.66	0.45	97284	1420
-19	-1.31	28.90	0.98	2.67	1.95	1.70	0.43	101667	1484
-20	-1.34	30.16	1.01	2.73	1.98	1.73	0.40	106113	1549
-21	-1.37	31.40	1.05	2.79	2.02	1.76	0.38	110623	1614
-22	-1.39	32.64	1.08	2.84	2.06	1.79	0.36	115194	1681
-23	-1.42	33.86	1.11	2.90	2.10	1.82	0.34	119827	1749
-24	-1.45	35.08	1.14	2.95	2.13	1.86	0.32	124521	1817
-25	-1.48	36.29	1.17	3.00	2.17	1.89	0.30	129274	1887
-26	-1.50	37.50	1.20	3.05	2.21	1.92	0.28	134086	1957
-26.33	-1.51	37.89	1.21	3.07	2.22	1.93	0.27	135687	1980
-26.33	-1.51	37.89	1.21	3.07	2.22	1.93	0.27	135687	1980
-27		38.70						135687	1980
-27.13		38.85						135687	1980
-29		41.10						#N/A	#N/A
-30		42.29						#N/A	#N/A
-31		43.49						#N/A	#N/A
-32		44.69						#N/A	#N/A
-33		45.89						#N/A	#N/A
-34		47.09						#N/A	#N/A
-35		48.29						#N/A	#N/A
-36		49.49						#N/A	#N/A
-36.18		49.71						#N/A	#N/A

Jet dissipation in the water / Spread jet boundaries / Jet core boundaries for plotting...

z (ft)	Jet core thickness, assume t_{core} at impact, tapering by 8° thereafter (ft)	Jet spread, assume t_{outer} at impact, spreading by 14° (ft)	Spread jet streampower per area in pool (ft-lb/s)/ft²	kW/m²	Lower edge x	Elev	Upper edge x	Elev	Peak streampower in spread jet	Average stream power intensity if broken up kW/m²	Lower core x	Elev	Upper core x	Elev
0					0.00	3121	0.45	3121.97		448	0.00	3121.00	0.45	3121.97
-1					1.93	3119.914	2.52	3120.99		414	1.98	3120.01	2.47	3120.90
-2					3.61	3118.846	4.32	3120.01		395	3.71	3119.02	4.22	3119.84
-3					5.12	3117.79	5.95	3119.02		384	5.28	3118.03	5.79	3118.78
-4					6.50	3116.742	7.43	3118.03		378	6.71	3117.03	7.22	3117.74
-5					7.77	3115.7	8.81	3117.03		374	8.04	3116.04	8.55	3116.69
-6					8.97	3114.664	10.11	3116.03		372	9.29	3115.04	9.79	3115.65
-7					10.10	3113.632	11.33	3115.03		371	10.46	3114.05	10.96	3114.62
-8					11.17	3112.603	12.49	3114.04		372	11.58	3113.05	12.08	3113.59
-9					12.19	3111.576	13.60	3113.04		373	12.65	3112.06	13.13	3112.56
-10					13.17	3110.553	14.66	3112.04		374	13.68	3111.06	14.15	3111.53
-11					14.11	3109.531	15.68	3111.04		376	14.67	3110.06	15.12	3110.50
-12					15.02	3108.511	16.66	3110.03		378	15.62	3109.07	16.06	3109.48
-13					15.89	3107.492	17.61	3109.03		380	16.54	3108.07	16.96	3108.46
-14					16.74	3106.475	18.53	3108.03		383	17.43	3107.07	17.84	3107.41
-15					17.56	3105.459	19.42	3107.03		386	18.29	3106.08	18.69	3106.42
-16					18.36	3104.444	20.29	3106.03		388	19.13	3105.08	19.52	3105.40
-17					19.14	3103.43	21.14	3105.03		391	19.95	3104.08	20.32	3104.38
-18					19.90	3102.417	21.96	3104.03		394	20.75	3103.09	21.11	3103.36
-19					20.64	3101.405	22.76	3103.03		397	21.53	3102.09	21.87	3102.35
-20					21.36	3100.393	23.55	3102.03		400	22.30	3101.09	22.62	3101.33
-21					22.07	3099.382	24.32	3101.03		403	23.04	3100.09	23.35	3100.32
-22					22.76	3098.372	25.07	3100.03		406	23.77	3099.10	24.06	3099.31
-23					23.44	3097.362	25.81	3099.03		409	24.49	3098.10	24.77	3098.29
-24					24.11	3096.352	26.54	3098.03		412	25.19	3097.10	25.48	3097.28
-25					24.76	3095.343	27.25	3097.03		415	25.88	3096.10	26.13	3096.27
-26					25.40	3094.334	27.95	3096.03		418	26.56	3095.10	26.79	3095.26
-26.33	0.27	3.07			25.61	3094.002	28.17	3095.70		419	26.78	3094.77	27.01	3094.92
-26.33	0.27	3.07	28712	419	25.61	3094.002	28.17	3095.70	1980	419	26.78	3094.77	27.01	3094.92
-27	0.05	3.47	25399	371	25.89	3093.221	28.78	3095.14	1980	371	27.32	3094.17	27.35	3094.19
-27.13	0.0014	3.55	24843	363	25.94	3093.07	28.90	3095.03	1980	363	27.42	3094.05	27.42	3094.05
-29	0.00	4.67	18892	276	26.71	3090.891	30.61	3093.47	276	276	#N/A	#N/A	#N/A	#N/A
-30	0.00	5.27	16747	244	27.13	3089.726	31.52	3092.63	244	244	#N/A	#N/A	#N/A	#N/A
-31	0.00	5.86	15039	219	27.54	3088.561	32.43	3091.80	219	219	#N/A	#N/A	#N/A	#N/A
-32	0.00	6.46	13647	199	27.95	3087.396	33.34	3090.96	199	199	#N/A	#N/A	#N/A	#N/A
-33	0.00	7.06	12491	182	28.36	3086.231	34.25	3090.13	182	182	#N/A	#N/A	#N/A	#N/A
-34	0.00	7.66	11516	168	28.78	3085.066	35.16	3089.29	168	168	#N/A	#N/A	#N/A	#N/A
-35	0.00	8.26	10682	156	29.19	3083.901	36.07	3088.46	156	156	#N/A	#N/A	#N/A	#N/A
-36	0.00	8.85	9960	145	29.60	3082.736	36.98	3087.62	145	145	#N/A	#N/A	#N/A	#N/A
-36.18	0.00	8.96	9841	144	29.68	3082.526	37.15	3087.47	144	144	#N/A	#N/A	#N/A	#N/A

Thief Valley Dam - Spillway Plunge Pool Jet

RWSE	3138.59 ft	100.000
Tailwater	3097.09 ft	
Q total	12,670	

SPILLWAY								DAM OVERTOPPING	
Crest of spillway, elev.	3133 ft			start of bucket angle, φ	47.1 °			Top of dam elev.	3146 ft
$H_{spillway}$	5.59 ft			Bucket curve, β	22.03 °			$H_{o,top}$	-7.41 ft
Spillway width, L	267.83 ft			Flip angle, α	-25.1 °	Use this as the take-off angle		Top of dam, length, L_{dam}	122.17 ft
$C_{d,spillway}$	3.58	d_{lip}	1.46 ft	A	-0.456831323			$C_{d,dam}$	2.64
$Q_{spillway}$	12,670 cfs	V_{lip}	32.37 ft/s	α_c	-22.96423442	But this is flatter than flip! (opposite to reported observation)		Q_{dam}	0 cfs
$q_{spillway}$	47 cfs/ft	$h_{v,lip}$	16.27 ft	α_j	-23.53	But this is flatter than flip! (opposite to reported observation)			
Lip of spillway	3121 ft	E_{lip}	17.59 ft	δ	11.43 °			Incline angle at top of dam, θ	0 °
Incline angle at lip of spillway	-25.1 °	H_{lip}	3138.59 ft	L_j	19.53 ft			d_{brink}	-3.53 ft
A	26.69644			Fr_j	4.718	no theta correction		V_{brink}	#NUM! ft/s
B_p	-0.46753							$h_{v,brink}$	#NUM! ft
L_p	12.92231							A	
T_s	0.04							Fr_j	#NUM!

This should be modified if the incline angle is not zero

This should be modified if the incline angle is not zero

Simple breakup length equation (Ervine et al. 1997), based on experimental data
33.7 ft

simple breakup length, Castillo (2006) - rectangular jet
28.8 ft

Castillo (2006)
φ 0.0321

Complex calculation of breakup length (round jet) | rectangular jet

round jet		rectangular jet	
C^2	1.0301268	C	1.014952
right side	1.0301268	right side	1.014952
difference	4.413E-07		
L_b	33.3 ft	L_b	25.97177 ft

Extremely simple estimate of breakup length (Ervin
L_b = 50 to 100 times initial diameter (thick

L_b low	73 ft
L_b high	146 ft

Horeni estimate for rectangular jets (must use metr
$L_b=6q^{0.32}$

L_b =	9.6 m
L_b =	31.6 ft

Jet Discharging from Spillway Flip Bucket

NO SPREAD

Drop z (ft)	Distance from brink x (ft)	Lower nappe elev. (ft)	Upper nappe elev. (ft)	V_j (ft/s)	V_x (ft/s)	V_y (ft/s)	t_{grav}, gravitational thickness (ft)	Θ		upper nappe, coordinate, perpendicular to lower nappe x	Elev.	CL nappe x	Elev.
0	0	3121	3122.61	32.37	29.32	13.70	1.46	25.1		0.62	3122.32	0.31	3121.66
-1	1.982197	3120	3121.61	33.35	29.32	15.88	1.42	28.4		2.66	3121.25	2.32	3120.62
-2	3.723681	3119	3120.61	34.30	29.32	17.79	1.38	31.3		4.44	3120.18	4.08	3119.59
-3	5.295346	3118	3119.61	35.22	29.32	19.52	1.34	33.7		6.04	3119.12	5.67	3118.56
-4	6.738904	3117	3118.61	36.13	29.32	21.10	1.31	35.7		7.50	3118.06	7.12	3117.53
-5	8.081355	3116	3117.61	37.01	29.32	22.58	1.28	37.6		8.86	3117.01	8.47	3116.51
-6	9.341369	3115	3116.61	37.87	29.32	23.96	1.25	39.3		10.13	3115.97	9.74	3115.48
-7	10.53249	3114	3115.61	38.71	29.32	25.27	1.22	40.8		11.33	3114.93	10.93	3114.46
-8	11.66492	3113	3114.61	39.53	29.32	26.51	1.20	42.1		12.47	3113.89	12.07	3113.44
-9	12.74657	3112	3113.61	40.34	29.32	27.70	1.17	43.4		13.55	3112.85	13.15	3112.43
-10	13.7837	3111	3112.61	41.13	29.32	28.84	1.15	44.5		14.59	3111.82	14.19	3111.41
-11	14.7814	3110	3111.61	41.90	29.32	29.94	1.13	45.6		15.59	3110.79	15.18	3110.39
-12	15.74386	3109	3110.61	42.67	29.32	30.99	1.11	46.6		16.55	3109.76	16.15	3109.38
-13	16.67456	3108	3109.61	43.41	29.32	32.02	1.09	47.5		17.48	3108.74	17.08	3108.37
-14	17.57645	3107	3108.61	44.15	29.32	33.01	1.07	48.4		18.38	3107.71	17.98	3107.36
-15	18.45205	3106	3107.61	44.87	29.32	33.97	1.05	49.2		19.25	3106.69	18.85	3106.34
-16	19.30354	3105	3106.61	45.58	29.32	34.90	1.04	50.0	1.4	20.10	3105.67	19.70	3105.33
-17	20.13281	3104	3105.61	46.29	29.32	35.81	1.02	50.7	1.3	20.92	3104.65	20.53	3104.32
-18	20.9415	3103	3104.61	46.98	29.32	36.70	1.01	51.4	1.3	21.73	3103.63	21.33	3103.31
-19	21.73109	3102	3103.61	47.66	29.32	37.57	0.99	52.0	1.3	22.51	3102.61	22.12	3102.31
-20	22.50285	3101	3102.61	48.33	29.32	38.42	0.98	52.6	1.2	23.28	3101.59	22.89	3101.30
-21	23.25796	3100	3101.61	48.99	29.32	39.25	0.97	53.2	1.2	24.03	3100.58	23.64	3100.29
-22	23.99743	3099	3100.61	49.64	29.32	40.06	0.95	53.8	1.2	24.77	3099.56	24.38	3099.28
-23	24.72221	3098	3099.61	50.29	29.32	40.85	0.94	54.3	1.2	25.49	3098.55	25.10	3098.27
-24	25.43314	3097	3098.61	50.92	29.32	41.63	0.93	54.8	1.1	26.19	3097.53	25.81	3097.27
-24.18	25.56	3096.82	3098.43	51.04	29.32	41.77	0.93	54.9		26.32	3097.35	25.94	3097.09
-24.18	25.56	3096.82	3098.43	51.04			0.93	54.9		26.31835127	3097.35	25.93902	3097.086
-25	26.40	3096.183						54.9		26.63	3096.35	26.51	3096.27
-25.84	27.10	3095.426						54.9		27.10	3095.43	27.10	3095.43
-27	27.92	#N/A						54.9		#N/A	3094.27	27.92	3094.27
-28	28.62	#N/A						54.9		#N/A	3093.27	28.62	3093.27
-29	29.32	#N/A						54.9		#N/A	3092.27	29.32	3092.27
-30	30.02	#N/A						54.9		#N/A	3091.27	30.02	3091.27
-31	30.73	#N/A						54.9		#N/A	3090.27	30.73	3090.27
-32	31.43	#N/A						54.9		#N/A	3089.27	31.43	3089.27
-33	32.13	#N/A						54.9		#N/A	3088.27	32.13	3088.27
-34	32.83	#N/A						54.9		#N/A	3087.27	32.83	3087.27
-35	33.53	#N/A						54.9		#N/A	3086.27	33.53	3086.27
-36	34.24	#N/A						54.9		#N/A	3085.27	34.24	3085.27
-36.27	34.43	#N/A						54.9		#N/A	3085.00	34.43	3085.00

Jet spread in the air, Ervine et al. (1997)

z (ft)	B	Arc length of jet, L_j (ft)	ε (ft)	t_{outer} spread thickness (Ervine et al. 1997) (ft)	Outer jet, spread thickness (Ervine & Falvey 1987) (ft)	Castillo (2006) (ft)	t_{core}, Inner jet thickness (0.5-1% angle of decay on each side) 0.50%	Jet core streampower at water surface impact, $q\gamma H/t_{core}$ (ft-lb/s)/ft²	kW/m²
0	-0.47	0.00	0.00	1.46	1.46	1.46	1.46	32851	479
-1	-0.54	2.22	0.10	1.61	1.53	1.48	1.40	35926	524
-2	-0.61	4.23	0.18	1.74	1.59	1.50	1.34	39092	571
-3	-0.67	6.09	0.26	1.85	1.65	1.53	1.28	42346	618
-4	-0.72	7.85	0.32	1.96	1.70	1.55	1.23	45685	667
-5	-0.77	9.52	0.38	2.05	1.75	1.58	1.18	49108	717
-6	-0.82	11.13	0.44	2.13	1.80	1.60	1.14	52613	768
-7	-0.86	12.69	0.50	2.21	1.85	1.63	1.10	56196	820
-8	-0.90	14.20	0.55	2.29	1.89	1.66	1.05	59858	874
-9	-0.94	15.67	0.60	2.36	1.94	1.69	1.02	63596	928
-10	-0.98	17.11	0.64	2.43	1.98	1.72	0.98	67409	984
-11	-1.02	18.52	0.69	2.50	2.02	1.74	0.94	71295	1040
-12	-1.06	19.91	0.73	2.57	2.07	1.77	0.91	75253	1098
-13	-1.09	21.28	0.77	2.63	2.11	1.80	0.88	79281	1157
-14	-1.13	22.63	0.81	2.69	2.15	1.83	0.85	83379	1217
-15	-1.16	23.96	0.85	2.75	2.19	1.86	0.81	87546	1278
-16	-1.19	25.27	0.89	2.81	2.23	1.89	0.79	91779	1339
-17	-1.22	26.57	0.92	2.87	2.27	1.92	0.76	96079	1402
-18	-1.25	27.85	0.96	2.93	2.31	1.95	0.73	100444	1466
-19	-1.28	29.13	0.99	2.98	2.35	1.98	0.70	104872	1530
-20	-1.31	30.39	1.03	3.04	2.39	2.01	0.67	109364	1596
-21	-1.34	31.65	1.06	3.09	2.42	2.04	0.65	113919	1663
-22	-1.37	32.89	1.10	3.14	2.46	2.07	0.62	118535	1730
-23	-1.39	34.12	1.13	3.20	2.50	2.10	0.60	123212	1798
-24	-1.42	35.35	1.16	3.25	2.54	2.13	0.58	127948	1867
-24.18	-1.42	35.57	1.16	3.26	2.54	2.13	0.57	128807	1880
-24.18	-1.42	35.57	1.16	3.26	2.54	2.13	0.57	128807	1880
-25		36.57						128807	1880
-25.84		37.60						128807	1880
-27		39.02						#N/A	#N/A
-28		40.24						#N/A	#N/A
-29		41.46						#N/A	#N/A
-30		42.68						#N/A	#N/A
-31		43.90						#N/A	#N/A
-32		45.13						#N/A	#N/A
-33		46.35						#N/A	#N/A
-34		47.57						#N/A	#N/A
-35		48.79						#N/A	#N/A
-36		50.01						#N/A	#N/A
-36.27		50.34						#N/A	#N/A

Jet dissipation in the water / Spread jet boundaries / Jet core boundaries for plotting...

z (ft)	Jet core thickness, assume t_{core} at impact, tapering by 8° thereafter (ft)	Jet spread, assume t_{outer} at impact, spreading by 14° (ft)	Spread jet streampower per area in pool (ft-lb/s)/ft²	kW/m²	Lower edge x	Elev	Upper edge x	Elev	Peak streampower in spread jet	Average stream power intensity if broken up kW/m²	Lower core x	Elev	Upper core x	Elev
0					0.00	3121	0.62	3122.32		479	0.00	3121.00	0.62	3122.32
-1					1.94	3119.914	2.70	3121.33		461	1.99	3120.01	2.65	3121.24
-2					3.63	3118.845	4.53	3120.33		452	3.73	3119.02	4.43	3120.16
-3					5.15	3117.787	6.18	3119.33		448	5.31	3118.03	6.02	3119.09
-4					6.55	3116.738	7.69	3118.32		447	6.76	3117.03	7.48	3118.03
-5					7.85	3115.695	9.10	3117.32		448	8.11	3116.04	8.83	3116.98
-6					9.06	3114.658	10.41	3116.31		450	9.38	3115.04	10.10	3115.92
-7					10.21	3113.625	11.65	3115.30		453	10.57	3114.05	11.29	3114.88
-8					11.30	3112.595	12.83	3114.29		456	11.71	3113.05	12.42	3113.83
-9					12.34	3111.567	13.96	3113.29		461	12.80	3112.06	13.50	3112.80
-10					13.33	3110.543	15.04	3112.28		465	13.84	3111.06	14.53	3111.76
-11					14.29	3109.52	16.08	3111.27		470	14.85	3110.06	15.52	3110.73
-12					15.21	3108.499	17.08	3110.26		474	15.82	3109.07	16.48	3109.69
-13					16.11	3107.48	18.05	3109.26		479	16.75	3108.07	17.40	3108.66
-14					16.97	3106.462	18.98	3108.25		484	17.66	3107.08	18.29	3107.64
-15					17.81	3105.445	19.89	3107.24		489	18.54	3106.08	19.16	3106.61
-16					18.62	3104.429	20.78	3106.24		494	19.40	3105.08	20.00	3105.59
-17					19.42	3103.415	21.64	3105.23		499	20.24	3104.08	20.82	3104.56
-18					20.19	3102.401	22.48	3104.23		504	21.05	3103.09	21.62	3103.54
-19					20.95	3101.388	23.30	3103.22		509	21.85	3102.09	22.40	3102.52
-20					21.68	3100.376	24.10	3102.22		514	22.62	3101.09	23.16	3101.50
-21					22.41	3099.364	24.88	3101.21		519	23.38	3100.09	23.90	3100.48
-22					23.11	3098.353	25.65	3100.21		524	24.13	3099.10	24.63	3099.47
-23					23.81	3097.343	26.40	3099.21		529	24.86	3098.10	25.35	3098.45
-24					24.49	3096.333	27.14	3098.20		534	25.58	3097.10	26.05	3097.43
-24.18	8.57	3.26			24.61	3096.151	27.27	3098.02		535	25.71	3096.92	26.17	3097.25
-24.18	8.57	3.26	36663	535	24.61	3096.151	27.27	3098.02	1880	535	25.71	3096.92	26.17	3097.25
-25	0.29	3.76	31786	464	24.98	3095.187	28.05	3097.35	1880	464	26.40	3096.18	26.63	3096.35
-25.84	0.0011	4.27	27975	408	25.36	3094.2	28.85	3096.65	1880	408	27.10	3095.43	27.10	3095.43
-27	0.00	4.97	24001	350	25.88	3092.837	29.95	3095.70	651	350	#N/A	#N/A	#N/A	#N/A
-28	0.00	5.58	21382	312	26.34	3091.662	30.91	3094.87	355	312	#N/A	#N/A	#N/A	#N/A
-29	0.00	6.19	19278	281	26.79	3090.487	31.86	3094.05	281	281	#N/A	#N/A	#N/A	#N/A
-30	0.00	6.80	17552	256	27.24	3089.312	32.81	3093.22	256	256	#N/A	#N/A	#N/A	#N/A
-31	0.00	7.41	16109	235	27.69	3088.137	33.76	3092.40	235	235	#N/A	#N/A	#N/A	#N/A
-32	0.00	8.02	14885	217	28.15	3086.962	34.71	3091.57	217	217	#N/A	#N/A	#N/A	#N/A
-33	0.00	8.63	13835	202	28.60	3085.787	35.66	3090.75	202	202	#N/A	#N/A	#N/A	#N/A
-34	0.00	9.24	12922	189	29.05	3084.612	36.61	3089.92	189	189	#N/A	#N/A	#N/A	#N/A
-35	0.00	9.85	12123	177	29.50	3083.437	37.56	3089.10	177	177	#N/A	#N/A	#N/A	#N/A
-36	0.00	10.46	11417	167	29.96	3082.262	38.52	3088.27	167	167	#N/A	#N/A	#N/A	#N/A
-36.27	0.00	10.62	11240	164	30.08	3081.945	38.77	3088.05	164	164	#N/A	#N/A	#N/A	#N/A

Thief Valley Dam - Spillway Plunge Pool Jet

RWSE	3139.75 ft		1,000,000
Tailwater	3099.54 ft		
Q total	17,187		

SPILLWAY

Crest of spillway, elev.	3133 ft			start of bucket angle, φ	47.1 °	
$H_{spillway}$	6.75 ft			Bucket curve, β	22.03 °	
Spillway width, L	267.83 ft			Flip angle, α	-25.1 °	Use this as the take-off angle.
$C_{spillway}$	3.66	d_{lip}	1.94 ft	λ	-0.451275288	
$Q_{spillway}$	17,187 cfs	V_{lip}	33.08 ft/s	α_U	-22.81898466	But this is flatter than flip! (opposite to reported observation)
$q_{spillway}$	64 cfs/ft	$h_{v,lip}$	16.99 ft	α_L	-23.39	But this is flatter than flip! (opposite to reported observation)
Lip of spillway	3121 ft	E_{lip}	18.75 ft	δ	11.43 °	
Incline angle at lip of spillway	-25.1 °	H_{lip}	3139.75 ft	L_j	29.21 ft	
A	27.88928			Fr_j	4.186	no theta correction
B_e	-0.46753					
L_p	13.4997					
T_s	0.04					

DAM OVERTOPPING

Top of dam elev.	3146 ft	
$H_{o\text{-}top}$	-6.25 ft	
Top of dam, length, L_{dam}	122.17 ft	
$C_{d,dam}$	2.64	
Q_{dam}	0 cfs	
Incline angle at top of dam, θ	0 °	
d_{brink}	-2.98 ft	This should be modified if the incline angle is not zero
V_{brink}	#NUM! ft/s	This should be modified if the incline angle is not zero
$h_{v,brink}$	#NUM! ft	
A		
Fr_j	#NUM!	

Simple breakup length equation (Ervine et al. 1997), based on experimental data
42.9 ft

simple breakup length, Castillo (2006) - rectangular jet
36.6 ft

Castillo (2006) φ 0.0321

Complex calculation of breakup length (round jet) | rectangular jet

round jet		rectangular jet	
C^2	0.6382576	C	0.79891
right side	0.6382586	right side	0.79891
difference	1.032E-06		
L_b	44.8 ft	L_b	33.59715 ft

Extremely simple estimate of breakup length (Ervin
L_b = 50 to 100 times initial diameter (thick

L_b low	97 ft
L_b high	194 ft

Horeni estimate for rectangular jets (must use metr
$L_b = 6q^{0.32}$

L_b =	10.6 m
L_b =	34.9 ft

Jet Discharging from Spillway Flip Bucket

NO SPREAD

Drop z (ft)	Distance from brink x (ft)	Lower nappe elev. (ft)	Upper nappe elev. (ft)	V_j (ft/s)	V_x (ft/s)	V_z (ft/s)	t_{gw}, gravitational thickness (ft)	θ		upper nappe, coordinate, perpendicular to lower nappe x	Elev.	CL nappe x	Elev.
0	0	3121	3123.14	33.08	29.97	14.01	1.94	25.1		0.82	3122.76	0.41	3121.88
-1	1.988041	3120	3122.14	34.04	29.97	16.14	1.89	28.3		2.88	3121.66	2.44	3120.83
-2	3.742153	3119	3121.14	34.97	29.97	18.03	1.83	31.0		4.69	3120.57	4.22	3119.79
-3	5.329488	3118	3120.14	35.88	29.97	19.73	1.79	33.4		6.31	3119.49	5.82	3118.75
-4	6.790142	3117	3119.14	36.77	29.97	21.30	1.75	35.4		7.80	3118.42	7.30	3117.71
-5	8.150334	3116	3118.14	37.63	29.97	22.76	1.71	37.2		9.18	3117.36	8.67	3116.68
-6	9.428319	3115	3117.14	38.48	29.97	24.14	1.67	38.8		10.47	3116.30	9.95	3115.65
-7	10.63741	3114	3116.14	39.31	29.97	25.44	1.63	40.3		11.69	3115.24	11.17	3114.62
-8	11.78769	3113	3115.14	40.12	29.97	26.67	1.60	41.7		12.85	3114.19	12.32	3113.60
-9	12.88697	3112	3114.14	40.91	29.97	27.85	1.57	42.9		13.95	3113.15	13.42	3112.57
-10	13.9415	3111	3113.14	41.69	29.97	28.99	1.54	44.0		15.01	3112.11	14.48	3111.55
-11	14.95633	3110	3112.14	42.46	29.97	30.08	1.51	45.1		16.03	3111.07	15.49	3110.53
-12	15.93563	3109	3111.14	43.21	29.97	31.13	1.49	46.1		17.01	3110.03	16.47	3109.51
-13	16.8829	3108	3110.14	43.95	29.97	32.15	1.46	47.0		17.95	3109.00	17.42	3108.50
-14	17.80108	3107	3109.14	44.68	29.97	33.13	1.44	47.9		18.87	3107.96	18.33	3107.48
-15	18.6927	3106	3108.14	45.39	29.97	34.09	1.41	48.7		19.75	3106.93	19.22	3106.47
-16	19.55994	3105	3107.14	46.09	29.97	35.02	1.39	49.4	1.8	20.62	3105.91	20.09	3105.45
-17	20.4047	3104	3106.14	46.79	29.97	35.93	1.37	50.2	1.8	21.46	3104.88	20.93	3104.44
-18	21.22864	3103	3105.14	47.47	29.97	36.82	1.35	50.9	1.7	22.28	3103.85	21.75	3103.43
-19	22.03323	3102	3104.14	48.14	29.97	37.68	1.33	51.5	1.7	23.08	3102.83	22.55	3102.41
-20	22.81977	3101	3103.14	48.81	29.97	38.53	1.31	52.1	1.7	23.86	3101.81	23.34	3101.40
-21	23.58942	3100	3102.14	49.46	29.97	39.35	1.30	52.7	1.6	24.62	3100.79	24.11	3100.39
-21.83	24.22	3099.17	3101.31	50.00	29.97	40.03	1.28	53.2		25.24	3099.94	24.73	3099.55
-21.83	24.22	3099.17	3101.31	50.00			1.28	53.2		25.24345646	3099.94	24.7298	3099.555
-22	24.50	3099.117						53.2			3099.65	24.86	3099.38
-23	25.39	3098.222						53.2		25.82	3098.55	25.61	3098.38
-24	26.28	3097.327						53.2		26.43	3097.44	26.35	3097.38
-24.54	26.76	3096.844						53.2		26.76	3096.85	26.76	3096.84
-26	27.85	#N/A						53.2		#N/A	3095.38	27.85	3095.38
-27	28.60	#N/A						53.2		#N/A	3094.38	28.60	3094.38
-28	29.35	#N/A						53.2		#N/A	3093.38	29.35	3093.38
-29	30.10	#N/A						53.2		#N/A	3092.38	30.10	3092.38
-30	30.85	#N/A						53.2		#N/A	3091.38	30.85	3091.38
-31	31.60	#N/A						53.2		#N/A	3090.38	31.60	3090.38
-32	32.34	#N/A						53.2		#N/A	3089.38	32.34	3089.38
-33	33.09	#N/A						53.2		#N/A	3088.38	33.09	3088.38
-34	33.84	#N/A						53.2		#N/A	3087.38	33.84	3087.38
-35	34.59	#N/A						53.2		#N/A	3086.38	34.59	3086.38
-36.38	35.62	#N/A						53.2		#N/A	3085.00	35.62	3085.00

Jet spread in the air, Ervine et al. (1997)

Drop z (ft)	B	Arc length of jet, L_j (ft)	α (ft)	t_{outer} spread thickness (Ervine et al. 1997) (ft)	Outer jet, spread thickness (Ervine & Falvey 1987) (ft)	Castillo (2006) (ft)	t_{core}, Inner jet thickness (0.5-1% angle of decay on each side) 0.50%	Jet core streampower at water surface impact, qH/t_{gw} (ft-lb/s)/ft²	kW/m²
0	-0.47	0.00	0.00	1.94	1.94	1.94	1.94	35077	512
-1	-0.54	2.23	0.10	2.08	2.01	1.95	1.86	38219	558
-2	-0.60	4.25	0.18	2.20	2.07	1.96	1.79	41449	605
-3	-0.66	6.12	0.26	2.30	2.13	1.97	1.73	44765	653
-4	-0.71	7.89	0.33	2.40	2.18	1.99	1.67	48165	703
-5	-0.76	9.58	0.39	2.48	2.23	2.01	1.61	51647	754
-6	-0.81	11.20	0.45	2.56	2.28	2.02	1.56	55210	806
-7	-0.85	12.77	0.50	2.64	2.33	2.04	1.50	58850	859
-8	-0.89	14.30	0.55	2.71	2.37	2.06	1.46	62567	913
-9	-0.93	15.78	0.60	2.77	2.42	2.09	1.41	66360	968
-10	-0.97	17.24	0.65	2.84	2.46	2.11	1.37	70226	1025
-11	-1.00	18.66	0.70	2.90	2.51	2.13	1.32	74164	1082
-12	-1.04	20.06	0.74	2.96	2.55	2.15	1.28	78174	1141
-13	-1.07	21.44	0.78	3.02	2.59	2.18	1.25	82253	1200
-14	-1.11	22.80	0.82	3.08	2.63	2.20	1.21	86401	1261
-15	-1.14	24.14	0.86	3.14	2.67	2.23	1.17	90616	1322
-16	-1.17	25.46	0.90	3.19	2.71	2.25	1.14	94898	1385
-17	-1.20	26.77	0.94	3.25	2.75	2.28	1.10	99245	1448
-18	-1.23	28.07	0.97	3.30	2.79	2.30	1.07	103656	1513
-19	-1.26	29.35	1.01	3.35	2.83	2.33	1.04	108131	1578
-20	-1.29	30.62	1.04	3.40	2.87	2.35	1.01	112669	1644
-21	-1.31	31.88	1.08	3.45	2.91	2.38	0.98	117268	1711
-21.83	-1.34	32.92	1.11	3.50	2.94	2.40	0.95	121131	1768
-21.83	-1.34	32.92	1.11	3.50	2.94	2.40	0.95	121131	1768
-22		33.14						121131	1768
-23		34.39						121131	1768
-24		35.64						121131	1768
-24.54		36.31						121131	1768
-26		38.13						#N/A	#N/A
-27		39.38						#N/A	#N/A
-28		40.63						#N/A	#N/A
-29		41.88						#N/A	#N/A
-30		43.13						#N/A	#N/A
-31		44.38						#N/A	#N/A
-32		45.63						#N/A	#N/A
-33		46.88						#N/A	#N/A
-34		48.13						#N/A	#N/A
-35		49.38						#N/A	#N/A
-36.38		51.10						#N/A	#N/A

Jet dissipation in the water / Spread jet boundaries / Jet core boundaries for plotting...

Drop z (ft)	Jet core thickness, assume t_{core} at impact, tapering by 8° thereafter (ft)	Jet spread, assume t_{outer} at impact, spreading by 14° (ft)	Spread jet streampower per area in pool (ft-lb/s)/ft²	kW/m²	Lower edge x	Elev	Upper edge x	Elev	Peak streampower in spread jet	Average stream power intensity if broken up kW/m²	Lower core x	Elev	Upper core x	Elev
0					0.00	3121	0.82	3122.76		512	0.00	3121.00	0.82	3122.76
-1					1.94	3119.913	2.93	3121.75		505	1.99	3120.01	2.88	3121.65
-2					3.65	3118.843	4.78	3120.73		504	3.75	3119.02	4.68	3120.55
-3					5.19	3117.785	6.45	3119.71		507	5.35	3118.03	6.30	3119.47
-4					6.60	3116.735	7.99	3118.69		512	6.81	3117.03	7.78	3118.39
-5					7.92	3115.691	9.42	3117.67		518	8.18	3116.04	9.15	3117.32
-6					9.15	3114.652	10.75	3116.65		525	9.46	3115.04	10.44	3116.26
-7					10.31	3113.618	12.02	3115.63		532	10.68	3114.05	11.65	3115.20
-8					11.42	3112.587	13.22	3114.61		540	11.84	3113.05	12.80	3114.14
-9					12.48	3111.559	14.36	3113.59		548	12.94	3112.06	13.90	3113.09
-10					13.49	3110.533	15.46	3112.57		556	14.00	3111.06	14.95	3112.04
-11					14.46	3109.509	16.52	3111.56		564	15.02	3110.07	15.96	3111.00
-12					15.40	3108.488	17.54	3110.54		572	16.01	3109.07	16.93	3109.96
-13					16.31	3107.468	18.52	3109.53		580	16.96	3108.07	17.87	3108.92
-14					17.19	3106.449	19.48	3108.51		588	17.89	3107.08	18.78	3107.89
-15					18.05	3105.431	20.40	3107.50		596	18.78	3106.08	19.66	3106.85
-16					18.88	3104.415	21.30	3106.49		604	19.66	3105.08	20.52	3105.82
-17					19.68	3103.4	22.18	3105.48		612	20.51	3104.09	21.36	3104.79
-18					20.47	3102.385	23.03	3104.47		620	21.34	3103.09	22.17	3103.76
-19					21.24	3101.372	23.87	3103.46		627	22.15	3102.09	22.96	3102.74
-20					22.00	3100.359	24.68	3102.45		635	22.94	3101.09	23.74	3101.71
-21					22.73	3099.347	25.48	3101.44		643	23.72	3100.10	24.49	3100.69
-21.83	0.95	3.50			23.33	3098.507	26.13	3100.60		649	24.35	3099.27	25.11	3099.84
-21.83	0.95	3.50	44465	649	23.33	3098.507	26.13	3100.60	1768	649	24.35	3099.27	25.11	3099.84
-22	0.89	3.60	43157	630	23.42	3098.305	26.30	3100.46	1768	630	24.50	3099.12	25.22	3099.65
-23	0.54	4.23	36794	537	23.91	3097.118	27.30	3099.65	1768	537	25.39	3098.22	25.82	3098.55
-24	0.19	4.85	32066	468	24.41	3095.932	28.29	3098.84	1768	468	26.28	3097.33	26.43	3097.44
-24.54	0.0025	5.18	29986	438	24.68	3095.291	28.83	3098.40	1768	438	26.76	3096.84	26.76	3096.85
-26	0.00	6.09	25510	372	25.41	3093.558	30.29	3097.21	747	372	#N/A	#N/A	#N/A	#N/A
-27	0.00	6.72	23144	338	25.91	3092.372	31.29	3096.40	486	338	#N/A	#N/A	#N/A	#N/A
-28	0.00	7.34	21180	309	26.41	3091.185	32.29	3095.58	341	309	#N/A	#N/A	#N/A	#N/A
-29	0.00	7.96	19523	285	26.91	3089.998	33.29	3094.77	285	285	#N/A	#N/A	#N/A	#N/A
-30	0.00	8.59	18106	264	27.41	3088.812	34.28	3093.96	264	264	#N/A	#N/A	#N/A	#N/A
-31	0.00	9.21	16882	246	27.91	3087.625	35.28	3093.14	246	246	#N/A	#N/A	#N/A	#N/A
-32	0.00	9.83	15812	231	28.41	3086.438	36.28	3092.33	231	231	#N/A	#N/A	#N/A	#N/A
-33	0.00	10.45	14870	217	28.91	3085.252	37.28	3091.52	217	217	#N/A	#N/A	#N/A	#N/A
-34	0.00	11.08	14034	205	29.41	3084.065	38.28	3090.70	205	205	#N/A	#N/A	#N/A	#N/A
-35	0.00	11.70	13286	194	29.91	3082.878	39.27	3089.89	194	194	#N/A	#N/A	#N/A	#N/A
-36.38	0.00	12.56	12377	181	30.60	3081.241	40.65	3088.77	181	181	#N/A	#N/A	#N/A	#N/A

Thief Valley Dam - Spillway Plunge Pool Jet

RWSE	3142.31 ft		100,000,000
Tailwater	3104.88 ft		
Q total	28,795		

SPILLWAY

Crest of spillway, elev.	3133 ft			start of bucket angle, φ	47.1 °		
$H_{spillway}$	9.31 ft			Bucket curve, β	22.03 °		
Spillway width, L	267.83 ft			flip angle, α	-25.1 °	Use this as the take-off angle.	
$C_{d,spillway}$	3.78	d_{lip}	3.12 ft	Λ	-0.44428457		
$Q_{spillway}$	28,795 cfs	V_{lip}	34.50 ft/s	α_v	-22.45036694	But this is flatter than flip! (opposite to reported observation)	
$q_{spillway}$	108 cfs/ft	$h_{v,lip}$	18.49 ft	α_s	-23.05	But this is flatter than flip! (opposite to reported observation)	
Lip of spillway	3121 ft	E_{lip}	21.31 ft	δ	11.43 °		
Incline angle at lip of spillway	-25.1 °	H_{lip}	3142.31 ft	l_b	57.01 ft		
A	30.34243			Fr_s	3.445	no theta correction	
B_0	-0.46753						
L_p	14.68714						
T_u	0.04						

DAM OVERTOPPING

Top of dam elev.	3146 ft	
$H_{o,top}$	-3.69 ft	
Top of dam, length, L_{dam}	122.17 ft	
$C_{d,dam}$	2.64	
Q_{dam}	0 cfs	
Incline angle at top of dam, θ	0 °	
d_{brink}	-1.76 ft	This should be modified if the incline angle is not zero
V_{brink}	#NUM! ft/s	This should be modified if the incline angle is not zero
$h_{v,brink}$	#NUM! ft	
A		
Fr_s	#NUM!	

Simple breakup length equation (Ervine et al. 1997), based on experimental data
64.2 ft

simple breakup length, Castillo (2006) - rectangular jet
54.8 ft

Castillo (2006)
φ 0.0321

Complex calculation of breakup length (round jet)		rectangular jet	
C^2	0.2928202	C	0.541129
right side	0.2928208	right side	0.541129
difference	6.36E-07		
L_b	73.9 ft	L_b	51.69889 ft

Jet Discharging from Spillway Flip Bucket

NO SPREAD

Drop / Distance from brink

z (ft)	x (ft)	Lower nappe elev. (ft)	Upper nappe elev. (ft)	V_j (ft/s)	V_x (ft/s)	V_y (ft/s)	t_{grav}, gravitational thickness (ft)	θ		upper nappe, coordinate, perpendicular to lower nappe: x	Elev.	CL nappe: x	CL nappe: Elev.
0	0	3121	3124.44	34.50	31.26	14.61	3.12	25.1		1.32	3123.82	0.66	3122.41
-1	1.998786	3120	3123.44	35.43	31.26	16.67	3.03	28.1		3.43	3122.68	2.71	3121.34
-2	3.776479	3119	3122.44	36.32	31.26	18.50	2.96	30.6		5.28	3121.55	4.53	3120.27
-3	5.393403	3118	3121.44	37.20	31.26	20.17	2.89	32.8		6.96	3120.43	6.18	3119.21
-4	6.886604	3117	3120.44	38.06	31.26	21.70	2.83	34.8		8.50	3119.32	7.69	3118.16
-5	8.280767	3116	3119.44	38.89	31.26	23.14	2.76	36.5		9.93	3118.22	9.10	3117.11
-6	9.593321	3115	3118.44	39.71	31.26	24.49	2.71	38.1		11.26	3117.13	10.43	3116.07
-7	10.83711	3114	3117.44	40.51	31.26	25.77	2.65	39.5		12.53	3116.05	11.68	3115.02
-8	12.02194	3113	3116.44	41.30	31.26	26.99	2.60	40.8		13.72	3114.97	12.87	3113.99
-9	13.15546	3112	3115.44	42.07	31.26	28.16	2.56	42.0		14.87	3113.90	14.01	3112.95
-10	14.24382	3111	3114.44	42.83	31.26	29.28	2.51	43.1		15.96	3112.83	15.10	3111.92
-11	15.29201	3110	3113.44	43.58	31.26	30.36	2.47	44.2		17.01	3111.77	16.15	3110.88
-12	16.30419	3109	3112.44	44.31	31.26	31.40	2.43	45.1		18.02	3110.71	17.16	3109.86
-13	17.28383	3108	3111.44	45.03	31.26	32.41	2.39	46.0		19.00	3109.66	18.14	3108.83
-14	18.23388	3107	3110.44	45.74	31.26	33.39	2.35	46.9		19.95	3108.61	19.09	3107.80
-15	19.15687	3106	3109.44	46.44	31.26	34.34	2.32	47.7		20.87	3107.56	20.01	3106.78
-16	20.05498	3105	3108.44	47.13	31.26	35.27	2.28	48.4	3.0	21.76	3106.51	20.91	3105.76
-16.86	20.81	3104.14	3107.58	47.71	31.26	36.04	2.25	49.1		22.51	3105.62	21.66	3104.88
-16.86	20.81	3104.14	3107.58	47.71			2.25	49.1		22.5112838	3105.62	21.6601	3104.878
-17	21.05	3104.105						49.1		22.51	3105.37	21.78	3104.74
-18	22.06	3103.227						49.1		23.24	3104.25	22.65	3103.74
-19	23.07	3102.349						49.1		23.96	3103.13	23.52	3102.74
-20	24.08	3101.471						49.1		24.69	3102.01	24.38	3101.74
-21	25.08	3100.593						49.1		25.42	3100.88	25.25	3100.74
-22.19	26.28	3099.548						49.1		26.28	3099.55	26.28	3099.55
-23	26.98	#N/A						49.1		#N/A	3098.74	26.98	3098.74
-24	27.85	#N/A						49.1		#N/A	3097.74	27.85	3097.74
-25	28.72	#N/A						49.1		#N/A	3096.74	28.72	3096.74
-26	29.59	#N/A						49.1		#N/A	3095.74	29.59	3095.74
-27	30.45	#N/A						49.1		#N/A	3094.74	30.45	3094.74
-28	31.32	#N/A						49.1		#N/A	3093.74	31.32	3093.74
-29	32.19	#N/A						49.1		#N/A	3092.74	32.19	3092.74
-30	33.06	#N/A						49.1		#N/A	3091.74	33.06	3091.74
-31	33.92	#N/A						49.1		#N/A	3090.74	33.92	3090.74
-32	34.79	#N/A						49.1		#N/A	3089.74	34.79	3089.74
-33	35.66	#N/A						49.1		#N/A	3088.74	35.66	3088.74
-34	36.52	#N/A						49.1		#N/A	3087.74	36.52	3087.74
-35	37.39	#N/A						49.1		#N/A	3086.74	37.39	3086.74
-36	38.26	#N/A						49.1		#N/A	3085.74	38.26	3085.74

Jet spread in the air, Ervine et al. (1997)

z (ft)	Integration parameter (B)	Arc length of jet, L_j (ft)	ε (ft)	t_{outer} spread thickness (Ervine et al. 1997) (ft)	Outer jet, spread thickness (Ervine & Falvey 1987) (ft)	Castillo (2006) (ft)	t_{core}, Inner jet thickness (0.5-1% angle of decay on each side) 0.50%	Jet core streampower at water surface impact, $q\gamma H/t_{grav}$ (ft-lb/s)/ft²	kW/m²
0	-0.47	0.00	0.00	3.12	3.12	3.12	3.12	39805	581
-1	-0.53	2.24	0.10	3.23	3.18	3.10	3.01	43078	629
-2	-0.59	4.28	0.18	3.33	3.25	3.08	2.92	46436	678
-3	-0.65	6.18	0.26	3.41	3.30	3.08	2.83	49877	728
-4	-0.69	7.97	0.33	3.49	3.36	3.07	2.75	53400	779
-5	-0.74	9.69	0.40	3.56	3.41	3.07	2.67	57001	832
-6	-0.78	11.34	0.46	3.62	3.46	3.07	2.59	60680	886
-7	-0.82	12.94	0.51	3.68	3.51	3.07	2.52	64434	940
-8	-0.86	14.49	0.57	3.73	3.56	3.07	2.46	68263	996
-9	-0.90	16.00	0.62	3.79	3.60	3.08	2.40	72165	1053
-10	-0.94	17.48	0.67	3.84	3.65	3.08	2.34	76139	1111
-11	-0.97	18.93	0.71	3.89	3.69	3.09	2.28	80183	1170
-12	-1.00	20.35	0.76	3.94	3.73	3.10	2.22	84296	1230
-13	-1.04	21.75	0.80	3.99	3.78	3.11	2.17	88478	1291
-14	-1.07	23.13	0.84	4.04	3.82	3.12	2.12	92726	1353
-15	-1.10	24.49	0.88	4.08	3.86	3.14	2.07	97040	1416
-16	-1.13	25.83	0.92	4.13	3.90	3.15	2.02	101419	1480
-16.86	-1.15	26.98	0.96	4.17	3.94	3.16	1.98	105236	1536
-16.86	-1.15	26.98	0.96	4.17	3.94	3.16	1.98	105236	1536
-17		27.16						105236	1536
-18		28.49						105236	1536
-19		29.81						105236	1536
-20		31.13						105236	1536
-21		32.46						105236	1536
-22.19		34.03						105236	1536
-23		35.11						#N/A	#N/A
-24		36.43						#N/A	#N/A
-25		37.75						#N/A	#N/A
-26		39.08						#N/A	#N/A
-27		40.40						#N/A	#N/A
-28		41.72						#N/A	#N/A
-29		43.05						#N/A	#N/A
-30		44.37						#N/A	#N/A
-31		45.69						#N/A	#N/A
-32		47.02						#N/A	#N/A
-33		48.34						#N/A	#N/A
-34		49.67						#N/A	#N/A
-35		50.99						#N/A	#N/A
-36		52.31						#N/A	#N/A

Jet dissipation in the water / Spread jet boundaries

z (ft)	Jet core thickness, assume t_{core} at impact, tapering by 8° thereafter (ft)	Jet spread, assume t_{outer} at impact, spreading by 14° (ft)	Spread jet streampower per area in pool (ft-lb/s)/ft²	Spread jet streampower per area in pool kW/m²	Lower edge x	Lower edge Elev	Upper edge x	Upper edge Elev	Peak streampower in spread jet kW/m²	Average stream power intensity if broken up kW/m²
0					0.00	3121	1.32	3123.82		581
-1					1.95	3119.913	3.47	3122.77		590
-2					3.68	3118.841	5.38	3121.71		602
-3					5.25	3117.78	7.10	3120.65		616
-4					6.70	3116.728	8.69	3119.59		631
-5					8.05	3115.682	10.16	3118.54		647
-6					9.31	3114.641	11.54	3117.49		663
-7					10.51	3113.605	12.85	3116.44		678
-8					11.65	3112.572	14.09	3115.40		694
-9					12.74	3111.542	15.28	3114.36		710
-10					13.79	3110.514	16.41	3113.32		726
-11					14.80	3109.489	17.51	3112.28		742
-12					15.77	3108.465	18.56	3111.25		757
-13					16.71	3107.444	19.58	3110.21		773
-14					17.62	3106.423	20.57	3109.18		788
-15					18.50	3105.405	21.52	3108.15		803
-16					19.36	3104.387	22.45	3107.13		817
-16.86	1.98	4.17			20.09	3103.512	23.24	3106.24		830
-16.86	1.98	4.17	56875	830	20.09	3103.512	23.24	3106.24	1536	830
-17	1.93	4.26	55642	812	20.17	3103.342	23.39	3106.13	1536	812
-18	1.56	4.92	48180	703	20.79	3102.126	24.51	3105.35	1536	703
-19	1.19	5.58	42483	620	21.41	3100.91	25.62	3104.57	1536	620
-20	0.82	6.24	37990	554	22.03	3099.693	26.74	3103.78	1536	554
-21	0.44	6.90	34357	501	22.64	3098.477	27.86	3103.00	1536	501
-22.19	0.0005	7.69	30847	450	23.38	3097.03	29.19	3102.07	1536	450
-23	0.00	8.22	28841	421	23.88	3096.045	30.09	3101.43	1157	421
-24	0.00	8.88	26698	390	24.50	3094.828	31.21	3100.65	856	390
-25	0.00	9.54	24851	363	25.11	3093.612	32.32	3099.86	658	363
-26	0.00	10.20	23243	339	25.73	3092.396	33.44	3099.08	522	339
-27	0.00	10.86	21831	319	26.35	3091.18	34.56	3098.30	424	319
-28	0.00	11.52	20580	300	26.97	3089.964	35.67	3097.51	352	300
-29	0.00	12.18	19465	284	27.59	3088.747	36.79	3096.73	296	284
-30	0.00	12.84	18465	269	28.20	3087.531	37.91	3095.95	269	269
-31	0.00	13.50	17562	256	28.82	3086.315	39.02	3095.16	256	256
-32	0.00	14.16	16744	244	29.44	3085.099	40.14	3094.38	244	244
-33	0.00	14.82	15998	233	30.06	3083.882	41.26	3093.59	233	233
-34	0.00	15.48	15316	224	30.68	3082.666	42.37	3092.81	224	224
-35	0.00	16.14	14690	214	31.29	3081.45	43.49	3092.03	214	214
-36	0.00	16.80	14113	206	31.91	3080.234	44.61	3091.24	206	206

Thief Valley Dam - Dam Overtopping Jets

RWSE	3159.99 ft		PMF
Tailwater Elev.	3136.16 ft		
	Q total	136,922	

DAM OVERTOPPING

Top of dam elev.	3146 ft	
$H_{o,top}$	13.99 ft	
Top of dam, length, L_{dam}	122.17 ft	
$C_{d,dam}$	2.64	
Q_{dam}	16877 cfs	
q_{dam}	138.14 cfs/ft	8.399789 0.005849112
Incline angle at top of dam, θ	0 °	
d_{brink}	6.02 ft	This should be modified if the incline angle is not zero
V_{brink}	22.95 ft/s	This should be modified if the incline angle is not zero
$h_{v,brink}$	8.181301 ft	
A	16.3626	
Fr_i	1.648876	
T_u	0.02	

Crest of spillway, elev.	3133 ft
$H_{spillway}$	26.99 ft
Spillway width, L	267.83 ft
$C_{d,spillway}$	3.1965
$Q_{spillway}$	120,045 cfs

Simple breakup length equation (Ervine et al. 1997), based on experimental data
168.0 ft

simple breakup length, Castillo (2006) - rectangular jet — Castillo (2006)
143.3 ft — φ 0.060322637

Complex calculation of breakup length (ro rectangular jet

C^2	0.003843	C	0.061988
right side	0.003843	right side	0.061988
difference	1.66E-08		
L_b	400.5 ft	L_b	161.0 ft

Extremely simple estimate of breakup length (Ervine and Falvey 1987)
L_b = 50 to 100 times initial diameter (thickness)
L_b low 300.916766 ft
L_b high 601.833532 ft

Horeni estimate for rectangular jets (must use metric q)
$L_b = 6q^{0.32}$
L_b = 13.6 m
L_b = 44.5 ft

Jet Overtopping Parapet Wall of Dam

NO SPREAD

Drop z (ft)	Distance from brink x (ft)	Lower nappe elev. (ft)	Upper nappe elev. (ft)	V_j (ft/s)	V_x (ft/s)	V_y (ft/s)	t_{grav}, gravitational thickness (ft)	θ	Upper nappe coordinates, perpendicular to lower nappe: x	Elev.	Nappe centerline: x	Elev.	Integration parameter B	L_j (ft)	ε (ft)	t_{outer} spread thickness (Ervine et al. 1997) (ft)	Outer jet, spread thickness (Ervine & Falvey 1987) (ft)	Castillo (2006) (ft)
0	0	3146	3152.018	22.95377	22.95	0	6.01833532	0.0	0.00	3152.02	0.00	3149.01	0	0	0.00	6.02	6.02	6.02
-0.25	2.86	3145.75	3151.768	23.30	22.95	4.012481	5.93	9.9	3.88	3151.59	3.37	3148.67	-0.21	3.39	0.07	6.07	6.07	5.96
-0.5	4.05	3145.5	3151.518	23.64	22.95	5.674504	5.84	13.9	5.45	3151.17	4.75	3148.34	-0.29	4.81	0.10	6.04	6.09	5.90
-0.75	4.95	3145.25	3151.268	23.98	22.95	6.94982	5.76	16.8	6.62	3150.76	5.79	3148.01	-0.35	5.91	0.12	5.99	6.11	5.85
-1	5.72	3145	3151.018	24.32	22.95	8.024961	5.68	19.3	7.60	3150.36	6.66	3147.68	-0.41	6.84	0.13	5.95	6.12	5.80
-2	8.09	3144	3150.018	25.61	22.95	11.34901	5.39	26.3	10.48	3148.84	9.29	3146.42	-0.57	9.76	0.18	5.75	6.17	5.62
-3	9.91	3143	3149.018	26.83	22.95	13.89964	5.15	31.2	12.57	3147.40	11.24	3145.20	-0.69	12.07	0.21	5.58	6.20	5.48
-4	11.44	3142	3148.018	28.01	22.95	16.04992	4.93	35.0	14.27	3146.04	12.85	3144.02	-0.79	14.08	0.24	5.42	6.23	5.37
-5	12.79	3141	3147.018	29.14	22.95	17.94436	4.74	38.0	15.71	3144.74	14.25	3142.87	-0.87	15.89	0.27	5.28	6.26	5.27
-6	14.01	3140	3146.018	30.22	22.95	19.65706	4.57	40.6	16.99	3143.47	15.50	3141.74	-0.95	17.58	0.29	5.15	6.29	5.20
-7	15.14	3139	3145.018	31.27	22.95	21.23205	4.42	42.8	18.14	3142.24	16.64	3140.62	-1.02	19.17	0.31	5.04	6.31	5.13
-8	16.18	3138	3144.018	32.28	22.95	22.69802	4.28	44.7	19.19	3141.04	17.68	3139.52	-1.08	20.69	0.33	4.93	6.33	5.08
-9	17.16	3137	3143.018	33.26	22.95	24.07488	4.15	46.4	20.17	3139.87	18.66	3138.43	-1.14	22.15	0.35	4.84	6.36	5.04
-10	18.09	3136	3142.018	34.22	22.95	25.37716	4.04	47.9	21.08	3138.71	19.59	3137.35	-1.20	23.57	0.36	4.76	6.38	5.01
-11	18.97	3135	3141.018	35.15	22.95	26.61578	3.93	49.2	21.95	3137.57	20.46	3136.28	-1.25	24.95	0.38	4.69	6.40	4.98
-11.3	19.23	3134.7	3140.718	35.42	22.95	26.97629	3.90	49.6	22.20	3137.23	20.72	3135.96	-1.27	25.36	0.38	4.66	6.40	4.97
-11.3	19.23	3134.7	3140.718	35.42	22.95	26.97629	3.90	49.6	22.20040769	3137.227	20.71523	3135.964	-1.27	25.36	0.38	4.66	6.40	4.97
-12	20.02	3134.166						49.6			21.31	3135.26		26.28				
-13	21.01	3133.285						49.6	23.31	3135.24	22.16	3134.26		27.59				
-14	22.00	3132.405						49.6	24.02	3134.12	23.01	3133.26		28.91				
-15	22.99	3131.525						49.6	24.73	3133.00	23.86	3132.26		30.22				
-16	23.99	3130.644						49.6	25.44	3131.88	24.71	3131.26		31.53				
-17	24.98	3129.764						49.6	26.15	3130.76	25.57	3130.26		32.85				
-18	25.97	3128.883						49.6	26.86	3129.64	26.42	3129.26		34.16				
-19	26.96	3128.003						49.6	27.57	3128.52	27.27	3128.26		35.47				
-20	27.95	3127.123						49.6	28.28	3127.40	28.12	3127.26		36.79				
-21	28.94	3126.242						49.6	28.99	3126.29	28.97	3126.26		38.10				
-21.1	29.04	3126.154						49.6	29.07	3126.17	29.05	3126.16		38.23				
-21.18	29.12	3126.084						49.6	29.12	3126.08	29.12	3126.08		38.33				
-24	31.52	#N/A						49.6	#N/A	3123.26	31.52	3123.26		42.04				
-25	32.37	#N/A						49.6	#N/A	3122.26	32.37	3122.26		43.35				
-26	33.22	#N/A						49.6	#N/A	3121.26	33.22	3121.26		44.66				
-27	34.07	#N/A						49.6	#N/A	3120.26	34.07	3120.26		45.98				
-28	34.93	#N/A						49.6	#N/A	3119.26	34.93	3119.26		47.29				
-29	35.78	#N/A						49.6	#N/A	3118.26	35.78	3118.26		48.60				
-30	36.63	#N/A						49.6	#N/A	3117.26	36.63	3117.26		49.92				
-31	37.48	#N/A						49.6	#N/A	3116.26	37.48	3116.26		51.23				
-32	38.33	#N/A						49.6	#N/A	3115.26	38.33	3115.26		52.54				
-33	39.18	#N/A						49.6	#N/A	3114.26	39.18	3114.26		53.85				
-34	40.03	#N/A						49.6	#N/A	3113.26	40.03	3113.26		55.17				
-35	40.88	#N/A						49.6	#N/A	3112.26	40.88	3112.26		56.48				
-36	41.73	#N/A						49.6	#N/A	3111.26	41.73	3111.26		57.79				
-37	42.58	#N/A						49.6	#N/A	3110.26	42.58	3110.26		59.11				
-38	43.43	#N/A						49.6	#N/A	3109.26	43.43	3109.26		60.42				
-39	44.28	#N/A						49.6	#N/A	3108.26	44.28	3108.26		61.73				
-40	45.14	#N/A						49.6	#N/A	3107.26	45.14	3107.26		63.05				
-41	45.99	#N/A						49.6	#N/A	3106.26	45.99	3106.26		64.36				
-42	46.84	#N/A						49.6	#N/A	3105.26	46.84	3105.26		65.67				
-43	47.69	#N/A						49.6	#N/A	3104.26	47.69	3104.26		66.98				
-44	48.54	#N/A						49.6	#N/A	3103.26	48.54	3103.26		68.30				
-45	49.39	#N/A						49.6	#N/A	3102.26	49.39	3102.26		69.61				
-46	50.24	#N/A						49.6	#N/A	3101.26	50.24	3101.26		70.92				
-47	51.09	#N/A						49.6	#N/A	3100.26	51.09	3100.26		72.24				
-48	51.94	#N/A						49.6	#N/A	3099.26	51.94	3099.26		73.55				
-49	52.79	#N/A						49.6	#N/A	3098.26	52.79	3098.26		74.86				
-50	53.64	#N/A						49.6	#N/A	3097.26	53.64	3097.26		76.18				
-51	54.50	#N/A						49.6	#N/A	3096.26	54.50	3096.26		77.49				
-52	55.35	#N/A						49.6	#N/A	3095.26	55.35	3095.26		78.80				
-53	56.20	#N/A						49.6	#N/A	3094.26	56.20	3094.26		80.12				
-54	57.05	#N/A						49.6	#N/A	3093.26	57.05	3093.26		81.43				
-55	57.90	#N/A						49.6	#N/A	3092.26	57.90	3092.26		82.74				
-56	58.75	#N/A						49.6	#N/A	3091.26	58.75	3091.26		84.05				
-57	59.60	#N/A						49.6	#N/A	3090.26	59.60	3090.26		85.37				
-58	60.45	#N/A						49.6	#N/A	3089.26	60.45	3089.26		86.68				
-59	61.30	#N/A						49.6	#N/A	3088.26	61.30	3088.26		87.99				
-60	62.15	#N/A						49.6	#N/A	3087.26	62.15	3087.26		89.31				
-61	63.00	#N/A						49.6	#N/A	3086.26	63.00	3086.26		90.62				
-62	63.86	#N/A						49.6	#N/A	3085.26	63.86	3085.26		91.93				
-62.49	64.27	#N/A						49.6	#N/A	3084.77	64.27	3084.77		92.58				

Drop z (ft)	t_{core}, inner jet thickness (0.5-1% angle of decay on each side) 0.50%	Jet core streampower at water surface impact, $\gamma qH/t_{gav}$ (ft-lb/s)/ft²	kW/m²	Jet core thickness, assume t_{core} at impact, tapering by 8° thereafter (ft)	Jet spread, assume t_{outer} at impact, spreading by 14° (ft)	Spread jet streampower per area in pool (ft-lb/s)/ft²	kW/m²	Lower edge x	Elev	Upper edge x	Elev	Peak streampower in spread jet	Average stream power intensity if broken up (kW/m²)	Lower core x	Elev	Upper core x	Elev
0	6.01833532							0.00	3146	0.00	3152.02			0.00	3146.00	0.00	3152.02
-0.25	5.894493686	12259	179					2.85	3145.68	3.89	3151.66		175	2.86	3145.77	3.88	3151.57
-0.5	5.794333366	12809	187					4.02	3145.406	5.47	3151.27		181	4.05	3145.52	5.44	3151.15
-0.75	5.701028857	13366	195					4.92	3145.139	6.66	3150.87		187	4.96	3145.28	6.61	3150.71
-1	5.612764753	13931	203					5.68	3144.875	7.64	3150.49		194	5.73	3145.03	7.58	3150.33
-2	5.297307086	16268	237					8.01	3143.839	10.56	3149.00		223	8.11	3144.04	10.46	3148.79
-3	5.027313389	18723	273					9.80	3142.817	12.69	3147.59		252	9.94	3143.05	12.54	3147.35
-4	4.791449525	21290	311					11.30	3141.801	14.41	3146.24		283	11.48	3142.06	14.23	3145.98
-5	4.582522119	23964	350					12.63	3140.79	15.88	3144.95		314	12.84	3141.06	15.66	3144.67
-6	4.395434283	26742	390					13.82	3139.781	17.17	3143.69		346	14.07	3140.07	16.93	3143.41
-7	4.226393425	29620	432					14.93	3138.773	18.35	3142.47		379	15.20	3139.07	18.07	3142.17
-8	4.072490048	32595	476					15.95	3137.767	19.42	3141.28		413	16.25	3138.07	19.12	3140.97
-9	3.931441697	35662	520					16.91	3136.762	20.42	3140.10		446	17.24	3137.08	20.09	3139.79
-10	3.801425718	38821	567					17.82	3135.757	21.35	3138.95		480	18.18	3136.08	21.00	3138.63
-11	3.680964922	42067	614					18.69	3134.753	22.24	3137.81		515	19.07	3135.08	21.86	3137.49
-11.3	3.646502847	43058	628	3.65	4.66			18.94	3134.452	22.49	3137.48		525	19.33	3134.78	22.10	3137.15
-11.3	3.646502847	43058	628	3.65	4.66	36000	525	18.94	3134.452	22.49	3137.48	628	525	19.33	3134.78	22.10	3137.15
-12		43058	628	3.39	5.12	32779	478	19.36	3133.604	23.26	3136.92	628	478	20.02	3134.17	22.60	3136.36
-13		43058	628	3.02	5.78	29065	424	19.96	3132.392	24.36	3136.14	628	424	21.01	3133.29	23.31	3135.24
-14		43058	628	2.65	6.43	26106	381	20.56	3131.179	25.46	3135.35	628	381	22.00	3132.41	24.02	3134.12
-15		43058	628	2.28	7.09	23695	346	21.16	3129.967	26.56	3134.56	628	346	22.99	3131.52	24.73	3133.00
-16		43058	628	1.91	7.74	21692	317	21.77	3128.755	27.66	3133.77	628	317	23.99	3130.64	25.44	3131.88
-17		43058	628	1.54	8.40	19999	292	22.37	3127.543	28.76	3132.98	628	292	24.98	3129.76	26.15	3130.76
-18		43058	628	1.17	9.05	18553	271	22.97	3126.331	29.86	3132.20	628	271	25.97	3128.88	26.86	3129.64
-19		43058	628	0.80	9.71	17301	252	23.57	3125.119	30.96	3131.41	628	252	26.96	3128.00	27.57	3128.52
-20		43058	628	0.44	10.36	16208	237	24.17	3123.907	32.06	3130.62	628	237	27.95	3127.12	28.28	3127.40
-21		43058	628	0.07	11.02	15245	222	24.77	3122.694	33.16	3129.83	628	222	28.94	3126.24	28.99	3126.29
-21.1		43058	628	0.03	11.08	15155	221	24.83	3122.573	33.27	3129.75	628	221	29.04	3126.15	29.07	3126.17
-21.18		43058	628	0.0001	11.13	15083	220	24.88	3122.476	33.36	3129.69	628	220	29.12	3126.08	29.12	3126.08
-24		#N/A	#N/A	0.00	12.98	12938	189	26.58	3119.058	36.46	3127.47	380	189	#N/A	#N/A	#N/A	#N/A
-25		#N/A	#N/A	0.00	13.63	12316	180	27.18	3117.846	37.56	3126.68	327	180	#N/A	#N/A	#N/A	#N/A
-26		#N/A	#N/A	0.00	14.29	11752	172	27.78	3116.634	38.66	3125.89	284	172	#N/A	#N/A	#N/A	#N/A
-27		#N/A	#N/A	0.00	14.94	11237	164	28.38	3115.421	39.76	3125.11	249	164	#N/A	#N/A	#N/A	#N/A
-28		#N/A	#N/A	0.00	15.60	10766	157	28.98	3114.209	40.87	3124.32	220	157	#N/A	#N/A	#N/A	#N/A
-29		#N/A	#N/A	0.00	16.25	10332	151	29.59	3112.997	41.97	3123.53	196	151	#N/A	#N/A	#N/A	#N/A
-30		#N/A	#N/A	0.00	16.91	9932	145	30.19	3111.785	43.07	3122.74	175	145	#N/A	#N/A	#N/A	#N/A
-31		#N/A	#N/A	0.00	17.56	9562	140	30.79	3110.573	44.17	3121.95	158	140	#N/A	#N/A	#N/A	#N/A
-32		#N/A	#N/A	0.00	18.22	9218	135	31.39	3109.361	45.27	3121.17	143	135	#N/A	#N/A	#N/A	#N/A
-33		#N/A	#N/A	0.00	18.87	8898	130	31.99	3108.149	46.37	3120.38	130	130	#N/A	#N/A	#N/A	#N/A
-34		#N/A	#N/A	0.00	19.53	8600	126	32.59	3106.936	47.47	3119.59	126	126	#N/A	#N/A	#N/A	#N/A
-35		#N/A	#N/A	0.00	20.18	8321	121	33.20	3105.724	48.57	3118.80	121	121	#N/A	#N/A	#N/A	#N/A
-36		#N/A	#N/A	0.00	20.84	8059	118	33.80	3104.512	49.67	3118.02	118	118	#N/A	#N/A	#N/A	#N/A
-37		#N/A	#N/A	0.00	21.49	7814	114	34.40	3103.3	50.77	3117.23	114	114	#N/A	#N/A	#N/A	#N/A
-38		#N/A	#N/A	0.00	22.15	7583	111	35.00	3102.088	51.87	3116.44	111	111	#N/A	#N/A	#N/A	#N/A
-39		#N/A	#N/A	0.00	22.80	7365	107	35.60	3100.876	52.97	3115.65	107	107	#N/A	#N/A	#N/A	#N/A
-40		#N/A	#N/A	0.00	23.46	7159	104	36.20	3099.664	54.07	3114.86	104	104	#N/A	#N/A	#N/A	#N/A
-41		#N/A	#N/A	0.00	24.11	6965	102	36.81	3098.451	55.17	3114.08	102	102	#N/A	#N/A	#N/A	#N/A
-42		#N/A	#N/A	0.00	24.77	6781	99	37.41	3097.239	56.27	3113.29	99	99	#N/A	#N/A	#N/A	#N/A
-43		#N/A	#N/A	0.00	25.42	6606	96	38.01	3096.027	57.37	3112.50	96	96	#N/A	#N/A	#N/A	#N/A
-44		#N/A	#N/A	0.00	26.07	6440	94	38.61	3094.815	58.47	3111.71	94	94	#N/A	#N/A	#N/A	#N/A
-45		#N/A	#N/A	0.00	26.73	6283	92	39.21	3093.603	59.57	3110.92	92	92	#N/A	#N/A	#N/A	#N/A
-46		#N/A	#N/A	0.00	27.38	6132	89	39.81	3092.391	60.67	3110.14	89	89	#N/A	#N/A	#N/A	#N/A
-47		#N/A	#N/A	0.00	28.04	5989	87	40.41	3091.178	61.77	3109.35	87	87	#N/A	#N/A	#N/A	#N/A
-48		#N/A	#N/A	0.00	28.69	5853	85	41.02	3089.966	62.87	3108.56	85	85	#N/A	#N/A	#N/A	#N/A
-49		#N/A	#N/A	0.00	29.35	5722	84	41.62	3088.754	63.97	3107.77	84	84	#N/A	#N/A	#N/A	#N/A
-50		#N/A	#N/A	0.00	30.00	5597	82	42.22	3087.542	65.07	3106.99	82	82	#N/A	#N/A	#N/A	#N/A
-51		#N/A	#N/A	0.00	30.66	5478	80	42.82	3086.33	66.17	3106.20	80	80	#N/A	#N/A	#N/A	#N/A
-52		#N/A	#N/A	0.00	31.31	5363	78	43.42	3085.118	67.27	3105.41	78	78	#N/A	#N/A	#N/A	#N/A
-53		#N/A	#N/A	0.00	31.97	5253	77	44.02	3083.906	68.37	3104.62	77	77	#N/A	#N/A	#N/A	#N/A
-54		#N/A	#N/A	0.00	32.62	5148	75	44.63	3082.693	69.47	3103.83	75	75	#N/A	#N/A	#N/A	#N/A
-55		#N/A	#N/A	0.00	33.28	5046	74	45.23	3081.481	70.57	3103.05	74	74	#N/A	#N/A	#N/A	#N/A
-56		#N/A	#N/A	0.00	33.93	4949	72	45.83	3080.269	71.67	3102.26	72	72	#N/A	#N/A	#N/A	#N/A
-57		#N/A	#N/A	0.00	34.59	4855	71	46.43	3079.057	72.77	3101.47	71	71	#N/A	#N/A	#N/A	#N/A
-58		#N/A	#N/A	0.00	35.24	4765	70	47.03	3077.845	73.87	3100.68	70	70	#N/A	#N/A	#N/A	#N/A
-59		#N/A	#N/A	0.00	35.90	4678	68	47.63	3076.633	74.97	3099.89	68	68	#N/A	#N/A	#N/A	#N/A
-60		#N/A	#N/A	0.00	36.55	4594	67	48.23	3075.421	76.07	3099.11	67	67	#N/A	#N/A	#N/A	#N/A
-61		#N/A	#N/A	0.00	37.21	4514	66	48.84	3074.208	77.17	3098.32	66	66	#N/A	#N/A	#N/A	#N/A
-62		#N/A	#N/A	0.00	37.86	4436	65	49.44	3072.996	78.27	3097.53	65	65	#N/A	#N/A	#N/A	#N/A
-62.49		#N/A	#N/A	0.00	38.18	4398	64	49.73	3072.402	78.81	3097.15	64	64	#N/A	#N/A	#N/A	#N/A

Appendix C – Drawings

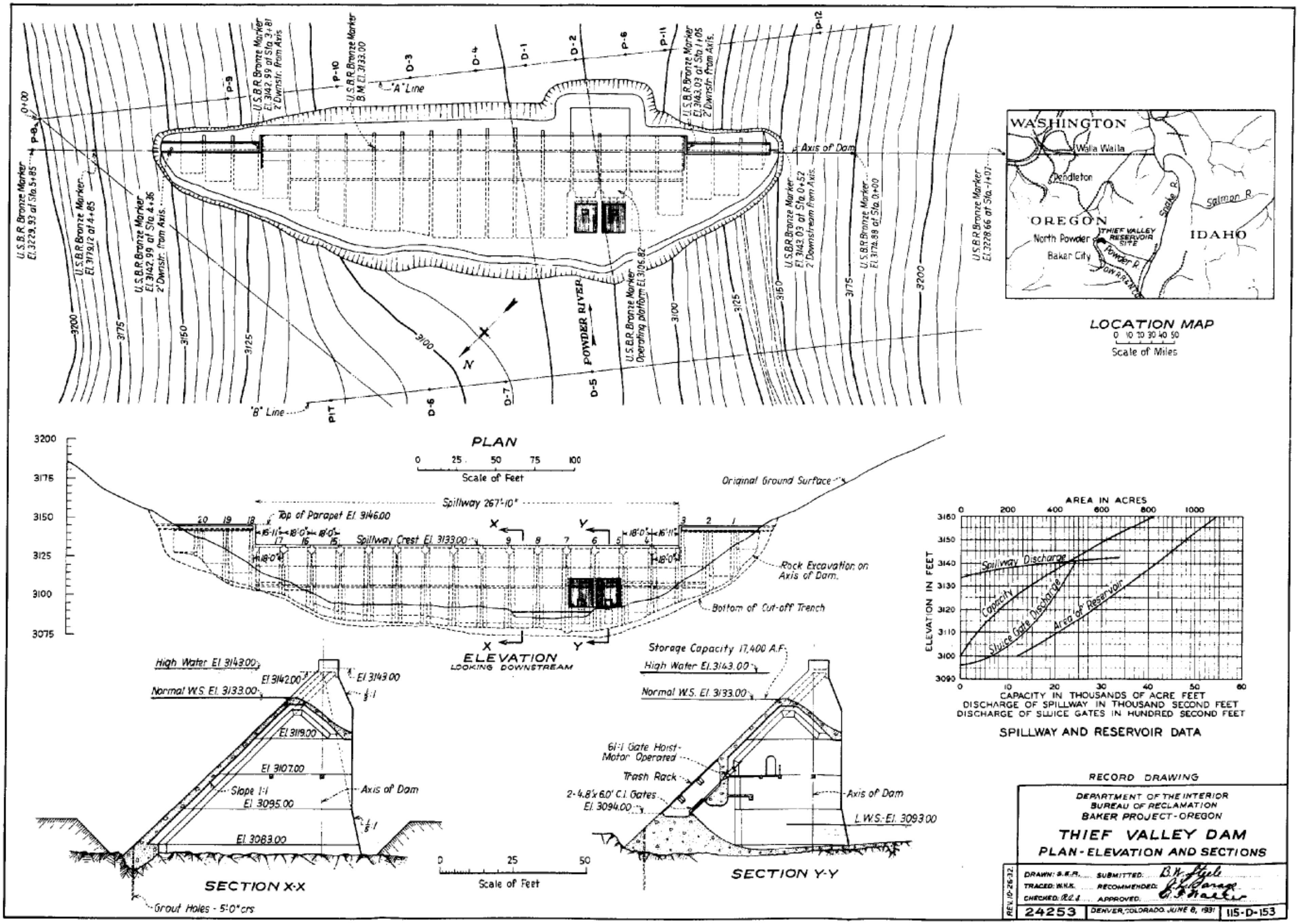
PLAN
Scale of Feet
0 25 50 75 100
"A" Line
"B" Line
Axis of Dam
POWDER RIVER
U.S.B.R. Bronze Marker El. 3229.93 at Sta. 5+85
U.S.B.R. Bronze Marker El. 3179.12 at 4+85
U.S.B.R. Bronze Marker El. 3142.99 at Sta. 4+36 2' Dwnstr. from Axis.
U.S.B.R. Bronze Marker El. 3142.99 at Sta. 3+81 2' Dwnstr. from Axis
U.S.B.R. Bronze Marker B.M. El. 3133.00
U.S.B.R. Bronze Marker El. 3143.03 at Sta. 1+05 2' Dwnstr. from Axis.
U.S.B.R. Bronze Marker Operating platform El. 3106.82
U.S.B.R. Bronze Marker El. 3143.03 at Sta. 0+52 2' Downstream from Axis.
U.S.B.R. Bronze Marker El. 3174.98 at Sta. 0+00
U.S.B.R. Bronze Marker El. 3228.66 at Sta. -1+07
LOCATION MAP
Scale of Miles
WASHINGTON
Walla Walla
Pendleton
OREGON
North Powder
Baker City
Powder R.
Snake R.
Salmon R.
IDAHO
THIEF VALLEY RESERVOIR SITE
ELEVATION
LOOKING DOWNSTREAM
Spillway 267'-10"
Top of Parapet El. 3146.00
Spillway Crest El. 3133.00
Original Ground Surface
Rock Excavation on Axis of Dam.
Bottom of Cut-off Trench
SPILLWAY AND RESERVOIR DATA
AREA IN ACRES
ELEVATION IN FEET
Spillway Discharge
Capacity
Sluice Gate Discharge
Area of Reservoir
CAPACITY IN THOUSANDS OF ACRE FEET
DISCHARGE OF SPILLWAY IN THOUSAND SECOND FEET
DISCHARGE OF SLUICE GATES IN HUNDRED SECOND FEET
SECTION X-X
High Water El. 3143.00
Normal W.S. El. 3133.00
El. 3142.00
El. 3143.00
El. 3119.00
El. 3107.00
Slope 1:1
El. 3095.00
El. 3083.00
Axis of Dam
Grout Holes - 5'-0" crs
Scale of Feet
SECTION Y-Y
Storage Capacity 17,400 A.F.
High Water El. 3143.00
Normal W.S. El. 3133.00
61:1 Gate Hoist-Motor Operated
Trash Rack
2-4.8'x6.0' C.I. Gates
El. 3094.00
Axis of Dam
L.W.S.-El. 3093.00
RECORD DRAWING
DEPARTMENT OF THE INTERIOR
BUREAU OF RECLAMATION
BAKER PROJECT-OREGON
THIEF VALLEY DAM
PLAN-ELEVATION AND SECTIONS
DRAWN
TRACED
CHECKED
SUBMITTED
RECOMMENDED
APPROVED
24253
DENVER, COLORADO JUNE 8, 1931
115-D-153

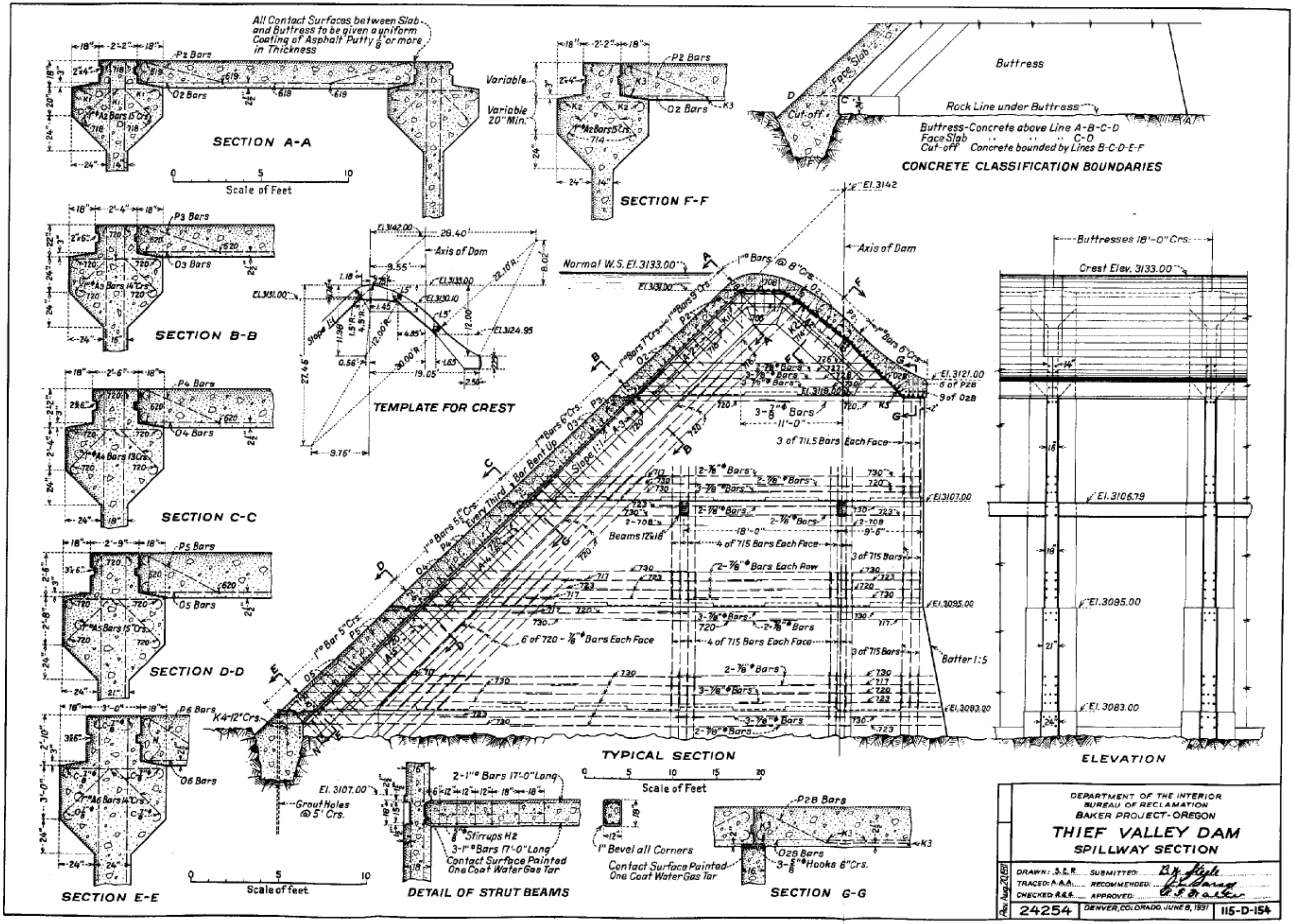
SECTION A-A
SECTION B-B
SECTION C-C
SECTION D-D
SECTION E-E
SECTION F-F
SECTION G-G
TEMPLATE FOR CREST
CONCRETE CLASSIFICATION BOUNDARIES
TYPICAL SECTION
ELEVATION
DETAIL OF STRUT BEAMS
All Contact Surfaces between Slab and Buttress to be given a uniform Coating of Asphalt Putty 1/8" or more in Thickness
Buttress-Concrete above Line A-B-C-D
Face Slab .. .. .. C-D
Cut-off Concrete bounded by Lines B-C-D-E-F
Rock Line under Buttress
Normal W.S. El. 3133.00
Axis of Dam
Buttresses 18'-0" Crs.
Crest Elev. 3133.00
Batter 1:5
Scale of Feet
DEPARTMENT OF THE INTERIOR
BUREAU OF RECLAMATION
BAKER PROJECT-OREGON
THIEF VALLEY DAM
SPILLWAY SECTION
DENVER, COLORADO, JUNE 8, 1931
24254
115-D-154

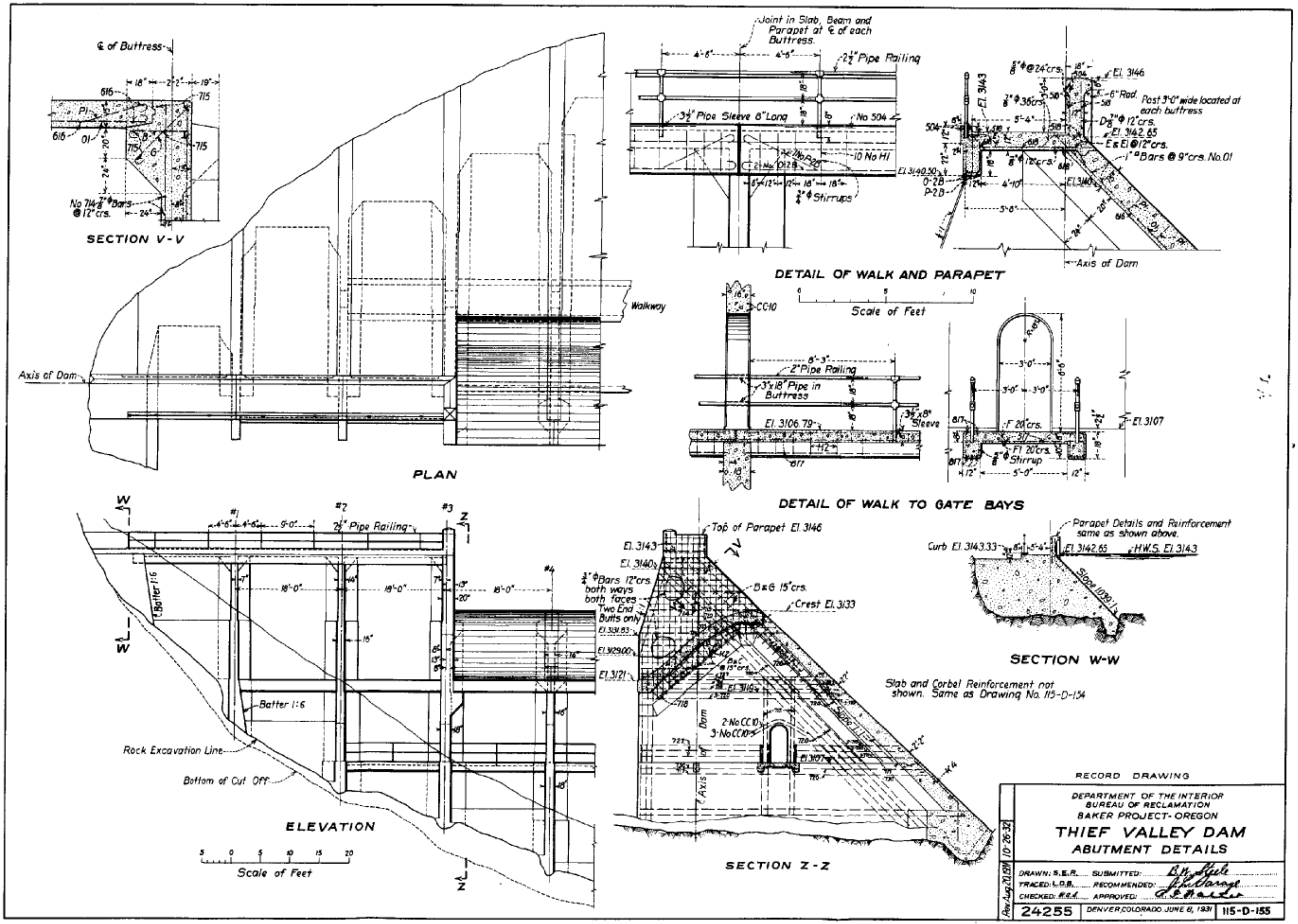
SECTION V-V
PLAN
Walkway
Axis of Dam
DETAIL OF WALK AND PARAPET
Joint in Slab, Beam and Parapet at ℄ of each Buttress.
2½" Pipe Railing
3½" Pipe Sleeve 8" Long
Post 3'-0" wide located at each buttress
Axis of Dam
Scale of Feet
DETAIL OF WALK TO GATE BAYS
2" Pipe Railing
3"x18" Pipe in Buttress
El. 3106.79
El. 3107
ELEVATION
2½" Pipe Railing
Batter 1:6
Rock Excavation Line
Bottom of Cut Off
Scale of Feet
SECTION Z-Z
Top of Parapet El. 3146
Crest El. 3133
SECTION W-W
Parapet Details and Reinforcement same as shown above.
Curb El. 3143.33
H.W.S. El. 3143
Slab and Corbel Reinforcement not shown. Same as Drawing No. 115-D-154
RECORD DRAWING
DEPARTMENT OF THE INTERIOR
BUREAU OF RECLAMATION
BAKER PROJECT-OREGON
THIEF VALLEY DAM
ABUTMENT DETAILS
DRAWN: S.E.R. SUBMITTED:
TRACED: L.D.B. RECOMMENDED:
CHECKED: APPROVED:
24255
DENVER, COLORADO, JUNE 8, 1931
115-D-155

Appendix D – Jet Impingement Maps

Maps that follow show the calculated impingement area for free jets discharged from the spillway flip bucket for frequency flood events ranging from 100 yr to 100,000,000 yr. Line definitions are illustrated on the example chart below:

- The axis of the dam is indicated by a straight blue line.
- A pair of jagged blue lines indicates the upper and lower nappe boundaries of the jet core at impingement on the downstream topography. Where the two lines are coincident, the jet core is calculated to be broken up and the single blue line indicates the center of the spread jet.
- A pair of jagged bright green lines indicates the upper and lower boundaries of the spread jet at impact with the downstream topography.
- Red contours highlight the expected tailwater elevation for each flood event.
- Note rapid diminishment of the jet core thickness and increasing width of the spread jet where impingement occurs below the tailwater elevation.

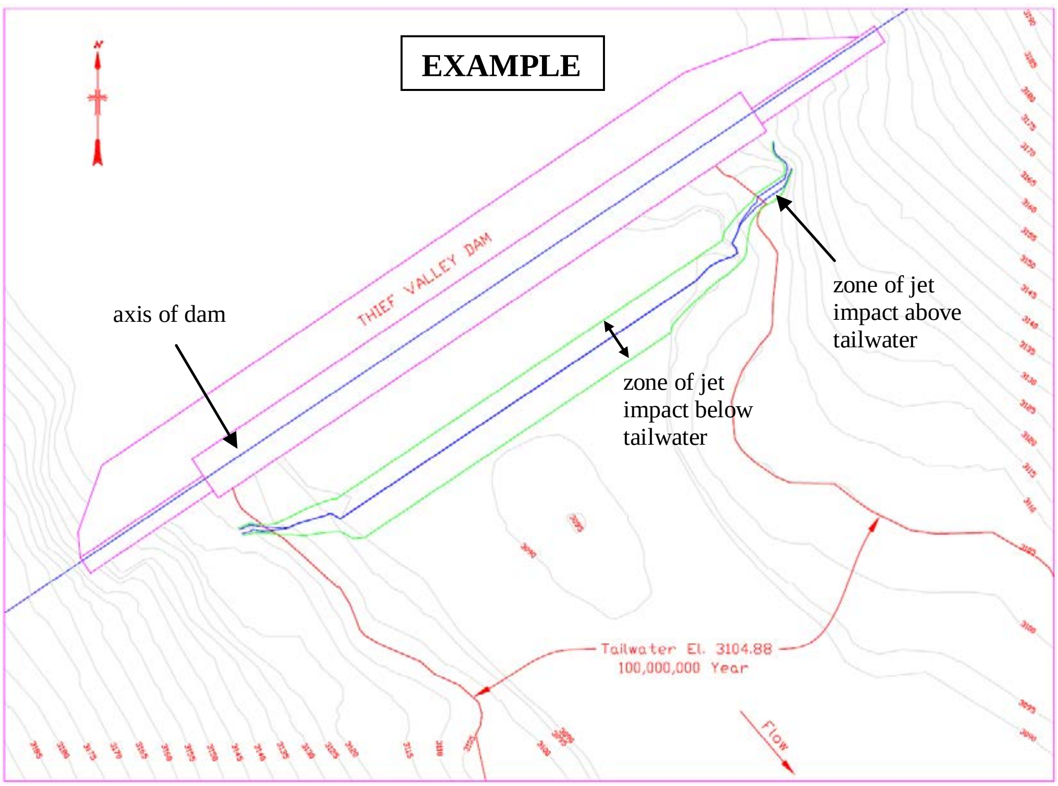

The final map in this appendix shows the calculated impingement area of free jets overtopping the dam parapet wall during the November PMF. The impingement area for associated spillways flows is not shown for the PMF case.

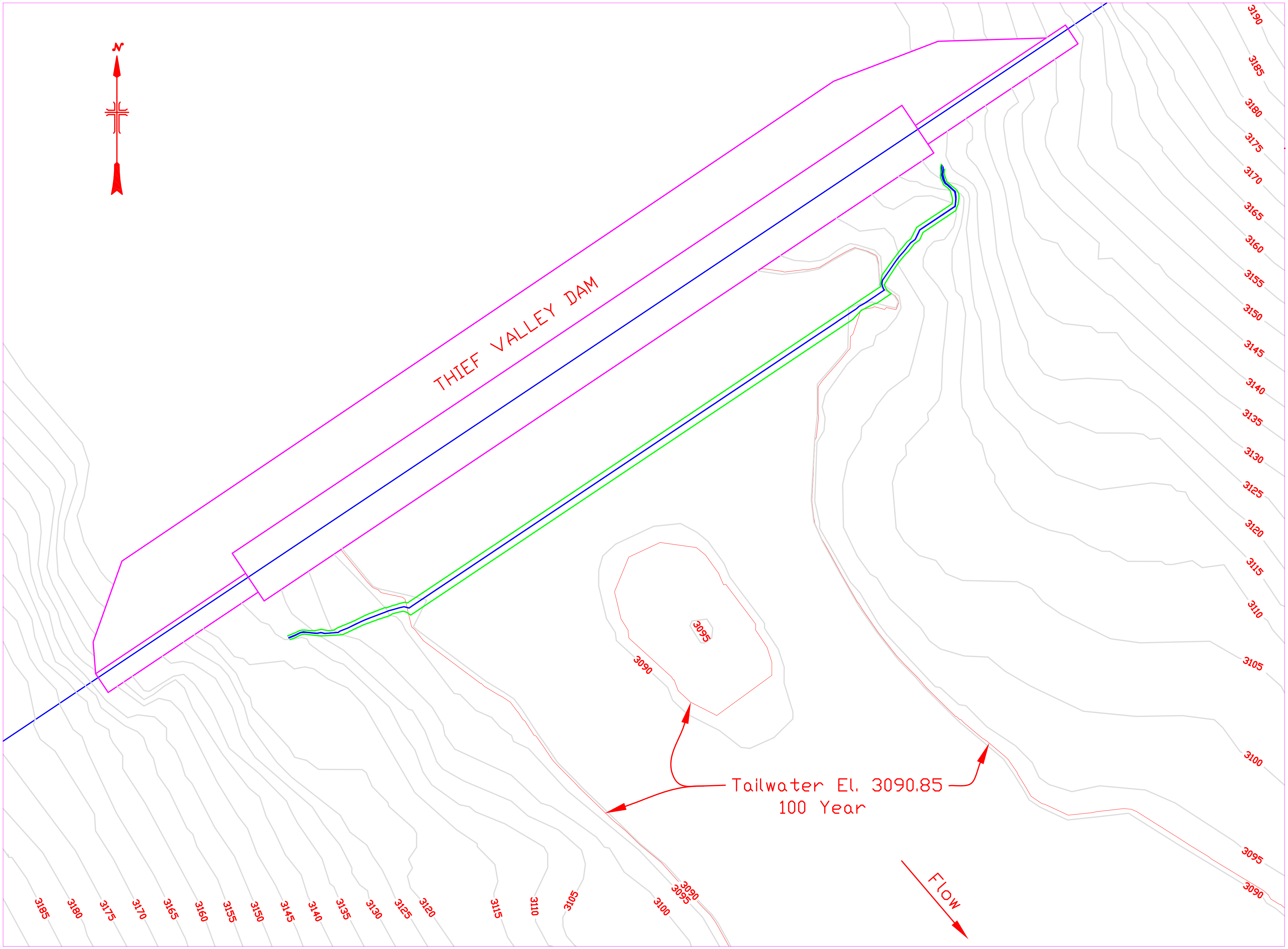
N
THIEF VALLEY DAM
Tailwater El. 3090.85
100 Year
Flow
3190
3185
3180
3175
3170
3165
3160
3155
3150
3145
3140
3135
3130
3125
3120
3115
3110
3105
3100
3095
3090

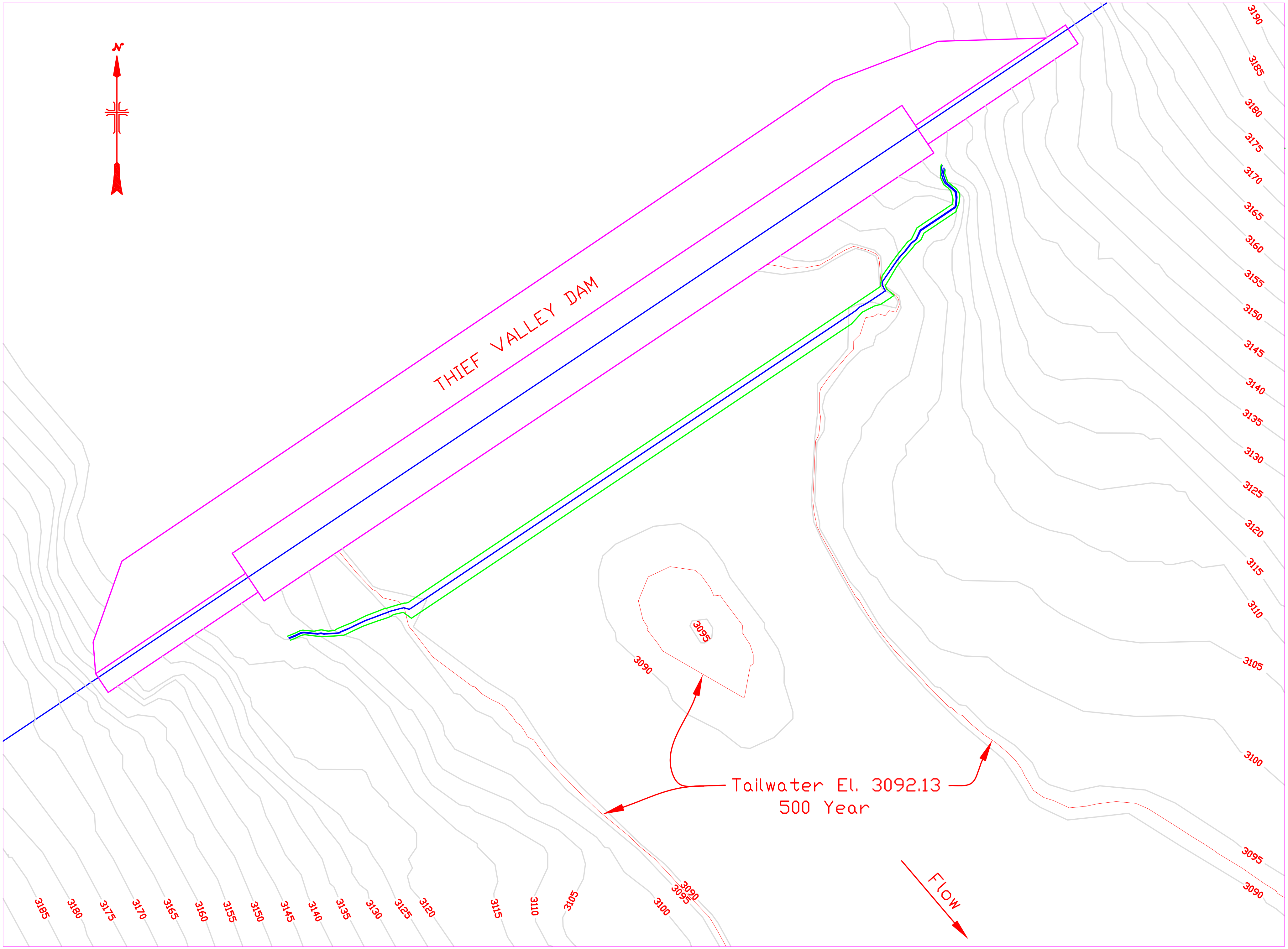
N
THIEF VALLEY DAM
Tailwater El. 3092.13
500 Year
Flow
3095
3090
3190
3185
3180
3175
3170
3165
3160
3155
3150
3145
3140
3135
3130
3125
3120
3115
3110
3105
3100
3095
3090

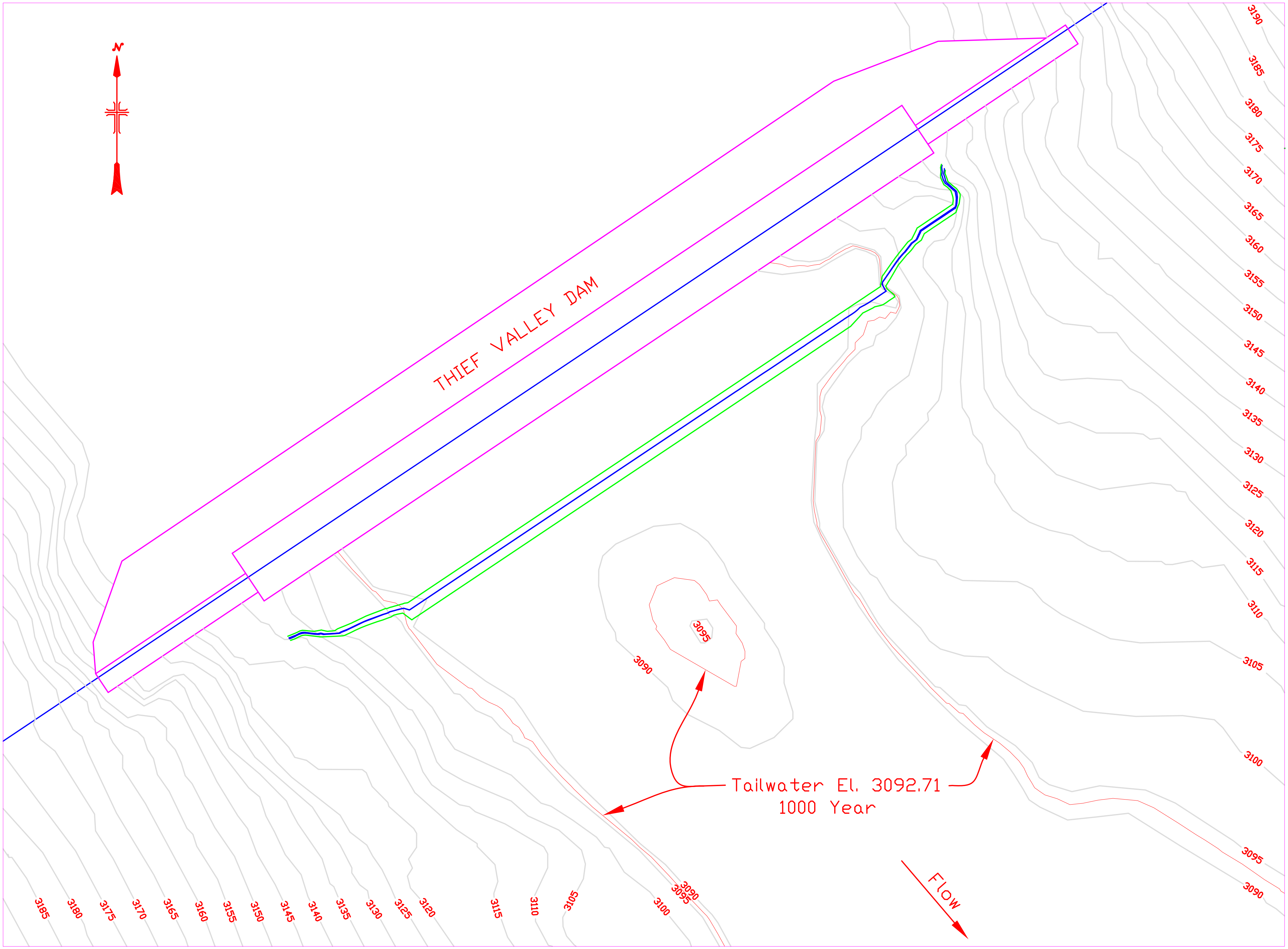

N
THIEF VALLEY DAM
Tailwater El. 3092.71
1000 Year
Flow
3190
3185
3180
3175
3170
3165
3160
3155
3150
3145
3140
3135
3130
3125
3120
3115
3110
3105
3100
3095
3090

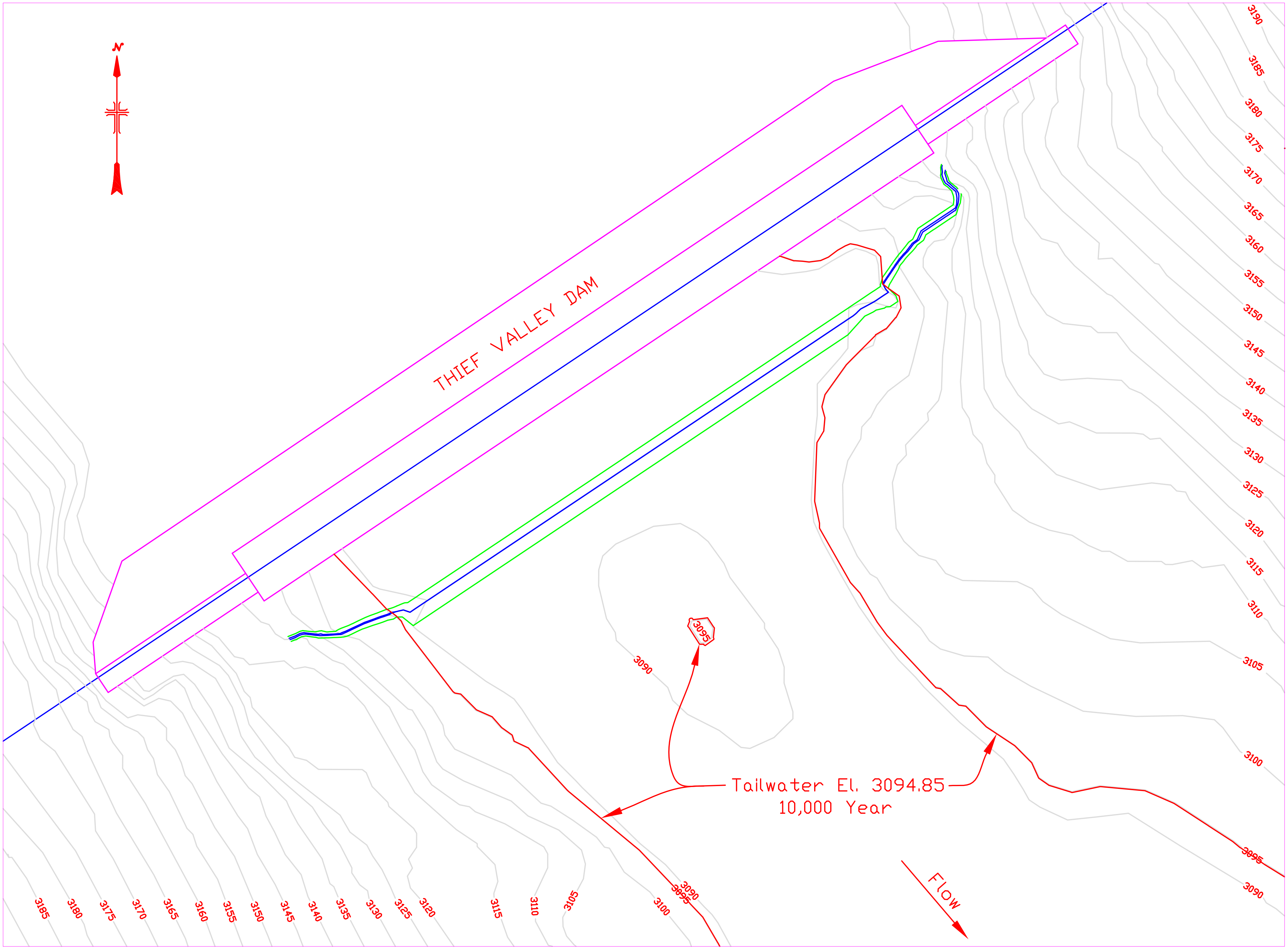

THIEF VALLEY DAM
Tailwater El. 3094.85
10,000 Year
Flow
N
3095
3090
3190
3185
3180
3175
3170
3165
3160
3155
3150
3145
3140
3135
3130
3125
3120
3115
3110
3105
3100

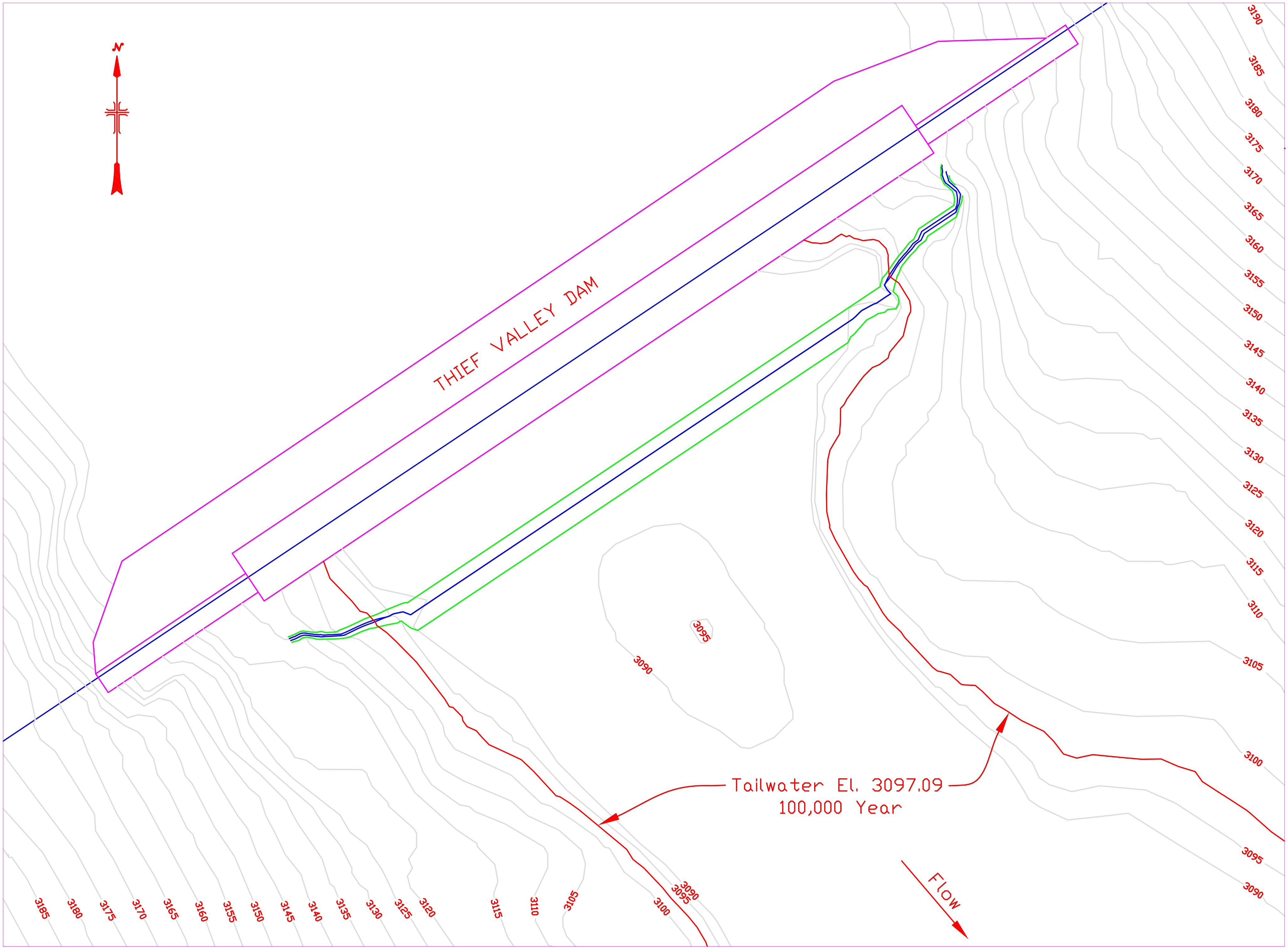

N
THIEF VALLEY DAM
Tailwater El. 3097.09
100,000 Year
Flow
3190
3185
3180
3175
3170
3165
3160
3155
3150
3145
3140
3135
3130
3125
3120
3115
3110
3105
3100
3095
3090

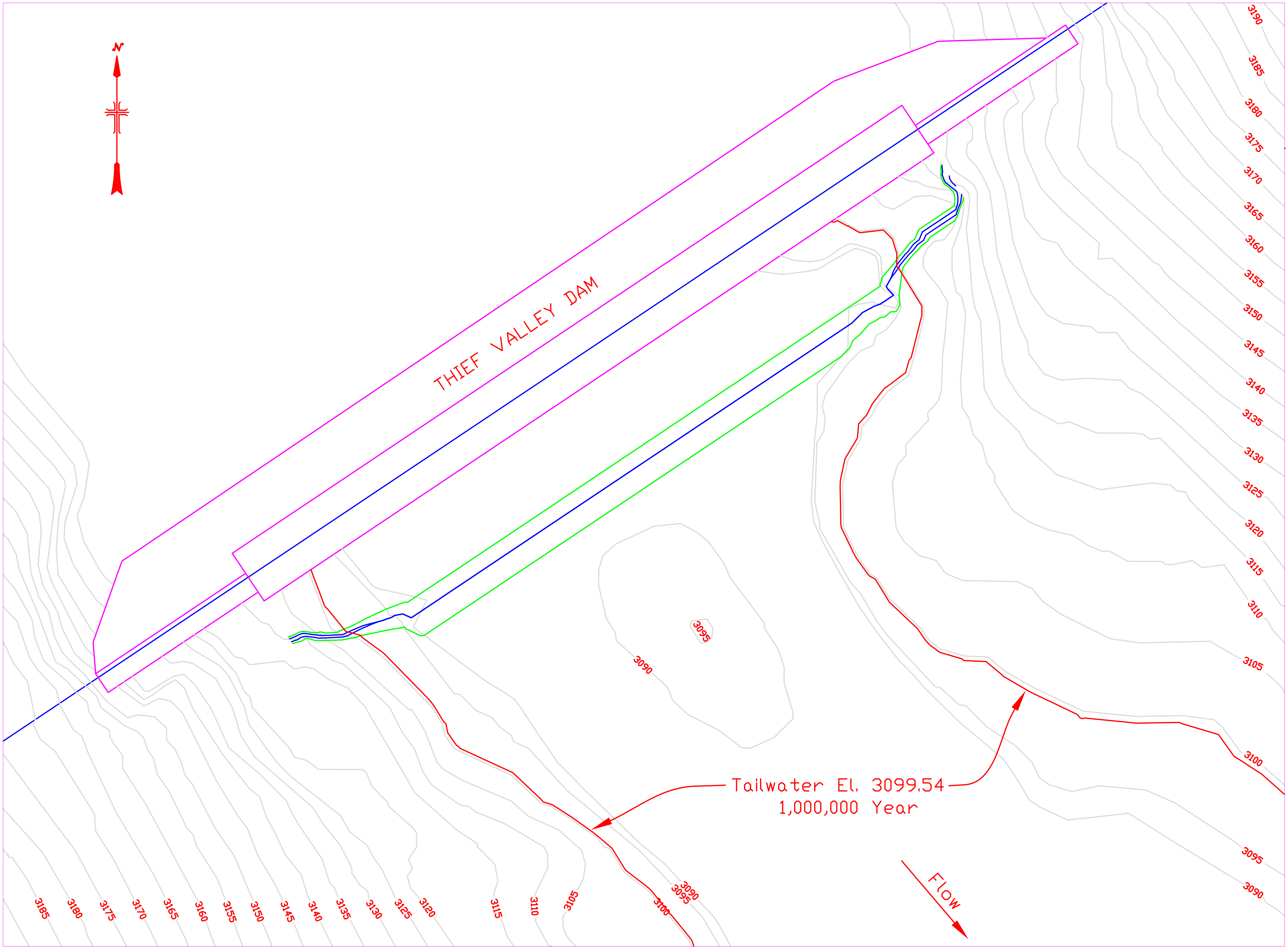

N
THIEF VALLEY DAM
Tailwater El. 3099.54
1,000,000 Year
Flow
3190
3185
3180
3175
3170
3165
3160
3155
3150
3145
3140
3135
3130
3125
3120
3115
3110
3105
3100
3095
3090

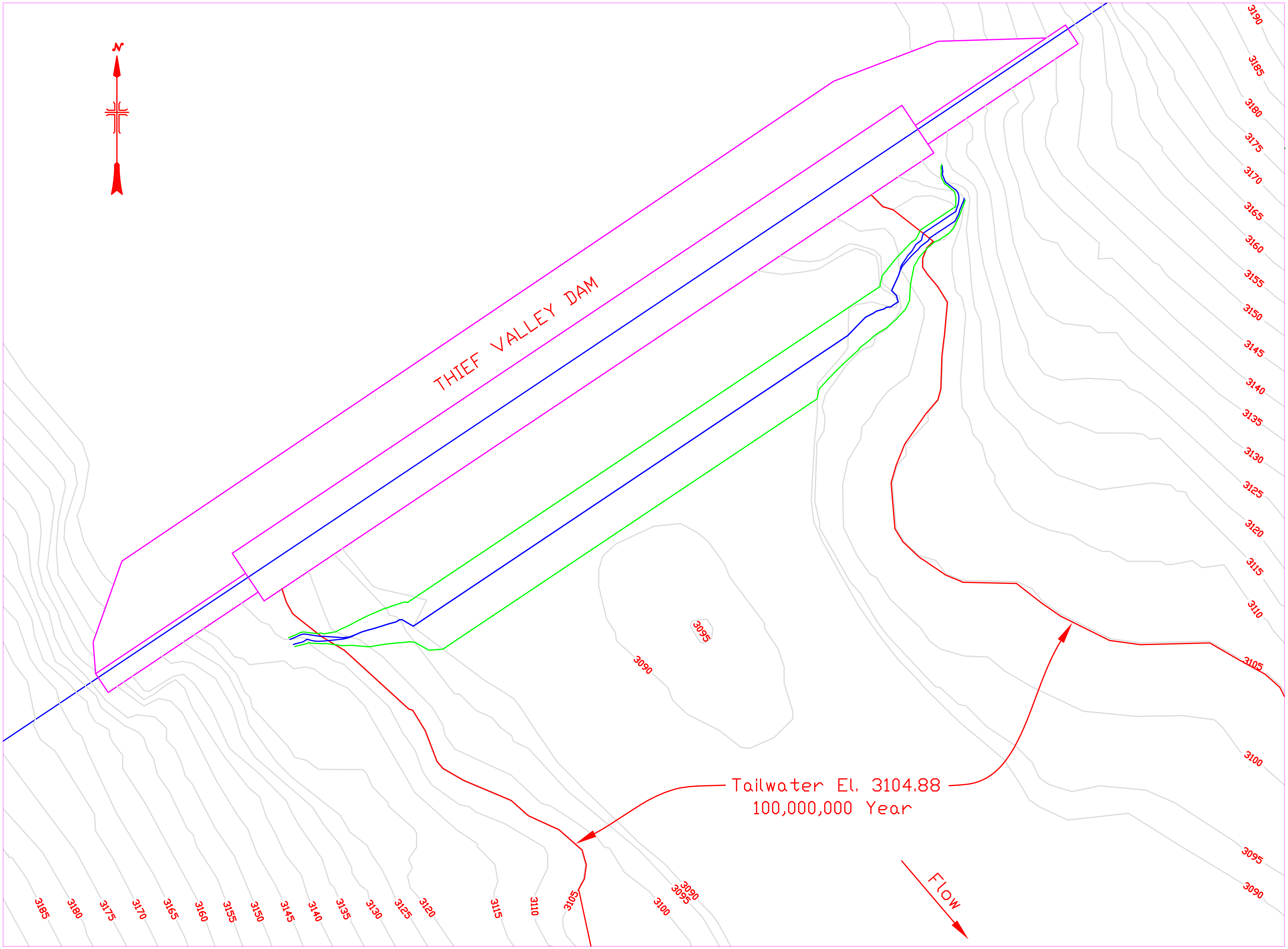

N
THIEF VALLEY DAM
Tailwater El. 3104.88
100,000,000 Year
Flow
3190
3185
3180
3175
3170
3165
3160
3155
3150
3145
3140
3135
3130
3125
3120
3115
3110
3105
3100
3095
3090

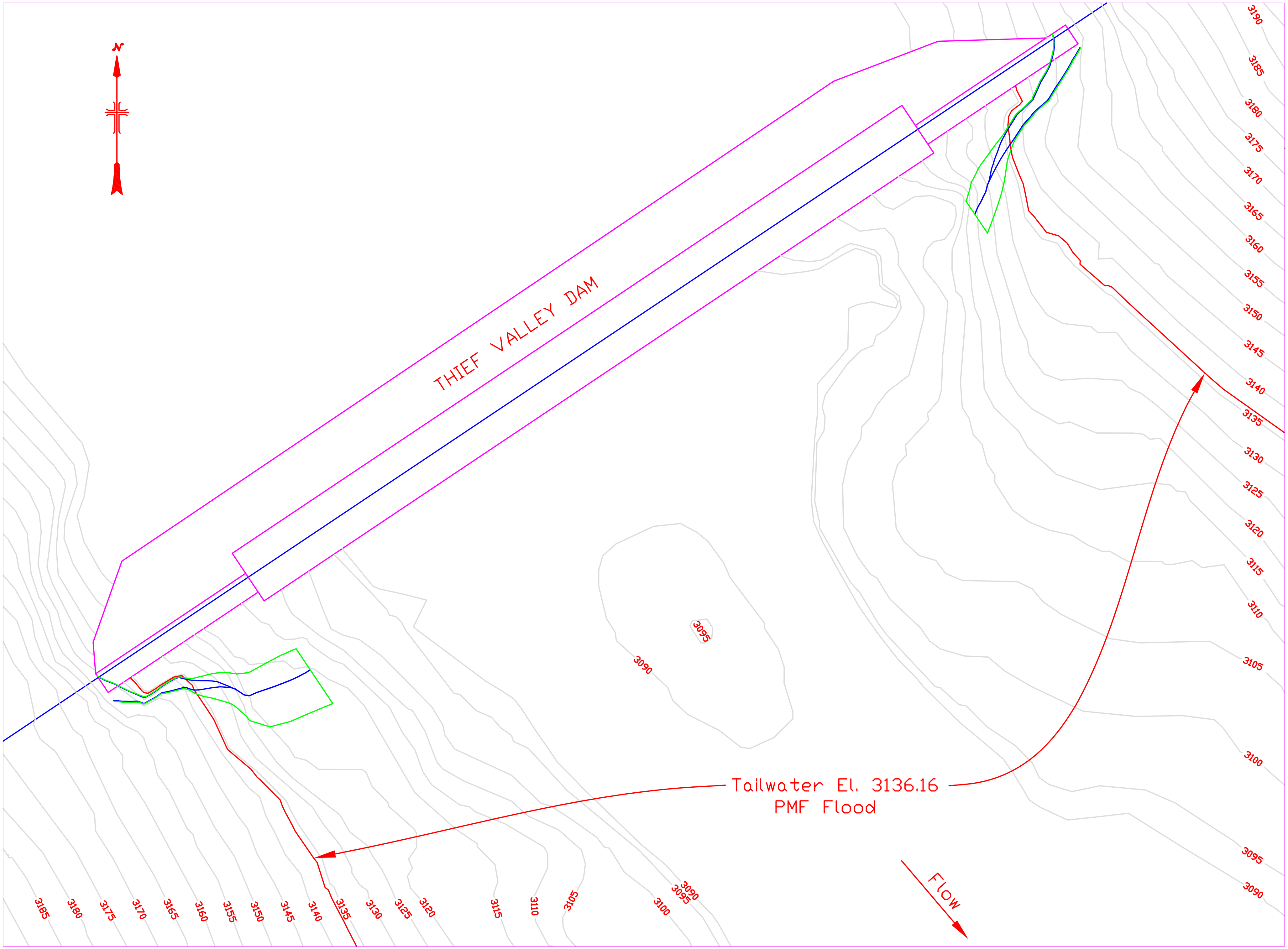

N
THIEF VALLEY DAM
Tailwater El. 3136.16
PMF Flood
Flow
3190
3185
3180
3175
3170
3165
3160
3155
3150
3145
3140
3135
3130
3125
3120
3115
3110
3105
3100
3095
3090